Embedded Watermarking for Image Verification in Telemedicine

by

Dominic Osborne

B.E. (Microelectronics, First Class Honours),
University of South Australia, 2001

Thesis submitted for the degree of

Doctor of Philosophy

in

Electrical and Electronic Engineering
University of Adelaide

2005

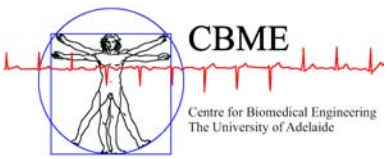

Contents

Abstract

Wireless communication technology has provided increased opportunity for applications such as telemedicine. This work focuses on the end application of teleradiology, targeting the communication of digital diagnostic images to remote locations for diagnosis and treatment. Medical images have conventionally been of large size and stored without loss of redundancy. Recent research has demonstrated that acceptable levels of Joint Picture Experts Group (JPEG) compression may be used on these image types without loss of diagnostic content. This has provided an opportunity for more rapid image transmission in wireless environments. One of the most pressing challenges that remain are techniques to verify the integrity of crucial diagnostic feature information that may be compromised with excessive use of standard compression methods.

An authentication watermarking technique is presented, which extracts critical feature information from the Region of Interest (ROI) and embeds a series of robust watermarks into the Region of Backgrounds (ROB) surrounding this location. This thesis will consider only the effects of distortions due to compression standards and presents a body of work that is a step towards a future study for considering compression together with channel noise introduced by the wireless environment.
The following key contributions have been made in this thesis:

- A novel technique to provide crucial feature authentication without introducing embedding distortions into these regions by using multiple robust watermarks
- Improved performance over earlier methods including superior robustness to DCT quantisation and complete JPEG image compression. Image fidelity is significantly improved with less distortion introduced. Smaller signatures can be used to authenticate essential image information than with conventional methods, decreasing overall system complexity
- Optimised JPEG survival levels that allow permissable JPEG compression levels to be specified.

Statement of Originality

This work contains no material that has been accepted for the award of any other degree or diploma in any university or other tertiary institution and, to the best of my knowledge and belief, contains no material previously published or written by another person, except where due reference has been made in the text.

I give consent to this copy of the thesis, when deposited in the University Library, being available for loan, photocopying and dissemination through the library digital thesis collection.

8th September, 2005

Signed

Date

Acknowledgments

Many people have collaborated to make this Ph.D. an interesting and rewarding part of my life. I extend my sincerest thanks to my family, friends, colleagues and supervisors.

I greatly appreciate the help I have received from my supervisor Associate Professor Derek Abbott for his excellent help and creative ideas that have assisted me in broadening my research skills. I appreciate his endless patience, positive outlook, ability to provide assistance and especially his willingness to put his students before his work. I thank him greatly for his meticulous proof reading of all of my published work.

I have had the pleasure of working with Dr Derek Rogers, an Adjunct Senior Lecturer from the School of Electrical and Electronic Engineering. His expert knowledge in wireless communications and engineering practice have assisted this research tremendously. His attention to detail and excellent standards have assisted me in developing sound research methods. Acknowledgements must be give to Mr Ross Frick, from the University of South Australia for his expert help and knowledge in mathematical areas. Thanks are due to Dr Matthew Sorell, Professor Reginald Coutts and Professor Jag Mazumdar for their support in the early stages of the project.

I have enjoyed interaction with colleagues from the University of Adelaide and collaborating with people with technical expertise within conferences. Thanks are also due to Dr Greg Harmer for the provision of an excellent LaTeX template. I thank my parents for their financial support and encouragement and my friends for their moral support and in helping me to have enjoyable breaks between work on the weekends. I gratefully acknowledge funding from the Australian Research Council and Motorola Software Corporation. Funding from the School of Electrical and Electronic Engineering has also been of great assistance for support on overseas conferences. Thanks are also due to the *Medpix™ Medical Image Database* (2005) for an excellent source of medical images.

Conventions

This thesis it typeset using the LaTeX2e software. WinEdt build 5.4 was used as an interface to LaTeX. Graphs and plots were generated using Matlab 7.0 (Mathworks Inc.) CorelDRAW 12 and Corel PHOTO-PAINT 12 were used to produce schematic and flow diagrams. The Kakadu JPEG-2000 software (David Taubman 2001) was used for the compression of imagery using an implementation of Part 1 of the JPEG-2000 standard.

The Harvard style is used for referencing and citation in this thesis. Australian English spelling is adopted, as defined by the Macquarie English Dictionary (Delbridge *et al.* 2001).

Publications

OSBORNE-D., ROGERS-D., AND ABBOTT-D. (2005a). Embedded watermarking for wireless image content authentication, *WSEAS Transactions on Communications*, **4**(7), pp. 505–513.

OSBORNE-D., ROGERS-D., AND ABBOTT-D. (2005b). Integrity assessment of diagnostic image content, *Proceedings of the 9th WSEAS International Conference on Communications*, Vouliagmeni, Athens, Greece, July 14-16. paper 479-308.

OSBORNE-D., ROGERS-D., SORELL-M., AND ABBOTT-D. (2005c). Multiple medical image ROI authentication using watermarking, *Proceedings of the SPIE - Biomedical Applications of Micro- and Nanoengineering II*, Vol. 5651, University of New South Wales, Sydney, Australia 12-15 December 2004, pp. 221–231.

OSBORNE-D., ABBOTT-D., SORELL-M., AND ROGERS-D. (2004a). Multiple embedding using robust watermarks for wireless medical images, *Proceedings of the 3rd International Conference on Mobile and Ubiquitous Multimedia (MUM-2004)*, Vol. 83 of *ACM International Conference Proceeding Series*, College Park, Maryland, U.S.A. October 27-29, pp. 245–250.

OSBORNE-D., ABBOTT-D., SORRELL-M., AND ROGERS-D. (2004b). Multiple embedding using semi-fragile watermarks for wireless medical images, *Proceedings of the IEEE: Electronics and Telecommunications (ETC-2004)*, Timisoara, Romania, October 22-23, Section 13(34), pp. 120–125.

OSBORNE-D., ROGERS-D., SORELL-M., AND ABBOTT-D. (2004c). Embedded importance watermarking for image verification in radiology, *Proceedings of the SPIE - BioMEMS and Nanotechnology*, Vol. 5275, University of Western Australia, Perth, December 10-12, pp. 383–390.

OSBORNE-D., ROGERS-D., MAZUMDAR-J., COUTTS-R., AND ABBOTT-D. (2002). An overview of wavelets for image processing for wireless applications, *Proceedings of the SPIE: Smart Structures, Devices and Systems*, Vol. 4935, University of Melbourne, Australia December 16-18, pp. 427–435.

List of Figures

List of Tables

Chapter 1

Introduction

WIRELESS communication technology has advanced to the point where efficient and rapid communication of all types of multimedia are possible using commercial 'off the shelf' systems. One of the most interesting and challenging end applications is for wireless telemedicine. Recent technology has shown an increase in the speed of transmission and a large drop in the cost of transmission bandwidth. This thesis brings together the technologies of wireless communication technology, JPEG image compression and embedded watermarking.

This chapter presents an overview of the thesis in Section 1.1, defines the area of telemedicine in Section 1.2 and the improvements in health care that result from it in Section 1.3. The primary problems encountered and their significance using this technology are discussed in Sections 1.4 and 1.5. The key challenges of lossy compression are shown to play an important role. Key contributions of this thesis are presented in Section 1.6. This provides an outline of the method as well as a summary of the original contributions. Delimitations of this work are addressed in Section 1.7.

1.1 Outline of Thesis

This research seeks to advance the new area of wireless telemedicine. Several close disciplines are addressed in this work including wireless communications, image processing and content authentication.

Chapter 2 contains a comprehensive literature review of the broad research area of wireless telemedicine to the specific concepts pertaining to semi-fragile watermarking. This chapter begins with examples containing practical applications of wireless telemedicine that have been undertaken worldwide. Such projects have been based on satellite communication, mobile phone telephony as well as radio-based technologies. Focus has been placed on communication infrastructure and standards, cost-effectiveness, ease of implementation as well as a critical summary to address key problem areas and highlight suggested improvements. Special attention is given to compliance with current image acquisition and compression standards developed by International Standard Organisations (ISO). Some of the most challenging problems include compression thresholds for optimal speed of transmission, quality assessment as well as content verification. The challenge of image authentication is addressed with focus placed on watermarking technologies that will not disrupt crucial image information and survive wireless communication processes focusing on standard compression techniques.

Chapter 3 defines some performance measures that are used to evaluate the effectiveness of watermarking methods that are designed and developed in this thesis. These include robustness, compression performance and image fidelity. Acceptable levels and thresholds are also defined to discern optimal system behavior from that which is unacceptable.

Chapter 4 provides a concise outline of the method adopted in this thesis, including theoretical techniques that are used to extract and embed a signature. A convenient approach to remove the perceptual distortion introduced by the watermark is also addressed. Further theoretical principles and theorems can be referred to in Section 2.7.1. Proof of these theorems are contained in Appendix D.

Chapter 5 compares the performance of an earlier system (Lin and Chang 2001) to

the method which is presented in Chapter 4. The metrics that are used for the comparisons are adopted from Chapter 3. The thesis is concluded with Chapters 6 and 7 that contain conclusions, discussions and recommendations. Focus is placed on improvements to the system, strengths and possible failure points. Potential end applications are also discussed.

1.2 What is Telemedicine?

Telemedicine is a subset of the much more broader commercial area of telematics that involves the use of computers or information systems to receive, store and distribute information over a distance using the technology of telecommunications. Examples can include The World Wide Web (WWW), Email, Videoconferencing, Dataconferencing, tele-servicing and tele-robotics.

Telemedicine is the collective union of medical related telematics technologies. Some examples taken from Youngberry (2004) include teleradiology, telepathology, telecare, telesurgery, teledermatology and teleneurology. This thesis has its focus on teleradiology, which is the wireless communication of radiological images. This is one of the oldest and well-established areas of telemedicine.

1.3 Improving Communication to Remote Locations

Many studies have found teleradiology to be a clinically beneficial and cost-effective alternative to conventional specialist treatment (Seidman 1997), (Wootton *et al.* 2003). This technology provides the infrastructure for rapid response to highly important medical care independent of the geographic barriers. Critically ill or injured patients can be treated locally by effective communication with a distant specialist provided by wireless technology (Tachakra *et al.* 2003). Flexible and rapid access to expert opinion and advice at the point of care is also provided, with improved management of medical resources (Osborne *et al.* 2002).

Patients requiring care would benefit from locally provided services as they would have immediate access to a second opinion if required. A likely scenario may be a patient in a remote location, who would have the flexibility to call their specialist. A

mobile phone could be used to discuss the management of a medical problem along with the transmission of diagnostic images.

Early methods of care for patients in these locations imply transportation to a hospital, assessment, admission and eventually results in the patient being discharged. Long journeys from remote locations to a central hospital is a problem for families and weakens the connection with primary health care and social services (Kaidu *et al.* 2004). If a local or remote hospital has the facilities for effective wireless telemedicine, diagnosing or treating specialists can know nearly as much about the patients as if they are examining them directly. Admission is less complex and may result in fewer patients requiring admission and treatment. This is a cost-effective solution for hospitals where funding may be limited. One of the most pressing challenges in communicating any type of medical data over long distances in a wireless environment is to maintain that the data has not changed in an undesirable way.

1.4 The Problem of Change

> *Even matter called inorganic, believed to be dead, responds to irritants and gives unmistakable evidence of a living principle within. Everything that exists, organic or inorganic, animated or inert, is susceptible to stimulus from the outside.* **Nikola Tesla** 1856-1943.

This quotation suggests that change occurs in all things as a result of many variables. This process is not acceptable in certain applications where critical judgement must be placed on information that must not be changed in an illegitimate way. Diagnostic images demand strict monitoring to ensure only the occurrence of acceptable distortions. Wireless telemedicine is a cutting edge technology that has many end applications in emergencies and diagnosis. Unfortunately, a wireless environment provides an ideal condition for changes to occur in diagnostic information. An undesirable outcome may ensue if essential information is lost or corrupted.

This work has a primary focus in providing an acceptable level of authentication for medical images that are required to be transmitted over a wireless link. This is very essential so that the distant specialist has assurance that essential information is present

within the transmitted image (Osborne *et al.* 2004c). A method is presented to eliminate the possibility of an erogenous diagnosis which may result from image compression distortions that are essential for effective transmission in a wireless environment. Transmitting medical images which are extremely large in size is a secondary problem, as it is not practical to transmit large amounts of data over a wireless link where transmission bandwidth is limited.

1.5 Significance of the Problem

Digital diagnostic images which are used in medicine contain highly important localised information. The relevant aspects of medical diagnostic images that influence their usefulness include the scale or size. Enough detail is mandatory to highlight specific diagnostic information. Location information is equally important to define the position of diagnostic information as well as its density and the way it is distributed in an image. All of these qualities allow for detailed diagnostic information to be accurately extracted from the medical image. Two classic examples that highlight this type of detail include a non-displaced hairline fracture shown in Figure 1.1 and a small tumor of a breast in Figure 1.2.

Displaced fractures typically involve bending of the bone and are not as interesting to use as performing a diagnosis is trivial. The Infant's Fracture in Figure 1.1 is a challenging type of medical image to work with as it is often missed on initial radiographs because of the fine structure shown in the fracture region. A fracture review clinic in (Palombo *et al.* 2003) was established using telemedicine. It was found on X-ray reporting that the only difference in transmitting the images digitally was the 'over diagnosis' of two out of 29 fractures. Fracture review clinics represent an increasing proportion of the workload of telemedicine, making fractures a particularly relevant type of medical image to use as examples. Diagnostic information that is difficult to identify makes this type of image especially challenging.

Small tumors could be considered more important, as diagnosis must be extremely accurate as it may result in a combination of surgery or radiotherapy treatment. Both of these require an exact location as well as detail of the tumor and surrounding tissue. The breast carcinoma in Figure 1.2 is a good example.

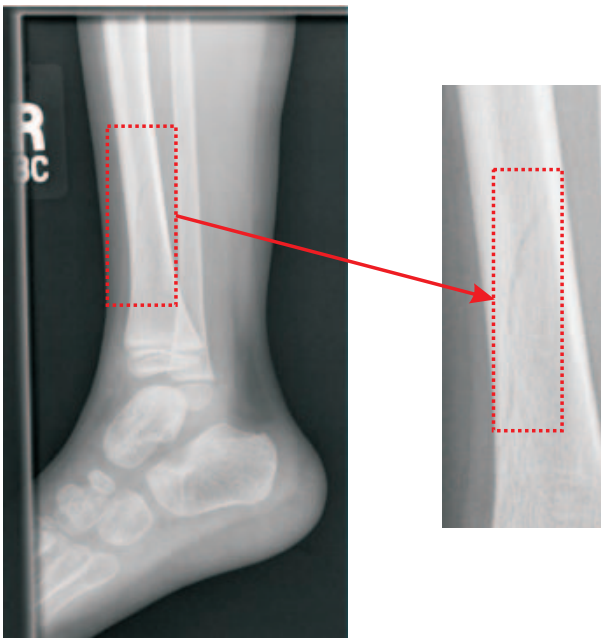

Figure 1.1. Infant's Fracture. This typically occurs in young children as a spiral hairline fracture often invisible on initial radiographs. Diagnosis can be verified if pain is reproduced with the application of torque stress across the fracture. The fracture can be seen within the dotted square.

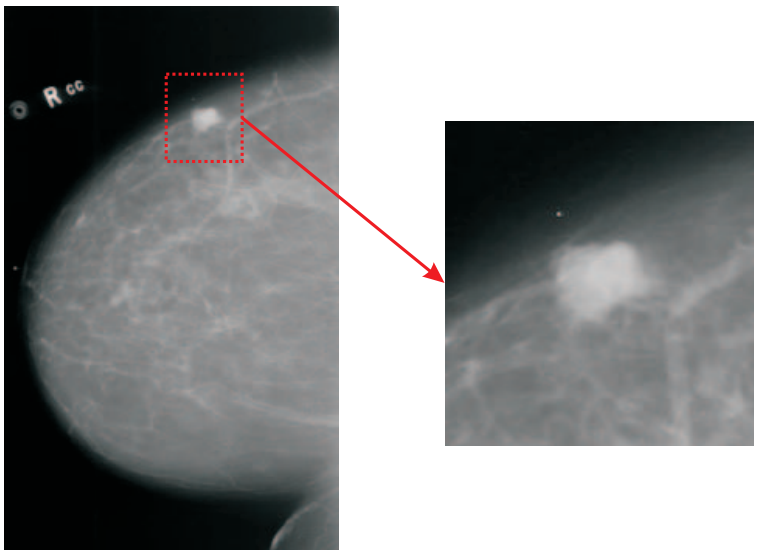

Figure 1.2. Encased papillary carcinoma of a breast. The findings in this mammogram show a dense lobulated high density nodule located at the 12 o'clock position. This corresponds to a mammographic abnormality.

1.5.1 The Need and Challenge of Using Compression

Medical images are typically acquired and stored digitally. This is especially true for greyscale diagnostic imagery that have applications in radiology. These images are typically of large size and number. Efficient compression makes it possible to increase the speed of transmission and reduce the cost of storage. Traditionally digital medical images have been of large size and stored without the loss of any information (Osborne *et al.* 2004a). The long term digital storage and mobile transmission of such images is prohibitive without the use of image compression to reduce the image file sizes.

A typical sized mammogram may be digitized at 2048×2048 pixels at 16 Bpp, leading to a file which is over 8 megabytes in size if no compression is used. On a typical 9.6 kilobit/s mobile link this would require a transmission time of nearly two hours. Although the cost of transmission bandwidth is decreasing there remains a strong demand for medical image compression.

As the speed of computers is increasing, the level of sophistication and complexity of compression methods, which are practical to use, is also increasing (Clunie 2000). Telemedicine networks as well as clinical Picture Archiving and Communication Systems (PACS) require effective storage and transmission of medical image data. Consequently efficient compression of this data is crucial. Table 1.1 summarises the storage requirements of a range of different types of medical images.

Table 1.1. Image size by modality. These figures clearly indicate that without compression, very large file sizes in the order of many megabytes will result. Typical mobile phone telephony will provide a bandwidth up to 9.6 KBps. For a typical Direct Radiography image of 18 Mb in size, this will take $\frac{18\times1000\times8}{9.6} = 15000$ seconds. This would take in excess of 4 hours for transmission, which is not cost-effective or practical for wireless diagnostic applications.

Modality	Size (Pixels)	Bit Depth	Size (Mb)
Computed Tomography (CT)	512 × 512	16-bit	0.52
Magnetic Resonance Imaging (MRI)	256 × 256	16-bit	0.13
Computed Radiography (CR)	2000 × 2500	16-bit	10.0
Direct Radiography (DR)	3000 × 3000	16-bit	18.0
Film Digitizer (FD)	2000 × 2500	16-bit	10.0
Ultrasound (US)	640 × 480	16-bit	0.614
Nuclear Medicine (NM)	256 × 256	16-bit	0.131
Digital Fluoroscopy (DF)	1024 × 1024	8-bit	1.05
Angiographic Radiology (Angio-R)	1024 × 1024	8-bit	1.05
Angiographic Cardiology (Angio-C)	1024 × 1024	8-bit	1.05

For cost-effective wireless transmission, compression must be used to discard some of the redundant image data to meet the mobile bandwidth constraint. This typically involves the use of the widely accepted Joint Picture Experts Group (JPEG) standards. The most commonly used of these is lossy baseline JPEG.

Images with slowly varying scene content and hence high correlation can be compressed efficiently as the image information can be concentrated into few coefficients in the frequency or transform domain. Projection radiographs are an exceptional type of medical image with this type of content. Coefficients that are not significant can be removed through quantisation, which results in a small file size for ease of transmission with negligible loss of image information. To the contrary, the images of interest to this work shown in Figures 1.1 and 1.2 contain high contrast edges and high levels of detail. More information must be retained in order to effectively reconstruct important picture information. This would also be expected in CT, MR and US images that may contain additional embedded text or speckled noise patterns that would otherwise be lost. Distortion is often visible in these types of images if excessive compression is used (Foos *et al.* 2000), (Osborne *et al.* 2005c).

Despite delivering impeccable quality most of the time, lossy compression can introduce false information or artifacts such as ringing and blurring which become apparent at very low bit rates. These distortions are shown in Figures 1.3 and 1.4 with a compression level of 0.1 Bpp using baseline JPEG and JPEG-2000.

These examples show that excessive lossy JPEG or JPEG-2000 compression will degrade these types of images and could affect the diagnostic outcome and hence patient treatment in telemedicine. Highly detailed information is also lost with large amounts of irreversible compression that cannot be recovered when the image is reconstructed. Spatial location information can be shifted around, which is a result of quantisation occurring on individual image blocks (Osborne *et al.* 2004b). This type of degradation can then pose the secondary problem of an erroneous diagnosis if detailed abnormalities are present in the original image.

1.6 Contribution of this Thesis

To address the concern of excessive compression, a technique is presented that can be used to verify the integrity of images with critically important Region of Interest (ROI)

Figure 1.3. Close up of an Infant's Fracture with extreme amounts lossy baseline JPEG and JPEG-2000 compression to 0.1 Bpp. From left to right the images include an uncompressed image, a baseline JPEG compressed image and a JPEG-2000 compressed image. The uncompressed image contains a high level of detail that highlights the spiral fracture information. This is a good example of the need for highly localised detail. The image in the center shows the effect of lossy Baseline JPEG compression to reduce the file size from uncompressed 8 Bits Per Pixel (Bpp) to 0.1 Bpp. Immediate loss of diagnostic information is apparent as the spiral hairline fracture is masked and displaced by block boundaries that result from discarding high frequency Discrete Cosine Transform (DCT) coefficients in the JPEG quantisation process. The lower part of the fracture also appears to have vanished. The image on the right represents the case when JPEG-2000 compression is used to reduce the image file size to 0.1 Bpp. In this instance there is a large amount of blurring which makes the fracture barely discernible and easily missed. Similarly this effect is from discarding high frequency wavelet coefficients in the EBCOT (Taubman and Marcellin 2001) quantisation process.

content prior to any informed judgements or decisions that are made after transmission. This method is designed to withstand acceptable levels of JPEG compression for ease of transmission. To ensure diagnostic integrity of these crucial regions, a multiple watermarking technique has been developed which can be used to verify the integrity of the ROI prior to diagnosis. The watermarking technique is designed for robustness to acceptable levels of baseline JPEG compression. This makes the technique compatible with most digital imaging systems that already employ the standard in their hardware and software infrastructures. This also encourages interoperability with existing consumer hardware that employ the standard.

Feature information is extracted from the ROI in the image received and compared to the signature extracted from the watermark. If there is a match within an acceptable

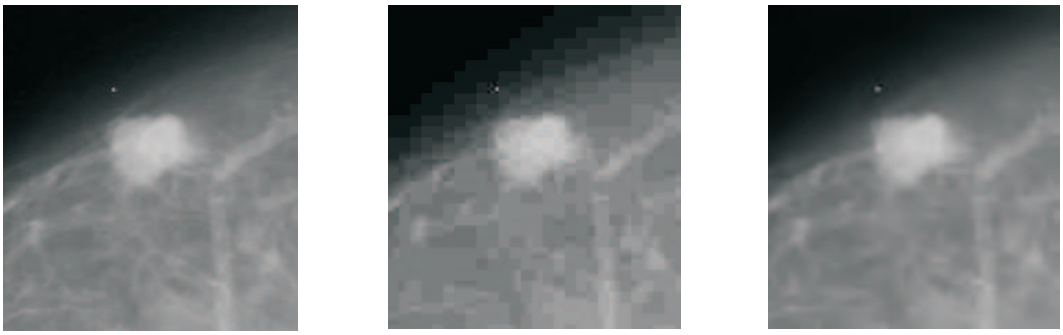

Figure 1.4. Close up of the encased breast carcinoma with extreme amounts lossy baseline JPEG and JPEG-2000 compression to 0.1 Bpp. From left to right the images include an uncompressed image, a baseline JPEG compressed image and a JPEG-2000 compressed image. The uncompressed breast carcinoma contains the most clearly visible diagnostic information matching as closely as possible that found in the original mammogram. This is a good example to use as the diagnostic information is highly localised. The image in the middle is indicative of an obvious loss of location information as the edges of the encased carcinoma are shifted to the block boundaries of the JPEG compressed image. Compression using JPEG-2000 as indicated by the image on the right does not appear to be as perceptually disturbing, but blurring is apparent. If either of these lossy compression schemes were to be used to transmit a mammogram to a remote specialist, caution should be taken or measures implemented to avoid applying such extreme compression levels.

limit, the image is considered authentic. Using similar methods proposed by Lin and Chang (2001), survival of the watermark is guaranteed by ensuring that this method is robust to:

1. Format transformation and lossless compression. A threshold is set for a match between the signature and watermark bits to disregard noise caused by integer rounding and decimation.

2. Application specific transformations including the DCT.

1.6.1 Overview of This Unique Approach

Critical feature information is extracted from the ROI that can be used as a signature. To avoid perceptual degradation of the crucial diagnostic region, robust watermarking is used around the ROI into the Region of Backgrounds (ROB) to provide authentication for these types of images. A simple method to multiply watermark involves

embedding the same authentication information in the eight regions surrounding the ROI or fewer regions if space in the ROB is unavailable. A visual overview of this method is shown in Figure 1.5. Multiple embedding can provide additional robust-

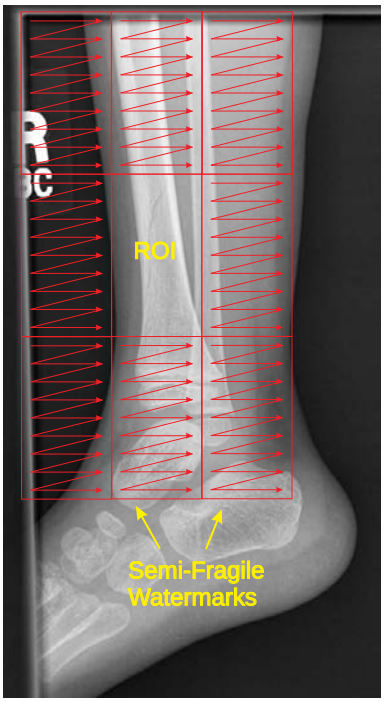

Figure 1.5. Multiple embedding in the ROB. The algorithm embeds a signature in the eight ROB regions surrounding the ROI or in fewer regions if space is unavailable. Similar watermarks could be used to occupy a smaller image area, which would require the capacity of the watermarking system to be increased.

ness if the image is cropped resulting in loss to some of the surrounding watermarks.

In this thesis there is a focus on identifying changes that have occurred to significantly important image regions. Localisation is useful as knowledge of where a work has been altered can be used to determine if the alteration is legitimate. For example if part of the fracture shown in Figure 1.1 had been lost and it did not occur in the ROI, authentication should still be possible. Many earlier approaches have had a focus on identifying localised changes in an image by embedding on a a pixel-by-pixel basis (Celik *et al.* 2003), (Kundur and Hatzinakos 2004) and on a block-wise basis (Yang *et al.* 2004), however these methods were not robust to JPEG compression and embedded authentication information into all image regions. Methods that had a focus on embedding a watermark outside of a crucial region (Wakatani 2002), (Lie *et al.* 2003) involved embedding authentication information in the wavelet transform domain and

were not designed for robustness to baseline JPEG compression.

This method does not involve embedding any information into the ROI, which eliminates the possibility of image deterioration as a result of watermark embedding or extraction. Because the watermark is based on JPEG invariant features from the crucial region, the ROI can be verified without requiring information embedded into it.

An overview of the complete authentication system is illustrated in Figure 1.6. This is expected to survive acceptable levels of JPEG compression whilst maintaining the integrity of the watermark.

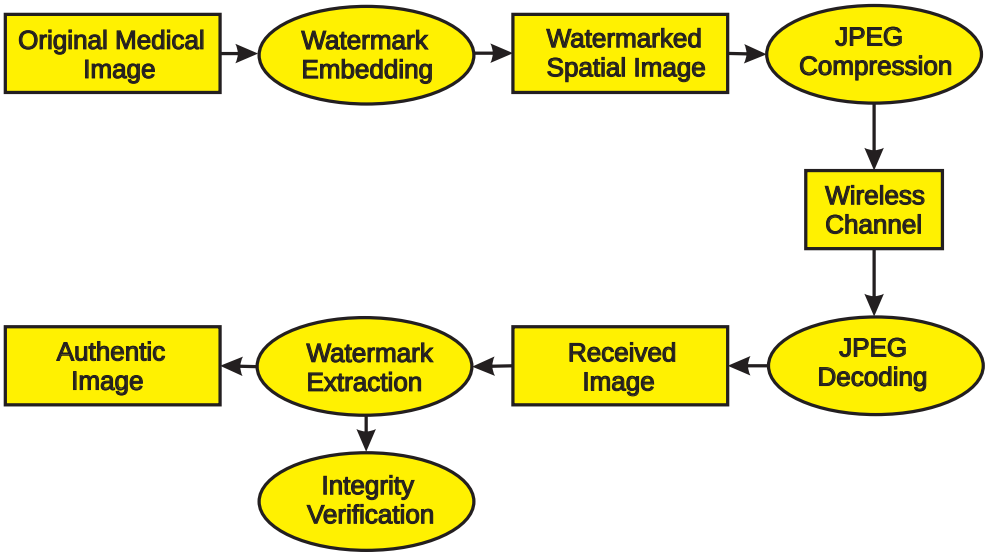

Figure 1.6. Systematic overview of watermarking method. The image is watermarked robustly to allow for acceptable distortions including conversion to and from spatial form as well as complete lossy JPEG encoding of the entire image to an acceptable bit rate. These include the distortions of integer rounding and DCT quantisation. This type of authentication technique could be extended to any image with a critically important region that requires authentication.

1.6.2 Summary of Original Contributions

The original contributions that are presented in this thesis in summary include:

1. **A Novel and Unique Technique:** Essential feature information can be verified using watermarking without introducing embedding distortions into these regions. Authentication information is taken from these locations and placed into

significantly less crucial image regions, hence losses that may occur in the ROI will correspond with a watermark mismatch in the ROB where the authentication information is placed.

2. **Improved Performance Over Earlier Methods:** robustness to DCT quantisation and complete JPEG image compression have been shown to be improved over an earlier method proposed by Lin and Chang (2001). Image fidelity has also been significantly improved, with less distortion introduced to the entire image. This is reflected with an improved average Peak Signal-to-Noise Ratio (PSNR). This is significantly better when fewer watermarks are used and a small ROI is selected for authentication. Fewer bits can be used to authenticate essential image information rather than an entire image. This lowers the amount of computation required to encode a watermark and authenticate an image.

3. **Targeted JPEG Survival Levels:** A user may specify a compression level targeting the acceptable compression range of authentication. This can be varied depending on the desired end application.

4. **Multiple Robust Watermarks**. The advantage being that the image can be clipped, yet still able to be authenticated. If one watermark fails another may be used.

1.7 Delimitations

Crucial JPEG invariant features are taken from the ROI by comparing essential DCT coefficients in known block pairs. Although corruption in specific block pairs can be located by this method, it is not possible to identify which block in the pair has been changed. This is not a significant problem for the end application in telemedicine, as the remote specialist only needs to know that the ROI is acceptable. This will be true provided that all of the blocks in the ROI have not changed. Boundary cropping may take place on medical images depending on the application. For example, a radiologist may choose to transmit only part of an image or the most significant region. This is depicted in Figure 1.7. This may present two problems. If clipping is too extreme, it may result in loss to all of the watermarks surrounding the ROI. This would render the diagnostic region content unable to be verified by watermarking. Secondly, authentication assumes a knowledge of the position of the ROI in the image and measures used to ensure that the new position is known. If the ROI location information is embedded

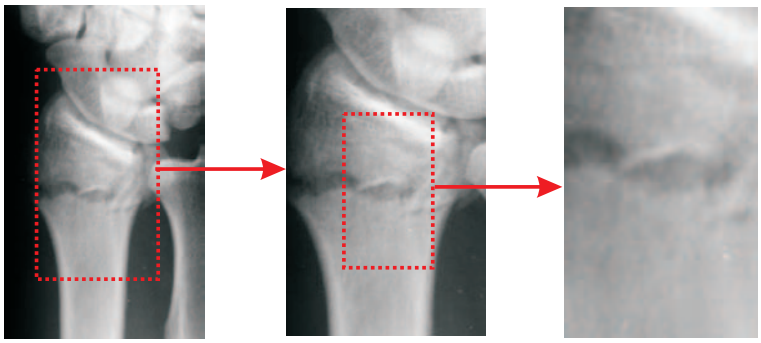

Figure 1.7. Clipping of fracture information. A fracture of the distal radius taken from a patient's arm. The transmitting radiologist may desire to clip contextual information not relevant to the diagnosis.

as a separate watermark on the edge of the image, clipping will remove knowledge of this region location.

This would assume that the ROB can be overlooked completely, which is an unlikely scenario given the high importance of these image types. If extreme cropping was still necessary, the watermarking approach could be modified by increasing its capacity so that it could occupy a lesser area.

Scaling is also a widespread image operation, especially if the mobile display device changes the image resolution to optimise the display capability. This may also occur at the transmitting end, for example a digital radiograph may be taken, watermarked and downsampled to a resolution acceptable for transmission to a remote receiver. The distribution of sampling noises can be modeled by a Gaussian function with a variance that is not significantly large (Lin and Chang 1999) and would not cause unacceptable changes to DCT coefficients. Hence the ROI watermark method could be changed by setting appropriate tolerance bounds. Design for robustness to scaling has not been investigated in this thesis.

Wavelet-based image compression techniques such as JPEG-2000 can behave as a type of low pass filter when applied to images with high levels of detail when low bit rate coding is used. This is depicted in Figures 1.3 and 1.4. Watermark survival to lossy JPEG-2000 compression is tested, but no thresholds for watermark detection are changed. Survival of the watermark to JPEG-2000 compression is treated as a side issue to explore the extended application of this system.

No attempt is made to automatically segment medical images into critical and non-critical regions. This is Presented in the Recommendations for possible future work. Furthermore, it is assumed that distortions introduced over the mobile link are insignificant and are eliminated with the appropriate channel coding methodologies. No effort is made to simulate transmission of these image types over a mobile communication channel.

1.8 Chapter Summary

This chapter has presented a concise introduction to the research problem and an outline of this thesis that provides an overview of the key chapters and agenda that is addressed. The key challenges faced in wireless communication and telemedicine are brought to the spotlight. Focus has been placed on the most significant challenges of the research problem focusing on lossy compression. The next chapter presents a extensive review of the literature relevant to this thesis. This is initiated with some literature pertaining to the broad commercial area of wireless telemedicine and includes the key topics that are crucial to the research area.

Chapter 2

Literature Review

A Number of technologies have been examined for their application in this thesis. A comprehensive review has been undertaken covering recent literature from the broad area of wireless telemedicine to the specific theorems describing image content authentication. Wireless telemedicine is presented in Section 2.1 and a number of telemedicine projects are reviewed in Sections 2.1.1 to 2.1.4 that discuss commercial applications of this technology. These are grouped according to their communication infrastructure and include satellite, Global System for Mobile (GSM) communications and Third Generation (3G) communications as well as analog methods including VHF and RF radio. The immediate need for quality assurance and standards is presented in Section 2.2 and the application of image compression is covered in Section 2.3. Approaches to minimise degradation in crucial diagnostic regions are then explored. The investigation of a JPEG compression threshold is discussed in Section 2.4. The importance of quality assessment for these image types is clarified in Section 2.5. This paves a path for the promising technology of authentication watermarking and its application for verifying the integrity of wireless radiological images in Section 2.6.

2.1 Overview of the Research Area

Most telemedicine is currently practiced in industrialised countries and can be used to improve equity of access to health care, quality of care as well as providing cost-effective and efficient delivery (Craig and Patterson 2005). This practice is most challenging when used in a wireless environment. A plethora of exciting developments in wireless telemedicine have emerged recently. The majority of these are experimental and designed to test the application and effectiveness of real-time telemedicine for use in primary health care. A particular interest is shown in emergency and diagnostic telemedicine imaging applications. Many of these projects demonstrate that wireless telemedicine is a cost-effective solution to providing specialist treatment to remote locations that would otherwise not receive help. Substantial costs are saved by eliminating transport time and unnecessary admissions. These improve follow-up visits through remote consultation, as well as improving the communication between specialists (Hersh *et al.* 2002) (Hjelm 2005).

Wireless telemedicine is most cost-effective when existing communication networks and infrastructure are used (Heslop *et al.* 2003). Financial benefits are maximised when consumer, rather than specialist hardware is used to display transmitted data including portable computers (Reponen *et al.* 1998), mobile handsets (Reponen *et al.* 2000b), Personal Digital Assistants (PDA's) (Reponen *et al.* 2000a), (Eastes 2001) and Webpads (Pagani *et al.* 2003). Constraints of the systems have been highlighted with improvements suggested.

2.1.1 Projects Using Satellite Networks

Satellite communication is one of the the most favorable wireless technologies, particularly because of its extensive coverage and large bandwidth (Lamminen 1999). One of the most interesting developments using this technology for mobile telemedicine was for the NASA space program where routine medical operation was conducted. This program consisted of the patient (astronaut), the flight surgeon, data acquisition and handling hardware, software and the telecommunications connection. A Telemedicine Instrumentation Pack (TIP) was designed to collect medical audio and

video information from the patient in space. Data capabilities included blood pressure and oxygenation monitoring, heart rate and electroencephalogram (ECG) waveforms. Video capabilities included general macro-imaging and close ups of eyes, skin, ears, nose and throat. Data collected with the TIP was sent back to earth by a satellite link (Tachakra *et al.* 2003).

In the Yonsei University of South Korea, a web-based Picture Archiving and Communication System (PACS) was established using satellite communication. This system provided the capability for doctors to study medical images from remote servers with a common browser without specialised software. This provided an opportunity for remote hospitals to acquire images using standard web browsers that did not have a land line connection.

This system infrastructure included client and server sections connected by a satellite link depicted in Figure 2.1. A telemedicine project called Multimed was developed in

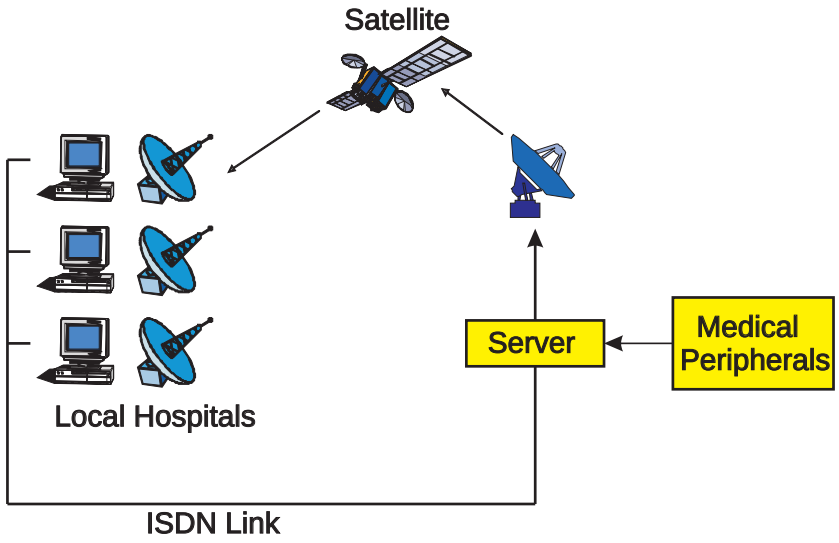

Figure 2.1. An overview of the web-based medical image viewer. This system was developed in the Yonsei University of South Korea to allow specialists in remote hospitals to obtain medical images using standard web browsers.

the Bristol Medical Simulation Centre, Guildford in the United Kingdom (Tooley *et al.* 1999). Extended access was provided to specialists that allowed them to be involved in simulated medical scenarios without the need for patients. This was designed to extend communication in rural areas and metropolitan hospitals. The communications

infrastructure was built around DirecPC, developed in Europe by HOT Telecommunications Ltd. Direct download of information was possible over a high bandwidth satellite link. Services provided included a 400 Kbs internet connection. Multimed utilised a combination of these services, without involving the end user in the complexities of accessing them. Further facilities at the centre included audiovisual equipment for the provision of live simulations that could be replayed and analysed. Figure 2.2 illustrates the communications infrastructure. Realtime ultrasound screening using a

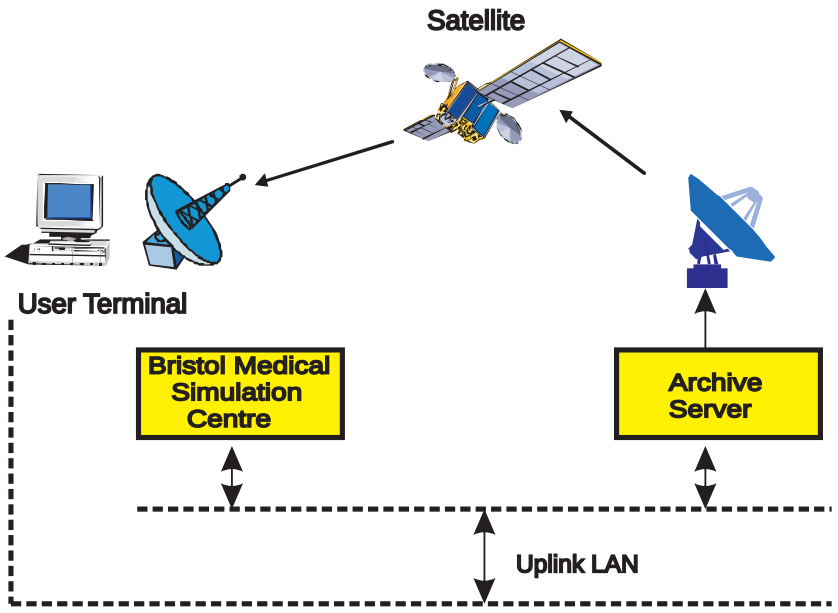

Figure 2.2. Overview of the communications infrastructure. An asymmetric satellite data service in the Multimed project allowed users to receive data at high bandwidth with a 60 cm satellite dish and a PC decoder card. Data requests were transmitted over a terrestrial link.

vehicle for medical examination was presented in Miyashita *et al.* (2003), which was equipped with an ultrasound scanner. Focus was to improve medical treatment in rural areas of Japan providing a satellite link. US Screening was performed on 205 people and comprised of 57 cardiac, 60 thyroid, 57 abdominal and 31 breast scans. A wireless bandwidth of 1.5 MBit/s was provided and allowed the resolution of the acquired images to be almost identical to the originals. Wireless telemedicine was proven to be cost-effective in providing health care in these rural areas.

A commercial broadband satellite based video communication system was available for commercial use by *Raytheon Pty Ltd* (2003). This was based on Mobile Very Small Aperture Terminal (MVSAT) technology. This was stated to be the first broadband

communications unit that could be deployed quickly and easily anywhere in the world using a fold-up patented 1.2 metre antenna and a telecom centre the size of a small suitcase. The MVSAT was designed to handle voice, video and data simultaneously with a transmission bandwidth of approximately 4 Mbps. The antenna could be assembled in less than 30 minutes and was designed for portability. This system had its main commercial focus on worldwide coverage for the broadcast and gathering of news, however other potential application areas could benefit including emergency telemedicine.

Figure 2.3. Commercial broadband communication system using mobile VSAT technology. Two parts of the portable system include the portable fold-up antenna (left) and the fixed system on the right. Diagnostic images and video used in telemedicine could be transmitted from the portable antenna to the hospital.

2.1.2 Telemedicine Developments Using GSM and 3G

A system called TeleCardio Mobile (Montoni *et al.* 2002) was designed in Brazil to allow Cardiologists at the Unit of Cardiology in the city to provide remote care for patients living in rural areas. This was proven to be cost effective and improved follow-up for discharged patients. The system took advantage of the larger bandwidth provided by Third Generation (3G) mobile phone telephony. Information was received through PDAs and mobile handsets connected to the internet by wireless modem cards. Remote consultation requests and results of medical procedures could be delivered to

physicians on mobile telephones.

In the Lion's Eye Institute in the University of Western Australia wireless telemedicine was used to transfer medical images using GSM communications. A set of medical images with a resolution of 267 × 234 pixels at a pixel depth of 24 Bpp (187K Byte) were compressed using JPEG to five different levels and transmitted to Perth from Indonesia. At a compression ratio of 1:5, the images were 36 kByte in size and took 29 seconds to transmit by mobile phone or 60 seconds by satellite phone. To measure the loss of quality, the Root Mean Square (RMS) error was calculated for each colour component for the transmitted and original images. Received images were considered to be of excellent quality and readily interpreted by ophthalmologists in terms of the likely presence of glaucoma (Yogesan *et al.* 2000). The most interesting feature of this work was the use of compression of imagery, which increased the speed of transmission. There was no stated acceptable level of compression or the point when the images lost their diagnostic value, which would have been an interesting feature in the project.

The European Momeda Project (Reponen *et al.* 2000b) used specialised software to provide for the transmission of computer tomography (CT), magnetic resonance (MR) images and patient information. This was transmitted by GSM to the mobile handset of a neurosurgeon from the hospital workstation for initial consultation and diagnosis. Re-use of GSM communication proved to be a cost-effective way of receiving the best possible expertise and appropriate course of treatment.

The Short Message Service (SMS) was tested for diabetes treatment in (Ferrer-Roca *et al.* 2004). A diabetes web management application used an SMS server to communicate with the patient's mobile phone via a GSM modem. Data such as blood glucose levels and body weight could be transmitted for effective management and treatment.

Much more recently, a generic, realtime, remote monitoring telemedicine system was evaluated through the Aalborg University of Denmark. This project used a combination of the general packet radio service for mobile phones and the Bluetooth protocol for the continuous monitoring of electrocardiograms (ECGs). This was found to be beneficial for clinical practice, as less than 10% of the ECGs were of unacceptable quality (Jasemian and Arendt-Nielsen 2005).

2.1.3 Ambulance Emergency Services Using GSM

The Hector research project was undertaken in Lancashire in the UK (Curry and Harrop 1998). Primary focus aimed at assessing and validating the best technology in the fields of telecommunications and information processing for real time systems. GSM communications provided to be cost-effective in transmitting video signals between a rapidly moving ambulance and a hospital. An additional television link was established between the ambulance and hospital. Two ambulances were in operation and were equipped with electrocardiogram (ECG) monitoring equipment.

Images were acquired with externally fixed cameras and one internal ambulance camera. A small helmet-mounted camera transmitted colour pictures to the ambulance using a microwave link. This was one interesting feature that provided improved acquisition of emergency imagery near the accident scene.

A mobile telemedicine system was established by Gagliano *et al.* (2000) for ambulance emergency services. This system comprised of a mobile unit for ambulance installation and a base station for hospital intranet connection. Real-time patient information transferred included data, audio and video. These were transmitted to a trauma centre at the hospital using digital cellular communication. The ambulance-based system included a video link provided with a portable camera in the ceiling of the ambulance situated above the patient's head to extract still images and video data. Images were compressed using extended JPEG and transmitted using up to four 'bonded' digital phone lines providing a bandwidth of about 20 Kbps. The wireless signals were transmitted to a server at the hospital where they could be viewed with a web browser. Video images were captured at 30 frames per second, but because of limited bandwidth, only one image was transmitted every 2.5 seconds with a resolution of 320 by 240 pixels with 24-bit colour depth. An option also allowed for emergency personnel to capture specific images and video clips at 5 frames per second (fps) if they were sent using a store-and-forward approach.

2.1.4 Rural Telemedicine System Using VHF and RF Radio

Voice and data communication facilities using a Very High Frequency (VHF) radio link was developed in 39 isolated rural health care facilities in the Amazon region of

Peru (Martinez *et al.* 2004). This study measured the reliability of telemedicine and the effect that it had on staff access to medical training and information. In 28% of the emergency cases, using emergency telemedicine saved the life of the patient. Communication technologies tailored to local needs were shown to solve many problems with the provision of voice and email communication.

A wearable monitoring device (Park and Kim 2003) made it possible to detect a electrocardiogram (ECG) output from a patient. This was aimed at determining the onset of emergency conditions based on communication of changes in heart or respiration rate. Radio Frequency (RF) transmission was used to communicate this information to specialists for real time medical treatment. This technology was chosen because of its low cost and simplicity.

2.2 Standards in Teleradiology

The biggest challenge facing telemedicine is the lack of standards to ensure an acceptable standard of care (Silverman 2003), (Gemmill 2005). There are three types of standards which are relevant to telemedicine. These include clinical, operational and technical guidelines. Standards most relevant to telemedicine include those published by the International Telecommunication Union (ITU) and the *Digital Imaging and Communication in Medicine (DICOM)* (2005) standard. Setting quality standards in telemedicine highlights critical factors that need to be considered for design and can improve education (Shershneva and Olson 2005). This can be regarded as a sign of maturity as telemedicine operations become more established (Loane and Wootton 2002).

Teleradiology is one of the oldest applications of telemedicine, which involves the wireless transmission of radiographic images. Standards relevant to the best practice of this area are published by the *American College of Radiology* (2005). These include information on technical standards as well as practice guidelines, which require periodic revision with clinical, scientific and technological advances. The structure of these guidelines is dynamic and it can be challenging to standardise all of the processes involved, especially for digital imaging (Yagi and Gilbertson 2005).

The most relevant standards applicable to this thesis include those pertaining to the equipment specifications. These state that all new equipment should comply with the

DICOM standard for digital image acquisition. The DICOM standard is internationally recognised for medical image communication. It was initially developed to allow for the effective transmission and storage of X-ray images, but could be extended to a wide variety of other image modality types. The DICOM standard specifies guidelines for image acquisition and display as well as transmission for diagnosis. Information relevant to file compression ratios, file transmission and display requirements, data storage and security are also included as part of the standard. Standardisation provides a high level of interoperability with other medical imaging equipment including X-ray, CT, MR, Nuclear Medicine, Ultrasound, Video Capture images and Digital Cardiology images (Loane and Wootton 2002). The DICOM subcommittee, working group IV is responsible for compression technology evaluation and specification definition for DICOM, which is of most interest to this work. Continual changes and additions to these specifications are frequent. Support has been included for JPEG lossless and lossy compression standards. These are specified as transfer syntaxes as the types of compression and storage that may be used and includes support for baseline JPEG compression standard, as well as JPEG-2000 compression as one of the most recent additions. The inclusion of lossy compression standards in the DICOM communication standard does not imply they are sanctioned for clinical use, only that the technology is provided for use by the end user or design engineer (Clunie 2000). The provision of a standard or metric that could guarantee that JPEG images were acceptable for diagnosis would make them particularly applicable to wireless telemedicine.

2.3 Medical Image Compression

Compressing medical images offers a method of reducing the cost of storage and increasing the speed of transmission. This is especially favorable if the end application is Teleradiology and transmission to a distant specialist must be as rapid as possible. Widespread consumer-level wireless display devices, such as PDAs require image compression for complete display of DICOM images (Nakata *et al.* 2005). This is essential when there is limited bandwidth.

Three types of compression are available. These include lossless, near-lossless and lossy compression. Lossless compression formats are widely accepted because no image information is discarded and data is interchangeable from one format to another.

Lossless compression techniques allow exact reconstruction of the original imagery and include schemes such as Bitmap (Bmp) and Tiff. Consistent visual appearance and diagnostic quality is guaranteed, at the expense of low compression levels. This is shown to be counter cost-effective for prompt wireless transmission.

Near-lossless compression techniques are based on the principle that a mathematical loss can exist before observable image degradation is apparent with the application of compression. This amount of lossy compression is also termed visually lossless (Daly 1990), as the compression and reconstructed image on subjective interpretation appear indistinguishable from each other.

Lossy image compression techniques are mathematically irreversible and aim to achieve much higher compression ratios by allowing some acceptable degradation of the image. According to Slone *et al.* (2003), an acceptable degree of lossy compression is dependent on many different parameters including the image modality, spatial resolution and type of digital image processing that is used. The degree of acceptable compression is also dependent on the Human Visual System (HVS) as well as reading tasks, conditions and experience.

Using industry wide standards, such as JPEG can be expected to reduce the cost and risk of compression and will not compromise interoperability with other equipment (Clunie 2000).

2.3.1 JPEG Standards

The most popular still image compression techniques are the international standards provided by the Joint Picture Experts Group (JPEG) (Wallace 1991). These are the most widespread and implemented compression standards and provide three possible compression types, including:

- Baseline Lossy JPEG.
- Extended Lossy Baseline JPEG.
- Lossless JPEG.
- JPEG-2000.

Baseline Lossy JPEG is one of the simplest and widespread image compression standards supporting a colour depth of 8 Bpp, found in most digital imaging hardware used in communications. Extended lossy JPEG can encode source images to a resolution of 12 Bpp. This has useful applications in specialist medical imaging applications when greater colour depth is demanded. It also supports progressive encoding, variable quantisation as well as arithmetic encoding. Much work has taken place to add lossy and lossless JPEG as a transfer syntaxes to DICOM (Olges *et al.* 2000).

Lossless JPEG is based on Differential Pulse Code Modulation (DPCM). This involves forming a prediction value for each pixel value based on the properties of surrounding pixels. The difference between pixel values is encoded and support is provided for source images with resolutions up to 16 Bpp. An improved standard for lossless compression was introduced by JPEG in 1997 called JPEG-LS (*JPEG-LS - Lossless and near-lossless compression of continuous-tone still images: ITU-T Rec. T.87, ISO/IEC 14495-1: Baseline* 1999) offering improved compression over earlier lossless JPEG. A near-lossless feature provided by JPEG-LS includes a specification of error tolerance that provides a trade-off between compression and image quality.

The most recent addition of JPEG-2000 (*JPEG 2000 Image Coding System: ITU-T Rec. T.800 08/2002, ISO/IEC 15444-1: Core Coding System* 2004), as a transfer syntax for use in medical imagery was the result of the combined effort of a large number of institutions, where visual quality of compressed images was assessed to provide clinical data to DICOM. Moreover, JPEG-2000 was compared to baseline JPEG in (Foos *et al.* 2000) and offered improved picture quality performance at a comparable bit rate. Other capabilities that are included as part of JPEG-2000 include support for ROI compression and handling of images with an extreme precision to 16 Bpp.

2.3.2 Region-Based JPEG Medical Image Compression

Region of Interest (ROI) based compression schemes identify regions of images that are determined by some criterion to be of highest clinical importance. The ROI is typically compressed using a lossless or near-lossless technique while the Region of Backgrounds (ROB) can be selectively compressed with greater loss to that of the ROI. This type of compression approach is relevant to the problem for the following key reasons:

- significant DCT or wavelet-based distortions may be applied to diagnostic medical images, provided that is does not occur in critical regions,
- this region is where all of the diagnostic information is stored. The rest of the image is useful in a contextual sense for analysis of the ROI in the image. Thus the image can be segmented into a region of high importance (ROI) and a region of relatively low importance (ROB).

Research pertaining to the segmentation and compression of medical imagery has shown that that diagnostically important regions must be preserved at high quality, while the rest of the image is important in a contextual sense and assists the viewer to observe the position of the ROI within the original image. This has been shown to improve compression efficiency (Arunoday *et al.* 2004), (Jia *et al.* 2004). An extreme example is provided in Figure 2.4, which shows that diagnostic content is still valid, even though the ROB has been quite distorted as a result of JPEG quantisation. Much more recent work was investigated by Engan *et al.* (2005), who implemented two different wavelet-based ROI coding methods. These included a Set Partitioning in Hierarchical Trees (SPIHT) scheme for the compression of mammograms as well as the JPEG-2000 standard. It was shown that mammograms could be compressed to less than 0.5 Bpp without any visual degradation or influence on the performance of a CAD system used to assist the radiologist in studying the mammograms.

Figure 2.4. Relative importance of diagnostic feature content. An infant's fracture is shown with the ROI near-losslessly compressed to a level of 2 Bpp, with the ROB coarsely quantised to a high level of 0.1 Bpp. The majority of the image data is used to encode the ROI if a variable quantisation table compression approach is adopted (Lin and Chang 1997). This would provide for very high compression levels, but assumes that the ROI is relatively small in comparison to the rest of the image. This example demonstrates that diagnostic feature information can still be retained as long as significant distortions do not occur in crucial regions.

DCT-Based JPEG ROI Methods

An investigation into region-based JPEG compression techniques demonstrated that many proprietary schemes have been proposed that are based around the standard or designed to enhance existing compression methods. Many of these schemes were also developed and presented before JPEG emerged as a standard and were referred to as hybrid coding or as Variable Scalar Quantisation (VSQ) compression schemes. These methods employed different quantisation tables scaled to varying levels and differed in the way the ROI was segmented from the ROB and the encoding method used.

Feature works include Wong *et al.* (1995), who investigated hybrid coding, based on discerning importance from background information for digital mammograms. This also involved developing and optimising JPEG compression to encode the ROI near-losslessly. A hybrid model of lossless ROI compression was later developed for use on CT and MRI imagery. This was shown to outperform the compression level of conventional JPEG and was extended for usage in video (Gokturk *et al.* 2001).

JPEG-2000 Based ROI Methods

Lossy compression based on the ROI capabilities of JPEG-2000 has been a popular research area. The lossy ROI capabilities of JPEG-2000 were analysed for compression efficiency in Penedo *et al.* (2003), where small improvements were found when ROI encoding was used. Further investigations by Agrafiotis *et al.* (2003) have involved hybrid coding 3-D medical image sets using the SPIHT coefficient encoding algorithm. Current work in this area has not been as popular as a result of the addition of ROI capabilities of this standard as a transfer syntax to DICOM.

Using JPEG-2000 ROI compression provides a non-uniform distribution of the available ‘bit budget’, which is achieved by varying the scaling of the background wavelet coefficients. The concept is very similar to VSQ adopted for baseline JPEG. The combination of lossy compression and the ROI capabilities of JPEG-2000 have been evaluated by Anastassopoulos and Skodras (2002) for their diagnostic usefulness in compressing medical images. Two different methods were used for ROI coding, including

MaxShift[1] ROI encoding, from Part 1 of the standard, as well as a scaling-based method (included in Part 2). ROI compression was applied to 42 kidney nephrostograms obtained from X-ray films and scanned at multiple resolutions in order to achieve optimal image quality. The ROI used was a *Lower Minor Calyx Fornix Rupture* in a patient's kidney.

These images were digitised losslessly at a greyscale constant pixel depth of 8 Bpp and with spatial resolution of 2240×2180 pixels.

Subjective image quality assessment was determined by the Mean Opinion Score (MOS) by a visual comparison of the ROI in the original and compressed imagery. These images were presented to six urologists for an evaluation of diagnostic value. The Peak Signal to Noise Ration (PSNR) was used for an objective comparison of the images. MaxShift ROI coding was found to be most effective, as it placed its entire 'bit budget' into the ROI before it started encoding the background information. Typical results of the bit rates achieved before the images lost their diagnostic value were around 0.03 Bpp, which could not be achieved with baseline JPEG.

Unfortunately 'off the shelf' type of hardware that could be used for the rapid wireless acquisition and transmission using this standard is not yet currently feasible. Moreover, JPEG-2000 hardware architectures are still are in their infancy stages. Many new ideas are still being proposed for the most cost-effective and efficient design of coders and decoders implemented in hardware. For example the development of 'on chip' wavelet transform with an embedded block coder incorporating an arithmetic encoder for the bitstream compression was presented in Freeman and Knowles (2004). A JPEG-2000 hardware and software co-processing architecture was also recently designed (Zhang and Fritts 2004) to complement existing software packages for more efficient and rapid coding based on the JPEG-2000 encoding processes.

[1]The MaxShift ROI encoding method was developed to minimise computational complexity and memory requirements of encoding a ROI. This is performed by scanning the quantised wavelet coefficients and choosing a scaling value so that the minimum coefficient magnitude in the ROI is larger than the maximum coefficient magnitude in the ROB.

2.4 Visually Lossless JPEG Compression

As outlined in Section 2.3.1, there are different types of JPEG compression that may be used. Lossy baseline JPEG is the most practical and cost-effective compression standard to use because of its ease of implementation, widespread use and high level of interoperability with most imaging equipment. An investigation into the degree of acceptable JPEG compression is highly relevant to wireless telemedicine as it allows the bit rate to be lowered as much as possible without affecting the diagnostic image quality. This decreases the image size resulting in more rapid transmission.

According to a work by Slone *et al.* (2003), the acceptable degree of lossy JPEG compression is dependent on several parameters. These include:

- **Image Source and Processing:** This may include image processing, frequency enhancement, tonal characteristics as well as display corrections. Aspects related to the source image include colour depth, modality, spatial resolution and type of digitisation prior to compression.
- **Reading Tasks and the HVS:** Including human-dependent parameters, such as experience, type of feature extraction as well as reading conditions.

Acceptable levels of lossy JPEG compression are based on the concept that a mathematical loss can exist before observable image degradation occurs. This is commonly referred to as *visually lossless* compression as the compressed and reconstructed images appear to be identical. A visually lossless threshold for the wavelet-based compression of a set of digitised mammograms is presented by Kocsis *et al.* (2003b) and for a DCT-based JPEG algorithm in (Kocsis *et al.* 2003a). Measurements were carried out using ROI operations on test image sets that had characteristics similar to radiographic images. Degradation of the test patterns was observed with the application of lossy JPEG compression to investigate a threshold. This approach was very similar to a method that was investigated earlier in the research (Osborne *et al.* 2004c). Alpha-numeric text was used as a test pattern in the investigation of a similar threshold. Letters were used in varying sizes that represented different types of detail that could be extracted by the reader or an automated Object Character Recognition (OCR) algorithm. Letters were used to represent a type of detail that had to be extracted similar to the way fractures and tumors could be extracted from a medical image. Hence if the letters could not

be recognised after using excessive compression, medical images containing a similar level of detail could not be extracted either. The loss of letters was intended to correlate with the score obtained from the OCR algorithm.

Parts of other types of test images were degraded and the number of detected objects as a function of size was used by Efstathopoulos *et al.* (2001). The amount of noise introduced to the test image was used to evaluate the optimum visually lossless threshold. Results suggested that a compression level of 1.0 Bpp could be used for lossy baseline JPEG compressed medical images. At this level, low contrast discrimination was not affected, image noise level was reduced and input and output grey level differences were also very small.

The loss of fidelity in JPEG compressed medical images and the investigation of a visually lossless threshold was evaluated by Slone *et al.* (2003). Subjective testing from specialists was used to evaluate the effectiveness of compressed digital chest radiographs compared to uncompressed images. A set of 144 posteroanterior radiographs of the shoulder were used, which were digitised at 16 Bpp using compression ratios of 10:1 20:1 and 50:1. This type of image was favored, as radiologists are especially sensitive to distortions in image areas of the shoulder. These results could be applied more broadly to images where sensitivity was less significant. The posteroanterior radiographs were compressed using extended lossy JPEG at a pixel depth of 12 Bpp. Excluding the initial data input and output, all calculations were completed in floating point form. Images were read on 14×17 inch transilluminated film as well as on 21-inch CRT displays with resolution of 2000×2500 pixels. The CRT display was designed to match as close as possible the luminance in film readings. Images were classified according to normal, abnormal and incidental and were randomised into one of four compression categories. These including the unaltered image and applied compression levels of 10:1, 20:1 and 50:1. Viewers were asked to limit the reading distance to typical clinical distances so that the conditions were as similar as possible to hospital environments. The percentage of images detected as indistinguishable from the unaltered image were determined from each compression level. When the percentage was equivalent to that for uncompressed images, images were considered indistinguishable from the originals. This criterion led to a visually lossless threshold. Readers differed in their ability to detect compressed and reconstructed images and as an entire group were unable to detect a compression ratio of 10:1. A compression level of 20:1 could sometimes be

detected, while 50:1 was usually detected. These results were consistent with both film and CRT displays.

An additional work in (Kocsis *et al.* 2003a) suggested that 1.0 Bpp is an ideal threshold for diagnostic interpretation. One of the most recent publications (Przelaskowski 2004) involved comparing the effectiveness of lossless compression with lossy wavelet-based coding. Irreversible compression of mammograms up to 1.0 Bpp was shown to preserve diagnostic accuracy according to opinions of the radiologists who subjectively evaluated the quality of the reconstructed mammograms. Much earlier studies have also confirmed that similar compression threshold levels are acceptable for use in JPEG-based diagnostic imagery. Some of these include (Okkalides 1998), (Kajiwara 1992), (Cosman *et al.* 1994), (Good *et al.* 1994) and (Cook *et al.* 1995). To conclude this section, recent works by (Efstathopoulos *et al.* 2001), (Kocsis *et al.* 2003a) and (Slone *et al.* 2003) strongly support that lossy JPEG compression can be used for the visually lossless compression of medical imagery safely to bit rates 1.0 Bpp.

2.5 Image Quality Assessment for Teleradiology

Quality assurance metrics are essential to evaluate the performance of lossy schemes or determine ideal thresholds for diagnostic use. However there are two known approaches to image quality assessment, which include:

- **Objective methods:** That are rapid and cost-effective solutions. These are based on known algorithms and involve testing the image without the need of a specialist
- **Subjective methods:** That require the educated impression of a well-trained specialist / s to give the image a score which is based on subjective interpretation.

Objective image quality metrics can be grouped according to the availability of an original image with a degraded image. The majority of existing image quality metrics are known as full reference, requiring an original image. If there is no reference image information available, the type of image quality measure is called blind or no-reference assessment. In a third type of metric, reference image information is only partially available as side information. this can be used to evaluate the quality of the degraded image and is referred to as reduced-reference image quality assessment. The most

commonly used full-reference objective quantitative metrics are based on the analysis of the pixels of the spatial image, such as Normalised Mean Square Error (NMSE), sum of absolute differences and Peak Signal-to-Noise Ratio (PSNR). These are the most simplest and widely used metrics as they are easy to calculate and are mathematically convenient. This type of measure does not always correlate well with the subjective opinions of medical specialists, but can be used for assessing compression algorithms.

Many new techniques are designed to assess the quality of images by comparing a degraded image with the original. For example Weken *et al.* (2004) compared images by using fuzzy sets and Wang *et al.* (2004) presented a method to determine the image quality of JPEG and JPEG2000 compressed images by quantifying the degradation of structural information. The requirement of full-reference image quality assessment limited the end application of this type of performance measure. Teleradiology cannot benefit from full-reference assessment as the original image is not present for a comparison. Identifying image quality measures without prior knowledge of the types of image distortion available is a challenging research problem.

Newer types of no-reference image quality assessment have also been a popular research area. image quality metrics based on the analysis of variance in the image were investigated in Avcibas *et al.* (2003). Quality measures have also been used to assess image quality by attempting to determine the extent of JPEG compression artifacts using arbitrary algorithms (Li 2002), (Luo *et al.* 2002). Perceived image quality was evaluated with the introduction of frequency distortion and the injection of noise by Zampolo and Seara (2003). Methods have also been investigated to obtain no-reference image quality metrics by learning through image examples without knowledge of the type of image distortion (Tong *et al.* 2005). Other methods have investigated the extent of pixel crosstalk in images (Estribeau and Magnan 2005). These techniques have not been thoroughly compared to observer performance targeting medical end applications.

A no-reference quality measurement algorithms was developed by Wang *et al.* (2002) for JPEG compressed images. Another method involved evaluating image quality using a film characteristic curve as a theoretical model. This was used to determine the medical image quality where contrast levels had been manipulated. Seven radiologists evaluated the distorted images and their interpretations were found to correlate with the film characteristic curve. This metric was aimed at determining the extent

of contrast in the image rather than the level of compression (Tingberg *et al.* 2004). Other approaches have targeted compressed image quality based on medical image parameters. The degradation of image quality was assessed by selecting some diagnostically important parameters in Efstathopoulos *et al.* (2001). These included image uniformity, input−output response, image noise level, geometric distortions as well as spatial resolution. A test film shown in Figure 2.5 was used to measure these variables. A reduced-reference metric based on the Human Visual System (HVS) was de-

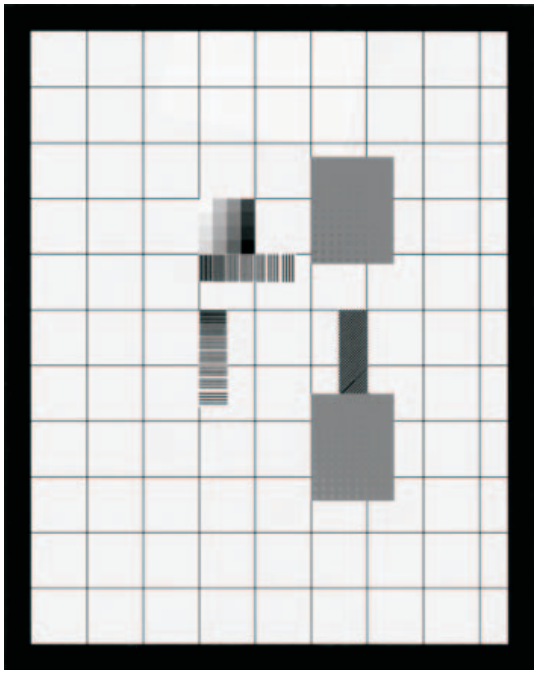

Figure 2.5. Test film used to measure image parameters. To assess the relationship between the density of the test film and pixel values of the digitised image, step patterns were used and consisted of 16 small squares of different optical densities. This was used to assess image parameters after image compression was applied. After (Efstathopoulos *et al.* 2001).

veloped by Weken *et al.* (2004). Structural information was extracted from an image and compared to local patterns of pixel intensities. This made it possible to quantify degradation with applied compression as loss if image quality correlated to loss of structural spatial information. This measure was found to match with subjective image ratings for images that had been compressed with both JPEG and JPEG-2000 compression schemes at varying bit rates. Although these methods could estimate image quality, a guarantee of image integrity was not possible.

Subjective or specialist human interpretation is also commonly used to interpret image

quality. A clinically well established subjective method is Receiver Operating Characteristic (ROC) analysis. This is based on comparing a degraded image with the original. ROC measures typically include the image sample size, the number of observers, normal to abnormal image ratio, thresholds for use, type of image degradation, image modality as well as the controlled display conditions (Kocsis *et al.* 2003a). Subjective methods of image quality assessment can be limiting as the opinion of radiologists is rarely exhaustively tested. Findings from studies in one area may also not be applicable to another. In practice these methods are not cost-effective as they are usually too inconvenient, time consuming and expensive.

2.6 Medical Content Authentication

There are two advantages in using watermarking for content authentication. The requirement of storing separate data, such as appended signatures is eliminated. This provides greater compatibility with existing file systems that cannot discern an authenticated work from an un-watermarked image. Hence greater interoperability with standard imaging systems is provided. The watermark also experiences the same manipulations as the cover work. If the image is corrupted in an undesirable way, the watermark will also be lost. An investigation targeting watermarking of medical imagery has revealed a plethora of publications incorporating many different modality types (Anand and Niranjan 1998), (Coatrieux *et al.* 2000), (Kong and Feng 2001), (K. Engan and Josefsen 2003), (Awrangjeb and Kankanhalli 2005) and (Woo *et al.* 2005). Unfortunately these methods were not designed for robustness to lossy JPEG compression. These approaches did not address the need of authenticating critically important image regions either. Techniques that have been proposed to authenticate such regions include works by (Wakatani 2002) and (Lie *et al.* 2003). Both have proposed methods that could be used to authenticate a ROI and were based on survival to DWT-based schemes. These had a similar focus in avoiding the distortion of the image data in the ROI as presented in this thesis. Current investigations by Planitz and Maeder (2005) have shown that medical image watermarking remains an open area for research.

2.6.1 ROI Authentication and Watermarking

Embedded watermarking around or in critically important image regions is highly relevant to the problem of authenticating diagnostic feature content, where deterioration

within these regions cannot be tolerated. Many of the works that have been based on watermarking segmented image regions have been based in the DWT domain. This has most likely been a result of research interest in wavelet-based JPEG-2000 providing the application of ROI coding.

One of the first ROI watermark approaches was developed by Su *et al.* (1999). Authentication information was placed into the ROI rather than embedding external to it. Information was embedded in individual subbands of the DWT domain. The EBCOT approach was used to encode the coefficients. The watermark was designed to be robust to distortions including lossy compression and low-pass filtering. The watermarked image was shown to maintain acceptable perceptual quality, but did not appear to survive significant levels of JPEG-2000 compression. Investigations by Wang *et al.* (1999) also suggested that using the combined spatial frequency characteristics of the wavelet transform provided a robust watermark that could resist undesirable attacks, when a ROI watermark scheme was used. Another method was investigated by Chen *et al.* (2001), where each ROI could be specified as an individual shape and could have priority over other regions. Decisions could be made to sequence the order of processing for the coefficients at the encoder and decoder. Watermark information based on textual information was embedded into the ROI and was placed into zero bits resulting from the left-shift process of SPIHT.

A particularly interesting method was investigated by Wakatani (2002), who proposed to embed multiple signature information around a known ROI, which is outlined in Section 2.6.1. Another especially interesting approach was proposed by Lie *et al.* (2003), shown in Section 2.6.1. The main end application of these works was copyright protection and ensuring that attacks on the watermark were prevented. To contrast the end application of this thesis involves providing image content integrity verification.

More recent ROI watermark approaches have been based on survival of JPEG-2000 compression. These have included a work published by Chen *et al.* (2004), who proposed a watermarking scheme to embed and extract signature information based on the JPEG-2000 codec process. This algorithm applied the *torus automorphism technique* to segment a signature which was embedded into the bitstream after the JPEG-2000 quantisation step. An interesting feature of this work was to minimise the distortions introduced by embedding. This method was also shown to be robust to some

blurring. Future work involving ROI watermarking has been proposed in a paper by Lee *et al.* (2004), based on exploiting the properties of wavelet coefficient signs experimentally found to be invariant to lossy compression standards including JPEG and JPEG-2000. Other methods have involved robustly coding the ROI for images, such as Sanchez *et al.* (2004), who optimally assigned channel protection to the ROI coded data according to the importance of individual packets in the bit stream. This was simulated over a Rayleigh fading channel, but could not guarantee ROI integrity.

Watermarking ROI Medical Images Using a Compressed Signature Image

A region-based watermark approach was proposed by Wakatani (2002), basing signature information on a progressively compressed version of a patient image. The most significant information was embedded into the region closest to a ROI in a spiral way, which is illustrated in Figure 2.6. The signature image could be detected with moder-

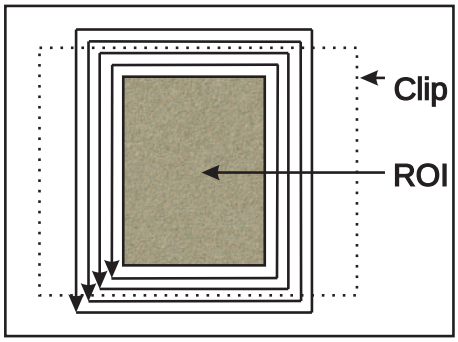

Figure 2.6. Bitstream embedded around a ROI. The ROI is the most crucial part of a medical image, which must be retained if the image is clipped. The signature image is compressed using Embedded Zerotree Wavelet (EZW) coding so that an entire image can be reproduced with variable quality, correlated to the length of the bitstream extracted.

ate quality from a clipped version of the image that included the ROI. This system was intended for application over web-based medical image database systems rather than wireless end applications. Focus was placed to ensure copyright, intellectual property protection and provide medical image integrity in long term storage. Watermarking took place in the DWT domain and involved decomposing the image into sub-bands, shown in Figure 2.7. The bitstream was encoded using the EZW process. As JPEG-2000 is based on the EBCOT wavelet coefficient encoding method, one of the failures of this approach was its non-compliance with compression standards. The proposed system was designed to gradually deteriorate the watermark during EZW wavelet compression, which is accomplished by losslessly preserving all of the bit-planes and hence all

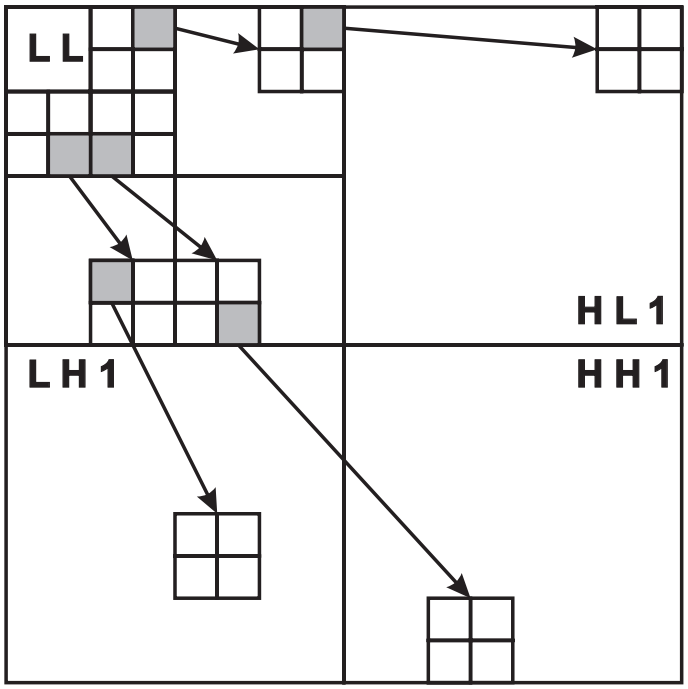

Figure 2.7. Sub-band decomposition. Sub-band decomposition of an image that has undergone a wavelet transformation. This compression algorithm exploits the correlation between lower bit-planes, the highest being 'LL' and the lower sub-bands, indicated in the direction of the arrows.

of the wavelet coefficients. This is unlike the work presented in this thesis, which uses acceptable levels of lossy JPEG compression to discard DCT coefficients, while at the same time maintaining diagnostic integrity. Multiple embedding around the ROI is useful when the medical image is clipped and one of the watermarks is lost.

Akiyoshi Wakatani (Wakatani 2002) proposed to divide the area around the ROI into d parts and embed the signature into each of the divided parts. If a clipped area included at least $1/d$ of the contour of the ROI, the signature could be detected. Figure 2.8 shows an example of four divided parts of a ROI and a clipped area. Although this only contains part of the watermark, the signature can be extracted from the ROB below the ROI and to the left of this region.

Dual Watermarking Proposed Using Wavelets

A scheme was proposed by Lie *et al.* (2003) to robustly watermark lossy JPEG-2000 ROI compressed images. A dual watermarking scheme was proposed in the DWT domain with one watermark being naturally fragile and the other robust. These schemes were

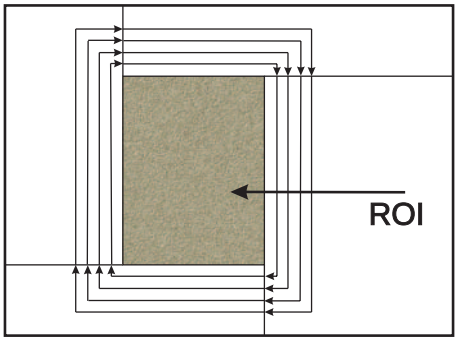

Figure 2.8. Dividing the contour around the ROI. Four regions are provided to embed a compressed signature image as proposed by Wakatani (2002).

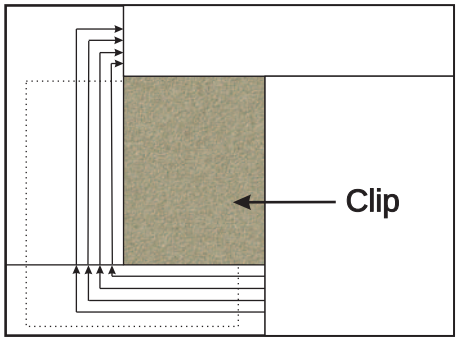

Figure 2.9. Clipped area with the ROI present. Clipping has not occurred in the ROI and another watermark can be used for authentication.

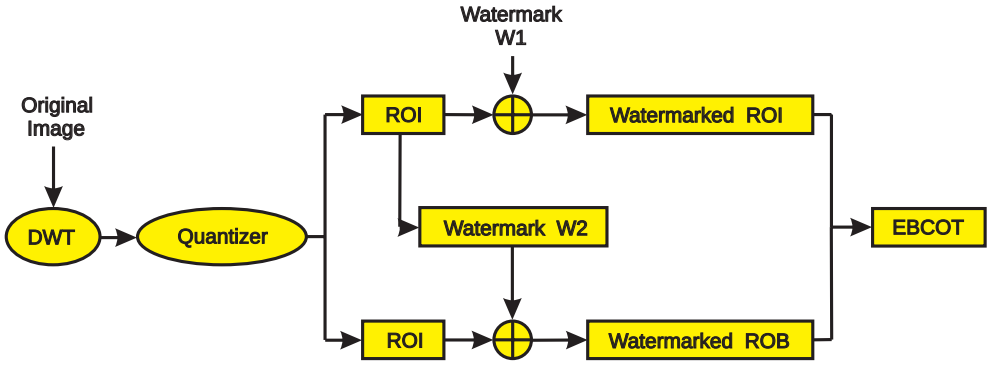

Figure 2.10. Block diagram of proposed dual watermarking scheme. ROI features are used for the watermark to be robustly embedded into the ROB as proposed by Lie *et al.* (2003). Unlike the method in this thesis, only one robust watermark is embedded in this region. This watermark is designed to withstand moderate levels of lossy JPEG-2000 compression. For this system coefficients are encoded using the EBCOT process.

designed to be embedded separately into the ROI and ROB. Embedding process took place at differing resolution layers to detect malicious changes and provide flexibility to determine the degree of alteration to discriminate intended attacks from unintended ones. To accurately detect which areas had been altered, the first watermark, W_1 which is sensitive and fragile was embedded into the ROI. This watermark could not survive after any intended or unintended manipulations on the ROI of the targeted image. The second watermark, W_2 was composed of features of mid-frequency sub-bands and robustly watermarked into the ROB using similar principles to this thesis. This is because features from the ROI were used as part of the embedding payload, which is depicted in Figure 2.10. Features were extracted from the ROI and embedded into the ROB

for the robust watermark. Acceptable distortions to maintain watermark survival included moderate levels of low-pass filtering and JPEG-2000 compression. Survival was not anticipated as a result of illegitimate distortions including malicious attacks, geometric distortions and block replacement. The robust watermark was based on invariant inter-sub band properties of the ROI depending on the types of desirable external manipulations. Almost identical to the way in which our watermark is extracted from the ROI, signature features were based on absolute differences between corresponding coefficients in the $LH3$ and $HH3$ subbands from 8×8 blocks. Similarly, the watermark used in this thesis is based on the absolute differences between invariant features of corresponding coefficients in randomly selected micro block pairs from inside the ROI. To ensure some compatibility with lossless JPEG-2000, robust watermark embedding was performed on a block level. The watermark was embedded into coefficients of the HL3, LH3 and HH3 subbands in the ROB.

2.7 Semi-Fragile Watermarking Robust to JPEG

Watermarking that is robust to JPEG compression is a type of selective image authentication, which is also termed *semi-fragile* or *robust* authentication watermarking. The more general goal of these techniques is to ensure that the watermark survives manipulation up to a point where the value of the work is lost. There are a few types of acceptable distortions that may be applied in the JPEG compression process, which include:

- **Integer rounding and Decimation:** Which may vary depending on the JPEG compressor or the type implemented in hardware
- **Application Specific Transforms:** Such as DCT quantisation
- **Image Cropping:** A result of cutting out important image features for transmission if the image is of a prohibitively large resolution or size.

One well known publication by Lin and Chang (2001) was proposed and partially implemented by Cox *et al.* (2001). This method can be used to authenticate images by allowing lossy JPEG compression up to an acceptable level and can be designed to survive the distortions listed above. This method is based on the invariant properties between DCT coefficients when JPEG compression is applied.

2.7.1 Authentication System Proposed By Lin and Chang

The image authentication method proposed by Lin and Chang (2001) is shown in Figure 2.11. The theorems and equations that are presented in the following sections are the basis behind the authentication system that is presented in this thesis.

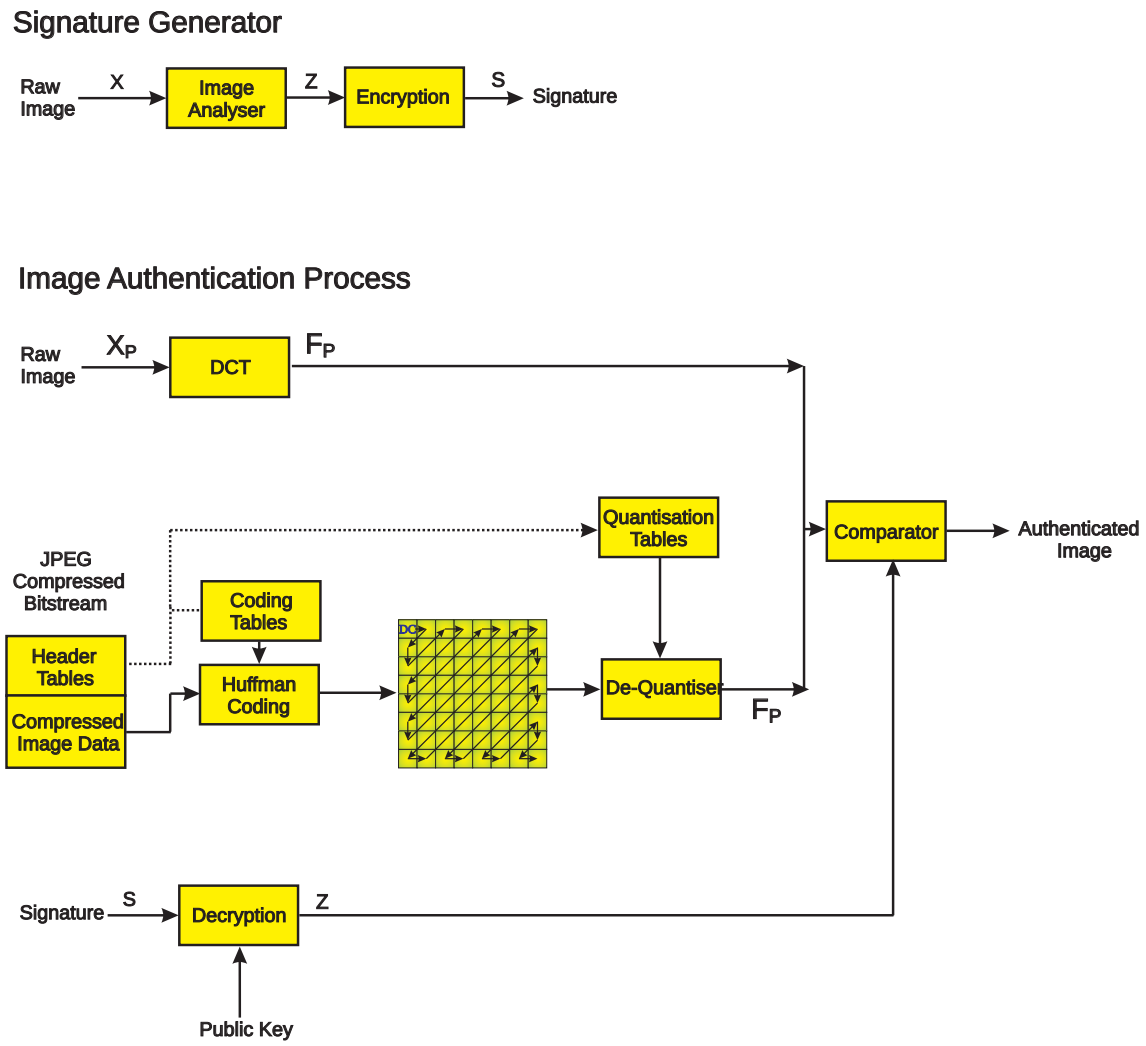

Figure 2.11. Overview of JPEG authentication system proposed by Lin and Chang. A raw image or JPEG file can be authenticated. The original image contains pixels values, X_P, which are transformed to DCT coefficient values, F_P. To generate a signature, the raw image is analysed to generate Z signature bits that are encrypted to create a signature, S. The signature is an encrypted signal based on features from the image. The way in which these features are obtained is presented in Chapter 4. In order to authenticate the image, the embedded watermark must be decrypted and compared to feature codes from the image. However in this thesis, feature codes are taken from the surrounding watermarks and compared to features taken from the ROI. If there is an acceptable match between the signals F_P and Z, the image is authenticated.

Theorems Used

Invariant features maintained through the compression process of JPEG make it possible to extract some quantitative and predictable properties. If robust feature codes are required, they must survive two steps including:

1. **Quantisation and rounding of the DCT coefficients**: A lossy operation which discards image information and changes the pixels values, but keeps essential visual characteristics.

2. **Huffman encoding**:A lossless method to encode the resulting coefficients to a minimal length sequence based on the frequency of each character in the sequence (Huffman 1952).

The following theorems taken from Lin and Chang (2001) provide a basis for the generation of these codes. Proofs of these theorems can be referred to in Appendix D. Please refer to Appendix C for an appreciation of the theorems and the transformations specific to JPEG.

Theorem 1 states that the sign of the DCT coefficient differences remains unchanged after quantisation. Hence it describes the invariant property of the sign of coefficients between two blocks, p and q, their difference being $\Delta F_{p,q}$.

The relationship between two DCT coefficients located at the same position in each micro block will remain unchanged after quantisation. According to Lin and Chang (2001), the only exception is if two points become "equal" as a result of integer rounding after quantisation. This theorem will hold true independently of the number of compression iterations or the quantisation table. Theorem 2 extends the first by showing that the values of coefficient differences remains unchanged.

Theorem 1: Consider F_p and F_q to be two DCT coefficient vectors taken from two 8×8 micro blocks of image X, and Q is the JPEG quantisation table used on the entire image.

$\forall i \in [1, ..., 64]$ and $p, q \in [1, ..., \rho]$, in which ρ is the total number of blocks, define $\Delta F_{p,q} \equiv F_p - F_q$ and $\Delta \tilde{F}_{p,q} \equiv \tilde{F}_p - F_q$ and the quantised approximation: $\tilde{F}_p(i) \equiv \text{ROUND}(\frac{F_p(i)}{Q(i)} \cdot Q(i))$, then the properties below must hold true:

1. If $\Delta F_{p,q}(i) > 0$, then $\Delta \tilde{F}_{p,q}(i) \geq 0$,

2. otherwise if $\Delta F_{p,q}(i) < 0$, then $\Delta \tilde{F}_{p,q}(i) \leq 0$,

3. otherwise $\Delta F_{p,q}(i) = 0$, then $\Delta \tilde{F}_{p,q}(i) = 0$.

Theorem 2: Assume a fixed threshold, k, where $k \in \Re$.
Define $\tilde{k}_i \equiv \text{ROUND}(\frac{k}{Q(i)})$, $\forall i$, then:

$$\text{if } \Delta F_{p,q}(i) > k,$$

$$\Delta \tilde{F}_{p,q}(i) \geq \begin{cases} \tilde{k}_i \cdot Q(i) & : \quad \frac{k}{Q(i)} \in Z \\ (\tilde{k}_i + 1) \cdot Q(i), & : \quad \text{elsewhere} \end{cases} \tag{2.1}$$

$$\text{otherwise if } \Delta F_{p,q}(i) < k,$$

$$\Delta \tilde{F}_{p,q}(i) \leq \begin{cases} \tilde{k}_i \cdot Q(i) & : \quad \frac{k}{Q(i)} \in Z \\ (\tilde{k}_i - 1) \cdot Q(i), & : \quad \text{elsewhere} \end{cases} \tag{2.2}$$

$$\text{otherwise if } \Delta F_{p,q}(i) = k,$$

$$\Delta \tilde{F}_{p,q}(i) = \begin{cases} \tilde{k}_i \cdot Q(i) & : \quad \frac{k}{Q(i)} \in Z \\ (\tilde{k}_i \text{ or } \tilde{k}_i \pm 1) \cdot Q(i), & : \quad \text{elsewhere.} \end{cases} \tag{2.3}$$

Hence, k is used as a threshold value to bound the difference of two DCT coefficients located at the same position in two micro blocks. It is possible to predict the difference relationships between coefficients after compression.

Both theorems allow feature codes to be extracted from an image, which are based on these invariant relationships. These codes can also be encrypted as a unique signature (Lin and Chang 2001). The image can be authenticated by comparing the DCT coefficient relationships with that in the signature. A similar principle has been adopted in this thesis.

System To Extract a Signature

The system flow diagram of the feature extraction process used by Lin and Chang is shown in Figure 2.12. There are 3 loops for the generation of a signature:

- Loop 1: N sets of feature codes are generated $Z_{n,p}$ for $n = 1{:}N$. Each of these has a different threshold k, as well as the number of DCT coefficients compared in each block pair b_n. In the implementation for this thesis $b_n = 8$, to allow for feature extraction from only the most significant DCT coefficients. This corresponds with extracting signature information from the first 8 coefficients of the JPEG zigzag scan and is discussed in detail in Chapter 4.
- Loop 2: Each of the block pairs, $p = p_1$ to $p_{\frac{\rho}{2}}$
- Loop 3: Iterate over each of the coefficients, b_n in the current micro block pair, which are indexed in the zigzag order.

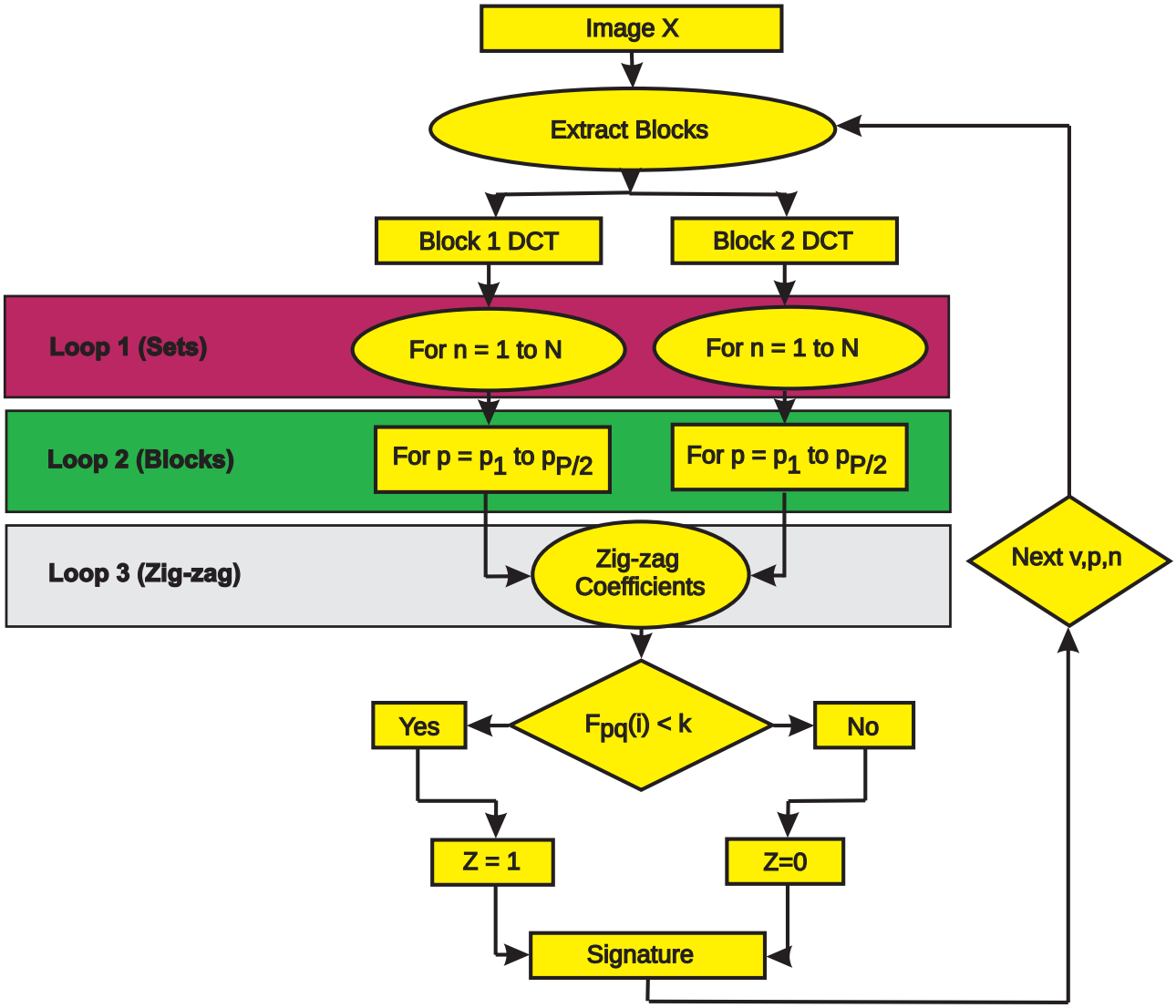

Figure 2.12. System to extract a signature. In loop 1, shaded in pink, N sets of feature codes are generated. In loop 2 the micro blocks are paired, this area is shaded green. The ROI watermark scheme provides a key to randomise this selection. The DCT coefficient difference between blocks p and q is determined. Loop 3, shaded in grey compares coefficients b_n in the current block pair. This approach is the same as the signature extraction process adopted in the research. An important difference is the extraction of a signature solely from the ROI in this thesis.

First Loop - Generate N Feature Codes:For the first loop b_n represents the number of bits generated in each block. The precision threshold specified in Theorem 2 is indicated by k and N sets of feature codes are generated.

Second loop - Iterating Over Block Pairs:In this loop the DCT coefficient difference is determined between blocks p and q. These blocks can be represented by two sets: $P_p = p_1, p_2, p_3, ..., p_{\frac{\varrho}{2}}$ and $P_q = q_1, q_2, q_3, ..., q_{\frac{\varrho}{2}}$. The grouping of blocks into pairs can be based on any mapping function, S, as long as the following conditions are met:

$$P_q = S(P_p) \tag{2.4}$$

and

$$P_q \bigcap P_q = 0,\ P_q \bigcup P_q = P. \tag{2.5}$$

The mapping function can provide greater levels of security as a seed can easily be used that is only known to an authorised person. Loop 3 compares corresponding coefficient pairs, b_n in each micro block. Initially the difference $\Delta F_{p,q}(1)$ is determined from blocks p and q. If this is smaller than a threshold, k, a signature bit of 0 is used, otherwise 1 is used. The two cases of "greater" and "equal" are classified into the same type, as the likelihood of $\Delta F_{p,q}(i) = 0$ is small (Lin and Chang 2001). It is beneficial to locate the b_n selected positions in lower DCT frequency bands. This is because they are much larger than their higher spatial frequency counterparts and smaller quantisation values are used. Hence their values are unlikely to be lost as a result of JPEG compression.

Authentication Process

An image that must be authenticated is transformed into the block-based DCT domain, $\tilde{F}$. If the image is received in spatial form this is simple, however a JPEG file must be reconstructed by Huffman decoding and de-quantisation. The signature S must also be extracted from the image to generate signature bits, Z. Here, $\tilde{F}$ and Z are used as inputs to the authentication system used, shown in Figure 2.13. Similar to the three loops used in the signature extractor, there are three loops required to obtain individual DCT coefficients. From Figure 2.13, in order for authentication to be possible for the case when $Z_n(i) = 0$, the following condition must be satisfied:

$$\Delta F_{p,q}(i) - \tilde{k} \leq 0$$

Thus if $\Delta F_{p,q}(i) - \tilde{k} > 0$, some parameters in blocks p or q must have been changed.

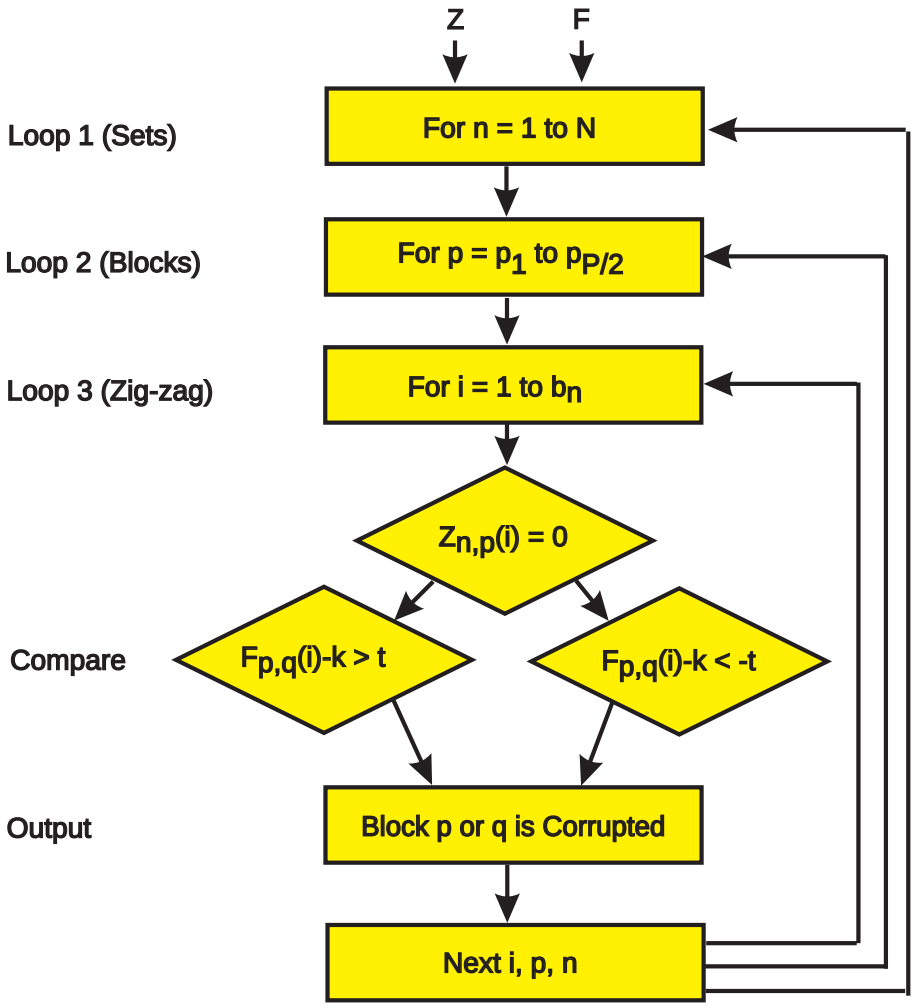

Figure 2.13. System to authenticate an image. The signature Z and DCT transformed image F are used as inputs to Lin and Chang's authentication system. Feature codes are extracted from individual blocks and compared to features of the signature Z against a known threshold. An acceptable match determines the authenticity of the blocks used for the comparison.

2.8 Chapter Summary

A few cutting edge technologies have been reviewed as well as their application to medical imaging. In order to meet the challenging requirements of a wireless link there is a need to reduce image size. Although the cost of transmission bandwidth has been falling, it is most cost-effective to use existing communication infrastructure wherever possible. At present cellular technology is the most practical option. Wireless transmission is fast and effective when diagnostic image information has been encoded for a channel in the most optimal way using efficient compression technologies. The cost of using compression must be taken into account as complex compression schemes

are expensive to develop and deploy, especially in consumer or specialist hardware. For these reasons focus has been placed on using international compression standards. JPEG compression is treated with caution as appropriate thresholds for use in diagnostic medical applications have been investigated. A bit rate of 1.0 Bpp is revealed as an acceptable limit for use in medicine. In the final sections of this chapter the embedded watermarking is presented as a novel approach to verify diagnostically important image regions and maintain compatibility with JPEG. The next chapter defines the performance measures used to evaluate the usefulness of the method presented in this thesis.

Chapter 3

Performance Measures

AN overview of the performance metrics used and the types of tests conducted to evaluate the effectiveness of the ROI watermarking method presented in this thesis are presented in this chapter. Target performance metrics include robustness, image fidelity and compression performance. Robustness testing is defined in Section 3.2, image fidelity in Section 3.3 and compression performance is presented in Section 3.4.

3.1 Overview of Performance Measures

Three performance metrics are presented that pertain to the most significant performance of the watermarking scheme. These include:

- **Robustness:** A measure of robustness is necessary to ensure acceptable survival of the watermark subject to the application specific transformation of DCT quantisation. Results are indicated by the percentage of a sample set of images detected as authentic.
- **Compression performance:** Desired compression standards must be able to compress the images that have been watermarked to a bit rate of 1.0 Bpp while maintaining watermark integrity. System failure or success will depend on watermark survival at this bit rate.
- **Image Fidelity:** A test used to quantify the degree of distortion introduced into a sample set of images with watermark embedding. Results are indicated by use of the Peak Signal-to-Noise Ratio (PSNR).

3.2 Watermark Robustness

Watermark robustness is defined as the ability to detect the watermark after the application of signal processing operations specific to JPEG. Robustness is determined by the extent of watermark survival to DCT quantisation. The loss of information present in the image can be acceptable as it contains redundancy that does not affect the diagnostic quality of the image. An ideal lossy compressor should quantise all perceptually equivalent images into a single consistent representation. If a robust watermark is to survive an acceptable level of lossy compression, it must withstand quantisation levels that correspond to the target compression range. It is equally important that the watermark does not survive unacceptable quantisation levels that significantly exceed the target compression range. This would otherwise be problematic, as the watermark would survive in an image that had a loss of diagnostic quality. The JPEG quantisation process is depicted in Figure 3.1. The quantisation step that occurs during compression is one of the most significant image distortions that can be modeled according to Equation 3.1, where q is the quantisation factor and $[x+0.5]$ rounds the coefficient, x to the nearest integer.

$$C_n[i] = q\left[\frac{C[i]}{q} + 0.5\right]. \tag{3.1}$$

Figure 3.1. JPEG quantisation process. Illustration of the lossy compression algorithm. Firstly the DCT is applied to the work and each of these are independently quantised on a block by block level. An inverse block-based DCT takes place to convert the image back to spatial representation.

Consider s to be a real valued scalar quantity and q_1 and q_2 as quantisation step sizes with $q_2 \leq q_1$, with quantisation operation $\bullet$, then

$$((s \bullet q_1) \bullet q_2) \bullet q_1 = s \bullet q_1. \tag{3.2}$$

If s is quantised to an even multiple of the larger step q_1 and then quantised by the smaller step q_2, the effect of the second quantisation step can be reversed (Cox *et al.* 2001). This property can be exploited by informing the watermark embedder and detector to transform coefficients by preselected step sizes. The watermark should survive as long as the quantisation that is performed during compression uses smaller step sizes. When larger step sizes are used the watermark should fail.

3.2.1 Approximations to Account for Acceptable Error

Noise may be introduced to this system with integer rounding and decimation resulting from spatial to DCT conversions in the JPEG compression process. This may also occur if the JPEG encoder does not calculate an accurate DCT. It is essential to incorporate a tolerance bound, π, for image authentication. Consider two image micro blocks, p and q, which must have changed if:

$$\Delta F_{p,q}(i) - \tilde{k} > \pi \tag{3.3}$$

in the case $\Delta F_{p,q}(i) - k < 0$, or if,

$$\Delta F_{p,q}(i) - \tilde{k} \leq -\pi \tag{3.4}$$

in the case $\Delta F_{p,q}(i) - k \geq 0$.
The tolerance is selected according to the average number of integer rounding errors. As this is largely dependent on the decimation algorithm used, this tolerance is set experimentally. Instead of selecting a threshold for individual coefficient pairs it is

more practical to set an acceptable limit to the number, N of bits in the signature, S and watermark, W to a threshold, ϵ. Thus for signature bits, S_i and watermark bits, W_i,

$$\frac{\Sigma(S_i - W_i)}{N} < \epsilon \tag{3.5}$$

This can be performed by applying DCT conversion and rounding on a sufficiently large sample set of watermarked images. The bit error rate between the signature and watermark can then be determined. When a sample set of 100 images were used this was experimentally found not to exceed 15%, which has been used as a tolerance bound introduced by these types of noises, thus:

$$\frac{\Sigma(S_i - W_i)}{N} < 0.15. \tag{3.6}$$

To test this performance practically, it is useful to determine the percentage of images that are detected as authentic for each embedding level that is used. It is also necessary to select another threshold that can be used to determine where this system fails. We have arbitrarily chosen a threshold of 85% of the images to be detected as authentic to indicate survival of image distortions.

3.3 Image Fidelity Performance With Watermarking

The fidelity of a watermarking system refers to the perceptual similarity between the original and watermarked images. It is useful to measure the degree of distortion that the watermarking introduces to the work for quality assessment. One trade-off of using robust watermarking is that the authenticated image contains perceptible distortions visible to the end user unless the watermark is removed.

The most established measures of objective perceptual image quality are Mean-Squared-Error (MSE) and Peak-Signal-to-Noise-Ratio (PSNR) techniques. The MSE between a reference image $r(n,m)$ and a watermarked image, $w(n,m)$ is,

$$\mathrm{MSE}(r,w) = \frac{1}{N \times M} \sum_{n=1}^{M} \sum_{m=1}^{N} [r(n,m) - w(n,m)]^2. \tag{3.7}$$

One problem with mean-squared error is that it depends strongly on the image intensity scaling. A mean-squared error of 100.0 for an 8-bit image (with pixel values in the range $0-255$) may be perceptually distorted, while a MSE of 100 for a 10-bit image

may appear to have very little distortion present.

The PSNR rectifies this problem by scaling the MSE according to the image range. This is similar to the MSE, however the peak pixel value, P is used in the computation as of Equation 3.8.

$$\text{PSNR} = 10\log_{10}[\frac{P^2}{MSE}] \tag{3.8}$$

The PSNR is measured in decibels (dB) and is useful to assess image fidelity when the original image is available for a comparison. It is also useful when there is only one type of distortion introduced into the authenticated image. One of the limits of this type of performance metric is the necessity of identical image resolution for images that are compared. Geometric distortions such as re-scaling are not highly probable, as images are of high importance and transmitted in standard resolution sizes. One exception may be a receiving device that rescales an image automatically. The PSNR is thus a valid measure of image quality to assess the immediate effects of watermarking at different embedding levels. This measure is also simple to determine, has a clear physical meaning and is mathematically convenient to calculate.

3.4 Compression Effectiveness and Metric Used

Compression effectiveness can be defined as survival of the watermark, given that an appropriate amount of complete JPEG compression is used. The compression ratio is used as a relative measure defined in Equation 3.9 of the uncompressed image size divided by the compressed image size,

$$\text{Compression Ratio} = \frac{\text{Uncompressed Image Size}}{\text{Compressed Image Size}}. \tag{3.9}$$

This type of image compression metric performs well for all images independent of the way that they are encoded as it is simply a ratio of sizes. Another method of determining the compression ratio is to compare the total number of bits in the uncompressed image to the number of bits in the compressed image file. This is useful for images that have a constant bit depth, however the number of bits in uncompressed medical imagery can often be difficult to determine (Clunie 2000). Many medical images may also contain a description of bit depth that does not allow of a useful indication of compression ratio. For instance, images used in Computed Tomography and Nuclear Medicine may specify a bit depth of 16 when the actual pixel values may be encoded

in fewer bits.

Another measure called the byte compression ratio involves comparing the number of bytes occupied by an uncompressed image divided by the number of bytes in the compressed image file. This is useful as uncompressed images are usually transmitted with their pixel values aligned to byte boundaries. A more realistic measure of image compression can be indicated by comparing the encoded bit rate (See Equation 3.10) with a measure of how much information is actually encoded encoded in the image. A well known measure is the "entropy" of the image (Shannon and Weaver 1949). This is the average amount of information per pixel in the compressed image.

Absolute measures have more widespread usage and the "bit rate" is used in this thesis. This is defined as the average number of bits used to encode a pixel and can be calculated from the total number of bits in the encoded picture file divided by the number of pixels,

$$\text{Bit Rate} = \frac{\text{Image File Size}}{\text{Total Number of Pixels}}. \tag{3.10}$$

This type measure is useful when comparing different compression methods applied to one image, or many images with a consistent bit depth. Its units are Bits Per Pixel (Bpp).

3.5 Chapter Summary

Three essential performance metrics have been presented as measures in evaluating the overall effectiveness in the system performance of watermarking methods tested in this thesis. These include quantisation and compression effectiveness, which is expressed in terms of bit rate. Image fidelity is also an important performance metric. This should be considered after watermark embedding and removal as it is undesirable for high levels of distortion to be present in watermarked diagnostic images used in wireless telemedicine. The next chapter discusses in detail the method used to authenticate a critically important image region.

Chapter 4

System Method

ROBUST watermarking schemes have previously been proposed to withstand DCT quantisation of image micro blocks (Lin and Chang 2001). In this chapter an outline of the method that uses multiple robust watermarks to authenticate critical feature information is presented. Two core stages are discussed that include extracting a signature from the critical image regions and embedding this information into the image in less significant regions. The signature extraction process is discussed in Section 4.1, while the embedding of this information is covered in Section 4.2. Appropriate thresholds used to detect the watermarks are discussed in Section 4.3. These are based on definitions outlined in Chapter 3. The chapter is concluded with a method to remove the watermark for improved image fidelity in Section 4.4.

4.1 Extracting the Signature

A ROI is specified at the location where the critical image information is segmented from a ROB. A signature is extracted from the low frequency DCT coefficients of the the micro blocks in the ROI and embedded into higher frequency terms of the ROB as a semi-fragile watermark, shown in Figure. 4.1. Similar ideas have been used in earlier literature including Maity *et al.* (2004), who extracted image features as part of the embedding payload for a robust watermark. The signature information and the water-

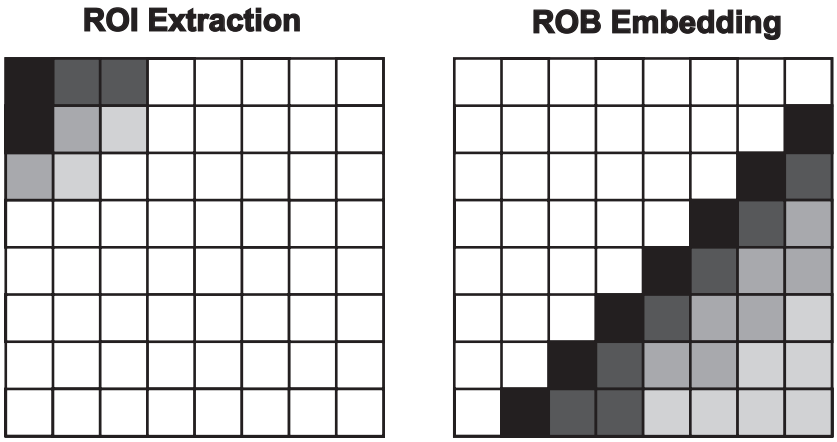

Figure 4.1. Obtaining a Signature From DCT Coefficients. Bits used to compute the signature are shown on the left in the ROI and the bits used for the watermark are depicted on the right. Matching shades indicate the transformation of signature bits to watermark bits. Low frequency DCT coefficients are used to generate the authentication signature, as they contain most important spatial information.

mark are designed to survive JPEG compression up to a given threshold specified as a quantisation multiplier or embedding strength, α. The signature is based on properties between randomly selected pairs of DCT coefficients that are invariant to JPEG compression. This technique is adopted from Lin and Chang (2001), which is discussed in Chapter 2.

For each pair of DCT blocks, 8 corresponding low frequency coefficients are compared to obtain 8 bits of the binary feature code sequence Z. Consider two blocks that have been grouped C_a and C_b, then the signature bit $b \in Z$ is determined by the relationship:

$$\text{signature bit} = \begin{cases} 0 & : \quad C_a[i,j] < C_b[i,j] \\ 1 & : \quad C_a[i,j] \geq C_b[i,j], \end{cases}$$

Table 4.1. Quantisation table used in JPEG. The top left value is the DC quantisation factor for each micro block, while the bottom right value represents the amount used to quantize the highest spatial frequency term. Greater levels of quantisation are used to progressively remove higher spatial frequency information, which is designed to exploit characteristics of the HVS. All of these values are multiplied by a global quantisation factor to obtain a scaled quantisation table. Redundant image information can be discarded, dependent on the a tradeoff between the desired image fidelity or bit-rate constraints. Recovery of the watermark will be dependent on the quantisation level applied to micro blocks in the image. Values in this quantisation table have been selected as a result of numerous subjective experiments performed by the JPEG organisation.

16	11	10	16	24	40	51	61
12	12	14	19	26	58	60	55
14	13	16	24	40	57	69	56
14	17	22	29	51	87	80	62
18	22	37	56	68	109	103	77
24	35	55	64	81	104	113	92
49	64	78	87	103	121	120	101
72	92	95	98	112	100	103	99

where i and j are the coordinates of a low frequency coefficient from Fig. 4.1. As a result of JPEG compression, each block is quantised by the same quantisation table in Table 4.1. Because one bit is generated from every two DCT coefficients that are compared, 8 signature bits are generated from every micro block pair in the ROI. These are embedded multiply into the ROB in the same shape as the ROI, but in multiple locations. For example, 5 watermarks can be can be seen for the breast carcinoma in Figure 4.2.

4.2 Embedding the Watermark

The method to embed the signature taken from the ROI takes an extra input parameter, α, which specifies the level of JPEG compression that the watermark should survive. This is expressed as the largest quantisation multiplier that can be applied to the quantisation matrix that results in the positive detection of a watermark. The watermark should degrade when the quantisation exceeds this level. The process of watermark

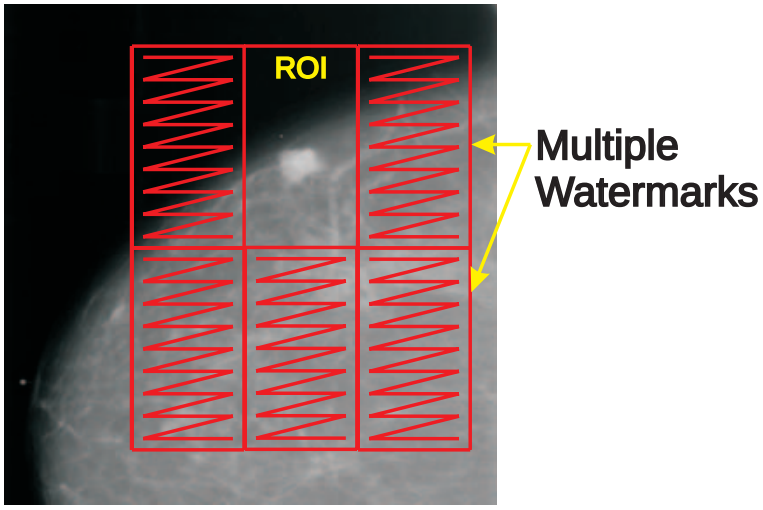

Figure 4.2. Multiple watermarking for the breast carcinoma. Five embedding regions are used around the ROI as there is limited space in the image. The entire signature generated from the ROI is separately embedded into each of these regions following the top-down zigzag sequence illustrated for each micro block in the ROB.

embedding is very similar to that used by Cox *et al.* (2001). Four signature bits are embedded into the high frequency DCT coefficients of each micro block in the image ROB. Let b be the value of one of the signature bits. This is embedded in the following process:

1. Select 7 coefficients from the set of 28 coefficients shown on the right side of Figure 4.1, $C[0], C[1], ...C[6]$. These coefficients are selected by following the JPEG zigzag scan process that is depicted in Figure 4.3.

2. The JPEG compression operation is performed on these coefficients and each is quantised by its corresponding quantisation factor and rounded to the nearest integer as of Equation 4.1

$$\tilde{f}_p[i] \;=\; \text{ROUND}\left[\frac{C[i]}{\alpha Q[i]}\right] \tag{4.1}$$

   The value $Q[i]$ is found in Table 4.1.

3. The least significant bit of the resulting integers $\tilde{f}_p$ are exclusive-or'd together to obtain the present bit value, b_e represented by the selected 7 coefficients.

4. If $b_e \neq b$, then the least significant bit of one of the integers is flipped. The integer that is changed is the one that results in least impact to image fidelity. The bit to

flip is the one that results in smallest error when the watermarked coefficient is unquantised by multiplying by its respective quantisation multiplier after the LSB has been flipped.

5. The resulting watermarked coefficients, $C_W[0], C_W[1], ...C_W[6]$ are multiplied by their corresponding quantisation factors to generate the watermarked DCT coefficients in Equation 4.2,

$$C_W[i] = \alpha Q[i] C_W[i]. \tag{4.2}$$

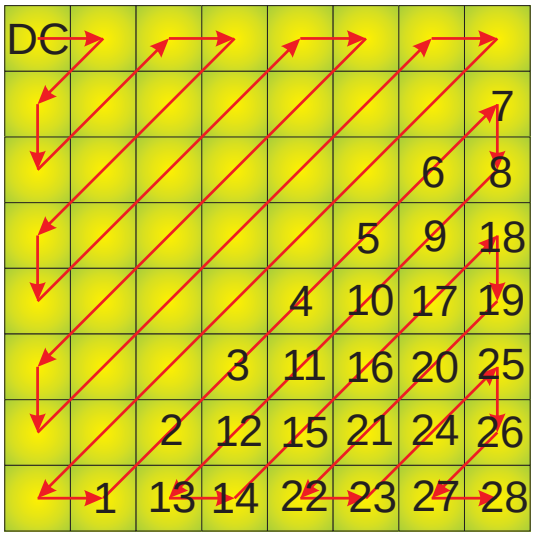

Figure 4.3. Zigzag scan used to trace DCT coefficients. DCT coefficients labeled 1 to 28 used as host coefficients for the watermark. Four bits are embedded in these coefficients. The implementation in this thesis ensures that only one group of 7 coefficients is used to host one bit. DC is used to represent the average or non-varying coefficient in the top left corner of the micro block.

Ideally this algorithm should embed all signature bits effectively after a singular embedding process. However rounding and decimation of DCT coefficients may cause some of these bits to flip their value. This problem can be resolved by running the embedder on the image until all signature bits are embedded correctly. For a detailed systematic implementation, please refer to Appendix B.

4.3 Detecting the Watermark

The watermark detection algorithm takes three arguments. These include the image to be authenticated, the location of the ROI within the diagnostic image as well as a seed

that generates a unique signature from the ROI by randomising the micro blocks in a known way. The method discussed in Section 4.1 is used to extract a signature from the ROI, which is followed by watermark extraction from the ROB. This involves performing the first three steps of the embedding process from one of the watermark regions in the ROB to extract each embedded bit, b_e. These are compared pair-wise with corresponding bits from the signature in the ROI. The percentage of bits that match are compared against a threshold. If this match exceeds a threshold, π_0 the ROI is declared as authentic. Ideally the threshold should be set at $\pi_0 = 100\%$, which would result in a perfect match. Clipping and round off error can occur with JPEG compression and decompression. This can occasionally corrupt embedded bits even if the quantisation multiplier is less than the watermark embedding strength, α. The threshold, π_0 is set to 85% because of the observed bit error rate discussed in Chapter 3. This threshold is also shown to be acceptable given the probability of a falsely generated signature in Section 5.

4.4 Removing the Watermark

Once image integrity has been verified, removing the watermark is an optional process for improving the image fidelity and has been treated as a side issue in this thesis. Lossy JPEG quantisation and integer rounding ensures that the majority of high frequency DCT coefficients have a high probability of being zero. An exception is for modified coefficients where the LSB has been flipped for watermarking. If these coefficients are set back to zero after authentication has taken place, it would not affect coefficients associated with retaining significant picture information in the ROB. The systematic process to remove the watermark is presented in Figure 4.4. The perceptual difference between a watermarked image and one with the watermark removed is shown in Figure 4.5.

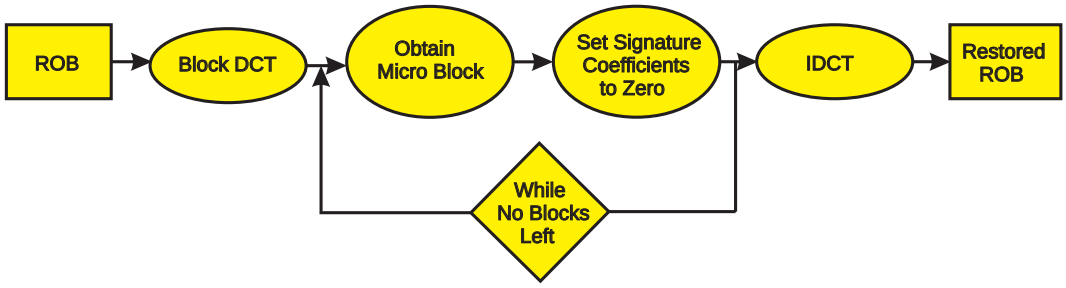

Figure 4.4. Removal of semi-fragile watermarks. Elimination of watermarks from the ROB takes place in the DCT domain, where individual micro blocks are extracted one by one. The set of 28 watermark coefficients are set back to zero. Resulting micro blocks contain no watermarking artifacts.

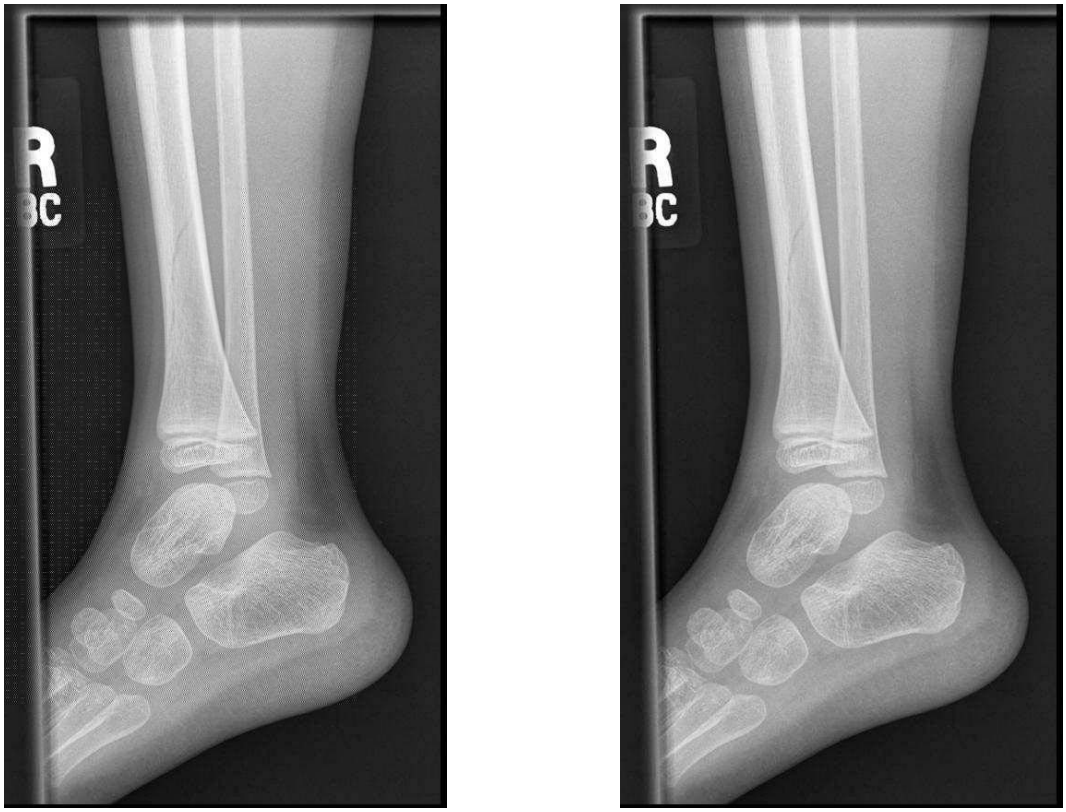

Figure 4.5. Removed watermark. The watermark is present in the received image (left) and has been embedded in five regions around the ROI as there was insufficient space for embedding in the three regions above. The watermark is apparent around the ROI in the form of high frequency noise that present as checkerboard patterns. Removing the watermark results in a perceptual improvement in image quality in the ROB with the checkerboard distortions removed.

4.5 Chapter Summary

An overview of the watermarking method is provided in this chapter. Techniques used to extract the signature and embed the watermark are presented. Watermark detection processes are explained as well as an approach to remove the perceptual distortion introduced by the watermark. Please refer to Appendix B for more detailed analysis of the systematic implementation in software. The next chapter compares the performance of this method with the proposed method by Lin and Chang (2001).

Chapter 5

Comparison To Other Methods

THE previous chapter presented an outline of the system method. In this chapter the system performance of the ROI watermarking scheme is compared to an earlier proposed method by Lin and Chang (2001). Three types of tests are used for these performance comparisons. These include quantisation testing, shown in Section 5.1 image fidelity in Section 5.2 and compression effectiveness seen in Section 5.3. Compression algorithms used include baseline JPEG and JPEG-2000. This chapter is drawn together in Section 5.4 which summarises the most significant results.

5.1 Quantisation Testing

5.1.1 Aim

DCT quantisation is one of the most perceptible distortions that results from quantising the micro blocks in the JPEG compression process. This distortion leads to most significant image distortion, as DCT coefficients are individually scaled by quantisation multipliers. Other distortions in the JPEG compression process that are less significant include decimation and rounding error. This is tested by complete JPEG compression in Section 5.3. The quantisation test will ensure that both the signature in the ROI and the watermarks contained in the ROB will survive acceptable levels of DCT quantisation. Robustness of the ROI watermark method is compared to the technique proposed by Lin and Chang (2001).

5.1.2 Hypothesis

As the degree of DCT quantisation is increased beyond a given acceptable level, fewer images should be detected as authentic. This is because quantisation has the effect of slowly removing the coefficients in each micro block by progressively scaling each DCT coefficient, which eventually round to zero. Successively greater scaling is used for higher frequency coefficients of each micro block, hence upper coefficients will be quantised and rounded to zero first that correspond to features of the watermark. The overall nature of image deterioration with DCT quantisation should be similar for all of the embedding strengths, α used. This ensures consistent robustness. The watermark should also fail shortly after the embedding strength is exceeded so that a harshly quantised image is not detected falsely as authentic. This could be expected if a watermark was retained at an unacceptable quantisation level.

5.1.3 Methods to Test Robustness

The images that are used to test watermark robustness include a sample set of 500 uncompressed greyscale medical images with resolutions varying between 512×512 and 2048×2048 pixels. These were saved as bitmap (BMP) images with a encoded bit depth of 8 Bpp. The robustness of the watermarking system to JPEG DCT quantisation is determined by embedding multiple watermarks into these set of images. The

embedding strength must be fixed at a constant level for each test. The percentage of images detected as authentic at the output after quantisation is used to approximate the watermark robustness. For the watermarking scheme to be sufficiently robust to quantisation, survival of the embedding levels of 0.62, 0.88 and 1.4 must ensure. These levels are obtained from the results in Appendix A.1, which experimentally show that the embedding levels correspond to acceptable compression levels over a range of 0.8 to 1.2 Bpp.

The testing process used is depicted in Figure 5.1 and involves basing a watermark on invariant DCT relationships within the ROI.

This region is adjusted to cover a 20% area of the image, which is a typical size for a crucial diagnostic image region. The ROI is specified to be based at the image center, which allows for 8 watermarks to be embedded around the ROI. A manual technique is adopted, whereby the images are grouped according to their resolutions with the ROI pre-specified.

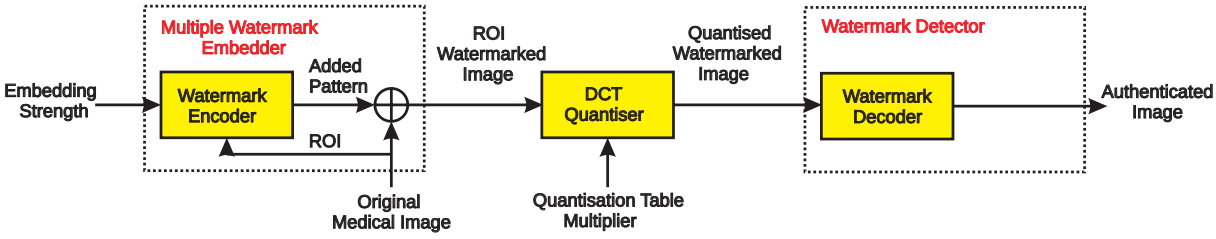

Figure 5.1. Method to test watermark and signature robustness. The quantisation test ensures that the complete watermarking system is robust to DCT quantisation. A medical image is manually segmented into a ROI and ROB. A unique signature is extracted from the ROI by the watermark encoder and embedded multiply as a watermark in the DCT domain of the ROB. The desired robustness is dependent on the embedding strength parameter α. The watermarked image (in DCT domain) is passed to the quantiser where variable levels of quantisation are applied in the block-based DCT domain. This is immediately followed by integer rounding of the coefficients. All micro blocks are quantised equally prior to passing the watermarked image (still in DCT domain) to the watermark detector for authentication. A key may be used to extract the unique signature from the ROI and compare it to a watermark in the ROB. A threshold, π_0 of 85% is set as an acceptable limit to the number of bits that must match in the signature and watermark for an authentic image.

5.1.4 Results of Robustness Testing

Performance comparisons between the ROI watermark method and the scheme proposed by Lin and Chang (2001) are shown in Figures 5.2 and 5.3.

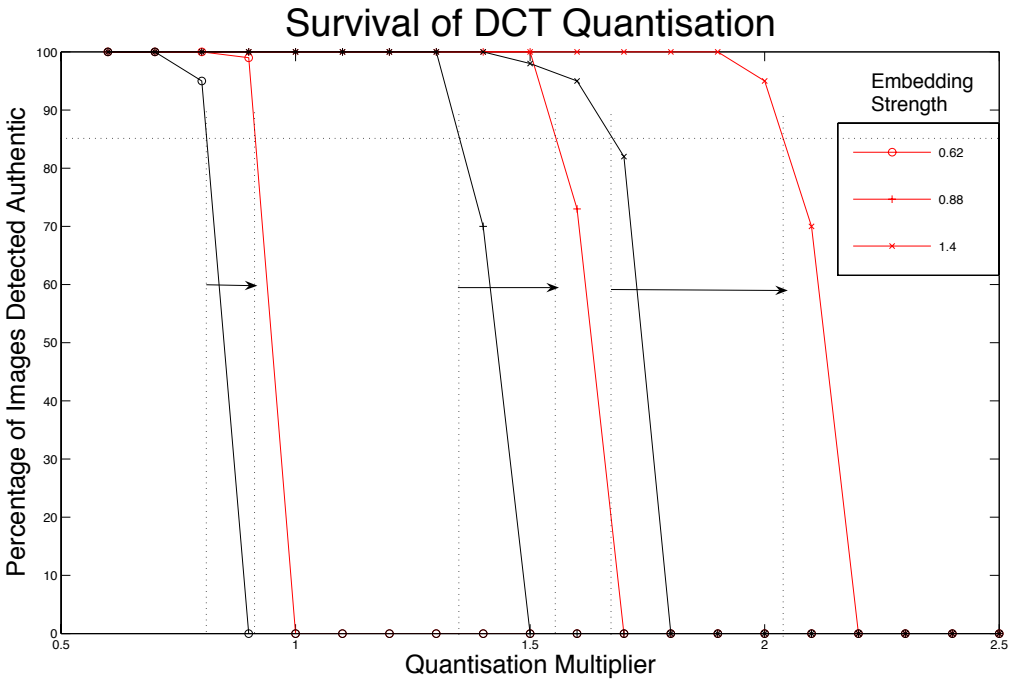

Figure 5.2. Robustness of ROI method and Lin and Chang's method. Testing the robustness of 500 images using the ROI watermark method (red) and Lin's approach designed to withstand JPEG compression with three selected embedding levels of 0.62, 0.88 and 1.4. It appears that the region-based watermarking scheme can survive greater levels of JPEG quantisation than for Lin's method especially when increased embedding strengths are used. A threshold of 85% matching bits has been used to discriminate an authentic image from a corrupted one. For the sample set of test images used, 85% must be detected as authentic for the watermarking system to be successful. When $\alpha = 0.62$ is used, the ROI watermark method fails when the quantisation level exceeds 0.90, while Lin's method fails when this exceeds 0.80. Also, when $\alpha = 0.88$ is used, the ROI watermark method fails when the quantisation level exceeds 1.55, while Lin's method fails when this exceeds 1.35. Finally, for $\alpha = 1.40$ is used, the ROI watermark method fails when the quantisation level exceeds 2.04, while Lin's method fails when this exceeds 1.68. Hence for embedding levels of 0.62, 0.88 and 1.40, the ROI watermarking approach outperforms Lin's proposed method by respective quantisation levels of 0.10, 0.20 and 1.36. Hence the ROI watermark method consistently outperforms Lin's proposed method when block-based DCT quantisation is applied.

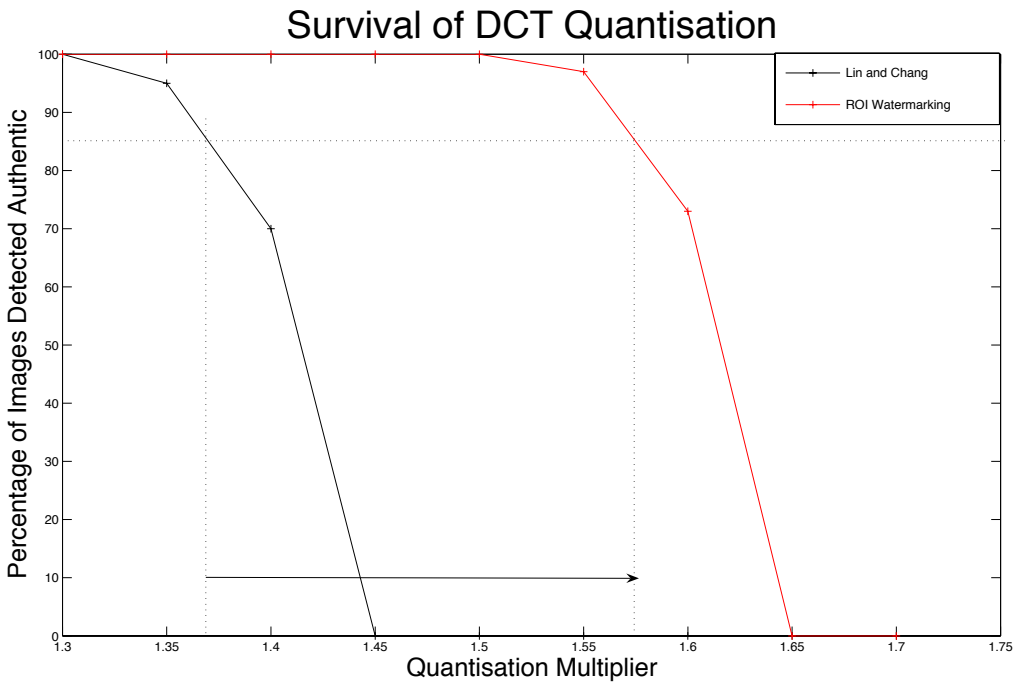

Figure 5.3. Analysis of failure point at an embedding level of 0.88 corresponding to 1.0 Bpp. At the point of watermark failure, an extra amount of DCT quantisation of approximately 0.2 can be applied to the image before failure when the ROI watermark approach is adopted. Hence over the most crucial quantisation level, our method out-performs Lin and Chang's proposed technique by allowing the quantisation to be exceeded by 0.2, while maintaining survival of the watermark.

5.1.5 Conclusion and Discussion

The ROI method is shown to outperform the method proposed by Lin and Chang for the JPEG quantisation tests. Hence the watermark will remain embedded in the image after greater levels of JPEG compression are used if the ROI watermark system is adopted rather than for Lin's method. One possible reason of this type of behavior could be attributed to Lin's method extracting a signature from every micro block in the image and embedding the signature into the same regions. Thus if any part of either the signature or watermark was lost it would be reported by the decoder as an error and may contribute to poorer quantisation survival. To the contrary, the ROI watermark method does not embed authentication information in the ROI or extract any signature information from the ROB. This means that there is less information required to authenticate the image, reducing the probability that the authentication information

can be corrupted by using a smaller signature.

Multiple embedding used in the ROI watermarking approach may also contribute to increased survival levels, as the authentication information is embedded in multiple locations. If one watermark is corrupted, another can used. This feature would not be expected to significantly increase the system robustness, as consistent levels of DCT quantisation are introduced to all micro blocks in the image. Consequently all watermarks would be expected to be lost at a similar quantisation level.

One of the adverse consequences of increased robustness is sustaining a watermark when excessive or unacceptable levels of quantisation are applied. The important question to raise is, are significant image features lost if the watermark survives more quantisation than that which correlates with an acceptable compression level? This is only anticipated to be a problem if the watermark embedding strength, α is not appropriately chosen. For example, setting $\alpha = 1.4$ informs the watermark embedder that this is the maximum level of quantisation that that watermark should survive, but does not guarantee it, as shown in Figure 5.2 where the watermark is lost when the quantisation multiplier exceeds 2.04. This would be considered unacceptable as it would correspond with a compression level lower than the accepted range of 0.8 to 1.2 Bpp. If α is set to a smaller value, such as 0.62, the watermark will most probably fail at a quantisation level of 0.9 that corresponds much more closely with the accepted bit rate of 1.0 Bpp. Because the watermark embedding does not significantly increase the resulting file size, this problem can be rectified by comparing the received file size with the image resolution to obtain the bit rate. This would give a realistic estimate of the applied compression level and watermarking would still provide assurance that critical feature information is present in the ROI.

Probability of a False Match Between Signature and Watermark

Another indication of robustness is the issue of false watermark detection. It is desired that the ROI watermarking system only authenticates the crucial region when an embedded watermark matches the signature. Testing for the probability that the authentication system could fail by authenticating a randomly generated watermark is essential for false error probability estimation. This is more likely to be probable when the signature length, n is small corresponding to a very small ROI. Hence it is useful

to investigate the probability that a randomly generated watermark matches the signature.

Assume that the two sequences are of length n. Assume without loss of generality that one sequence, say S_1, consists entirely of ones and represents the binary feature codes taken from the ROI. The other sequence, S_2 is randomly generated, so that a symbol in a randomly chosen position in the sequence is equally likely to be a 0 or a 1.

Let X be the number of 1s in S_2. Then the probability of a perfect match is the probability that all symbols in S_2 are 1s,

$$P_r(X = n) = \left(\frac{1}{2}\right)^n.$$

Suppose that a sequence is deemed to provide an acceptable match if the proportion of pair-wise matches is at least π_0. Then the probability of an acceptable match is given by the binomial probabilities:

$$P_r(X \geq n\pi_0) = \sum_{x=n\pi_0}^{n} \binom{n}{x} \left(\frac{1}{2}\right)^n.$$

If n is large (say, $n > 40$), an acceptable approximation to the binomial probabilities may be obtained from the Gaussian distribution (Abramowitz and Stegun 1974):

$$P_r(X \geq n\pi_0) \approx P_r\left(Z \geq \frac{\pi_0 - \frac{1}{2}}{\sqrt{\frac{1}{4n}}}\right),$$

where Z is the unit Gaussian random variable.
The Gaussian right tail probability, as a function of z, is known as the Q-function, that is,

$$P_r(Z \geq z) = Q(z) = \int_z^\infty e^{\frac{-t^2}{2}} dt$$

and this may be approximated in terms of the error function:

$$\text{erf}(x) = \frac{2}{\sqrt{\pi}} \int_0^x e^{-t^2} dt.$$

In particular,

$$Q(z) = \frac{1}{2}\left(1 - \text{erf}\left(\frac{z}{\sqrt{2}}\right)\right).$$

While its inverse may be found from the inverse error function,

$$Q^{-1}(y) = \sqrt{2}\text{erf}^{-1}(1 - 2y).$$

The error function and its inverse is available in Matlab.
Consider the following decision structure:

- The null hypothesis is H_0: the sequence S_2 is random.
- The alternative is H_1: the sequence S_2 has a structure, which is deemed acceptable according to the criterion that the proportion of pair-wise matches with S_1 is at least π_0. Hence the test statistic is X, the number of pair-wise matches.
- Reject H_0 in favour of H_1 if $P_r(X \geq n\pi_0) \leq \tau$, where τ is an appropriate significance level.

Then the base acceptance level,

$$\tau = P_r(X \geq n\pi_0) \approx Q\left(\frac{\pi_0 - \frac{1}{2}}{\sqrt{\frac{1}{4n}}}\right)$$

$$\pi_0 \approx \frac{1}{2} + \frac{Q^{-1}(\tau)}{2\sqrt{n}} = \frac{1}{2} + \text{erf}^{-1}\frac{1-2\tau}{\sqrt{2n}}.$$

This may be used to find the criterion proportion for acceptance of a sequence, for a given sequence length and significance level. The following Matlab code is included:

```
tau = [0.05, 0.01, 0.005, 0.001, 0.0005, 0.0001, 0.00005, 0.00001];
n = [10, 50, 100, 500, 1000, 5000, 10000, 50000]; for i=1:7
    for j=1:7
        pi0(i,j)=0.5+erfinv(1-2*tau(i))/sqrt(2*n(j))
    end
end
```

The results are:

$\tau : n$	1×10^1	5×10^1	1×10^2	5×10^2	1×10^3	5×10^3	1×10^4	5×10^4
5×10^-2	0.7601	0.6163	0.5822	0.5368	0.5260	0.5116	0.5082	0.5037
1×10^-2	0.8678	0.6645	0.6163	0.5520	0.5368	0.5164	0.5116	0.5052
5×10^-3	0.9073	0.6821	0.6288	0.5576	0.5407	0.5182	0.5129	0.5058
1×10^-3	0.9886	0.7185	0.6545	0.5691	0.5489	0.5219	0.5155	0.5069
5×10^-4	1.0203	0.7327	0.6645	0.5736	0.5520	0.5233	0.5165	0.5074
1×10^-4	1.0880	0.7630	0.6860	0.5832	0.5588	0.5263	0.5186	0.5083
5×10^-5	1.1152	0.7751	0.6945	0.5870	0.5615	0.5275	0.5195	0.5087
1×10^-5	1.1743	0.8016	0.7132	0.5954	0.5674	0.5302	0.5213	0.5095

These results indicate that, for example, if $n = 50$ and $\pi_0 = 80.2\%$, then, $P_r(X > n\pi_0) = 0.00001$.

As the watermark is only chosen to be acceptable given $\pi_0 \geq 85\%$ with a typically larger choice of n, it can be expected that the probability of false watermark detection is extremely low.

A typical ROI selection may include a pixel area of, say 160×160 pixels, which would contain 400 micro blocks. If four bits are taken from each micro block to generate the signature sequence S_1, this would correspond to a length $n = 1600$. Thus the choice of pi_0 could be lowered to 57% and the false error probability would still be as low as 0.00001. This indicates that the error threshold $\pi_0 = 85\%$ sets a very low limit on the number of false errors.

5.2 Image Fidelity Testing

For any watermarking system, desired properties usually must be traded off with other parameters. One of the drawbacks of increased watermark robustness is an elevation in the degree of perceptible artifacts. This is shown in Figure 5.4. For a close analysis of the type of visual distortion over the target embedding levels, multiple watermark embedding has taken place and is shown in Figure 5.5. Although these artifacts can be eliminated by removing the watermark, it is useful to evaluate the extent of image degradation for monitoring purposes while the watermark is in place.

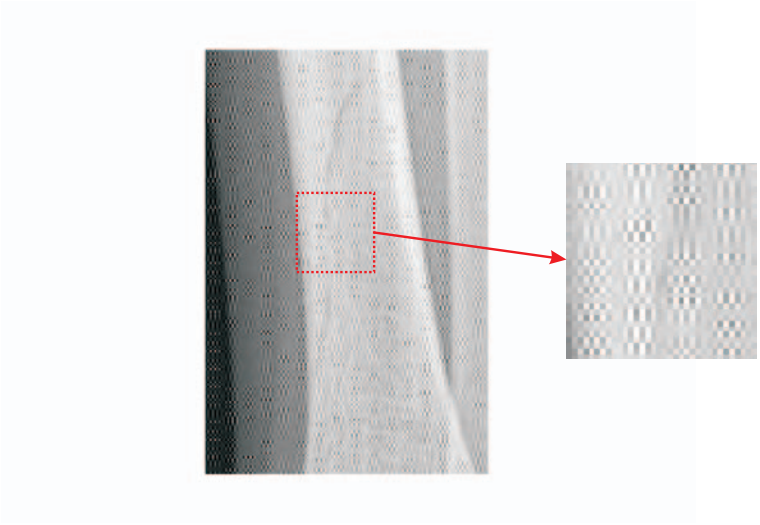

Figure 5.4. Introduction of watermark artifacts. The semi-fragile watermark method designed for robustness to JPEG compression, proposed by Lin and Chang is used for the infant's fracture. When this type of watermarking is used on the entirety of the image, the perceptual degradation is most noticeable. This appears in the form of 8×8 checkerboard patterns that resemble the spatial basis functions used in JPEG compression. Watermarking has taken place with an embedding strength $\alpha = 1.0$, which is necessary so that the fracture can be compressed to an acceptable diagnostic level of 1.0 Bpp, while still retaining an authentication watermark and fail after this level is exceeded.

5.2.1 Aim

The purpose of this test is to quantify the extent of image deterioration by introducing watermark artifacts. The ROI watermark method is compared to the technique proposed by Lin and Chang (2001).

5.2.2 Hypothesis

It could be expected that the PSNR of the watermarked images will on average decrease as the watermark embedding strength is increased. This is expected to result from increasing difference between the the pixel values of the original and watermarked images. As the number of watermarks is also increased, the PSNR should be lowered as the watermarks will cover a larger area. This will also lead to increased difference between both image sets. Removal of the watermark should lead to increased perceptual quality as well as an increased PSNR.

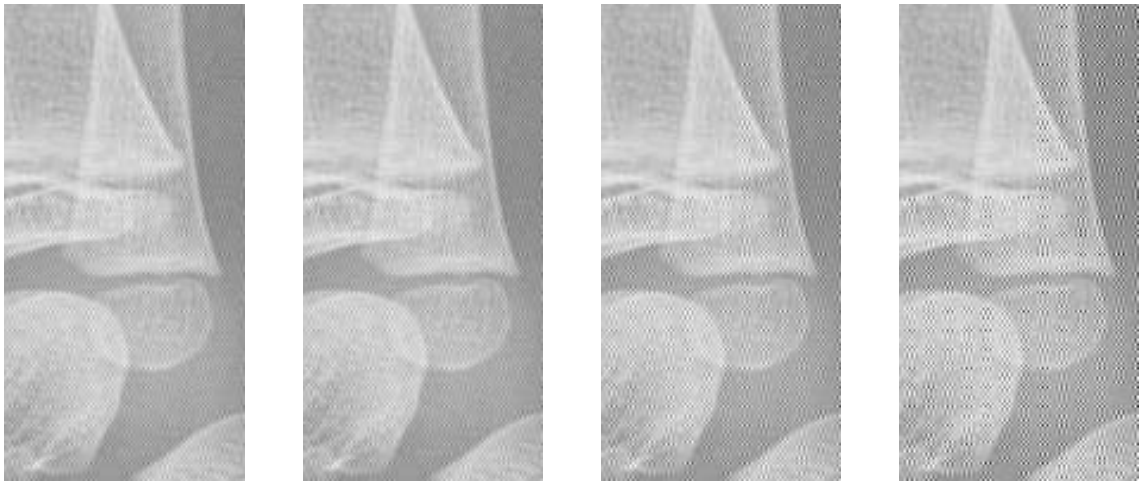

Figure 5.5. Embedding strengths of 0.62, 0.88, 1.4 **and** 2.5. These close ups were taken from the infant's fracture of the bottom right corner of the selected ROI where 8 surrounding watermarks in which 3 are visible when a zoom level of 300× is used. An additional embedding strength of 2.5 was also chosen as it was also the largest strength tested for distortions. Pronounced watermarking artifacts are present at this level that highlight the nature of the distortions. The bottom right hand corner of a selected ROI of the infant's fracture is shown in these diagrams to show the difference between watermarking in the ROB and having no watermark in the ROI. The degree of watermarking artifacts most likely seen are present in the second image from the left and corresponds to using an embedding strength of 0.88 corresponding to a JPEG compression level of 1.0 Bpp.

5.2.3 Methods to Test Image Fidelity

The images that have been used in testing image fidelity and making comparisons between systems include a sample set of 500 uncompressed greyscale medical images with resolutions varying from 512×512 to 2048×2048 pixels. These were saved as bitmap (BMP) images with a encoded bit depth of 8 Bpp.

The PSNR is calculated for the watermark embedding strengths, α of 0.62, 0.88 and 1.4. The system used to test image PSNR is shown in Figure 5.6. This system is also used to evaluate minor distortions following removal of the watermark to eliminate perceptually disturbing visible artifacts that have been introduced as a result of watermark embedding.

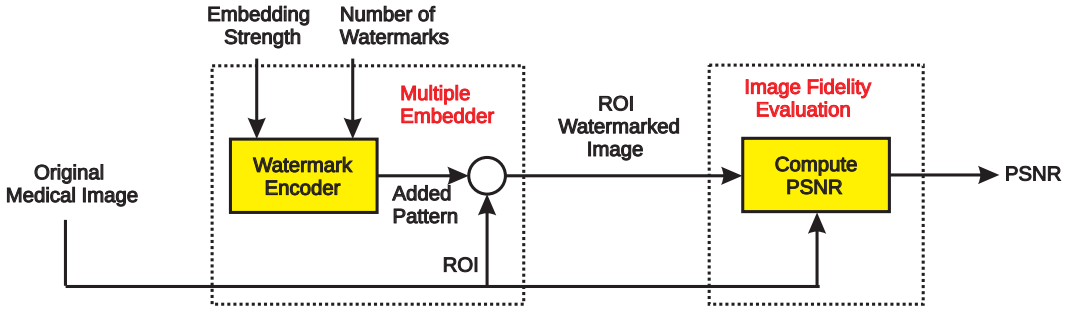

Figure 5.6. System used to test image fidelity. An embedding strength and the number of watermarks is specified to the watermark embedder prior to embedding at least one watermark around the ROI. The original unwatermarked medical image is used as a known reference to evaluate the distortions introduced by watermarking. These distortions appear as checkerboard patterns, shown in Figure 5.4 and are a result of flipping bits in the micro blocks of the ROB. This pattern can vary in its appearance and is the key factor that contributes to a lowered PSNR.

5.2.4 Results

PSNR image fidelity evaluation took place with different numbers of watermarks used for comparison to Lin's scheme. The results are shown in Figures 5.7 and 5.8.

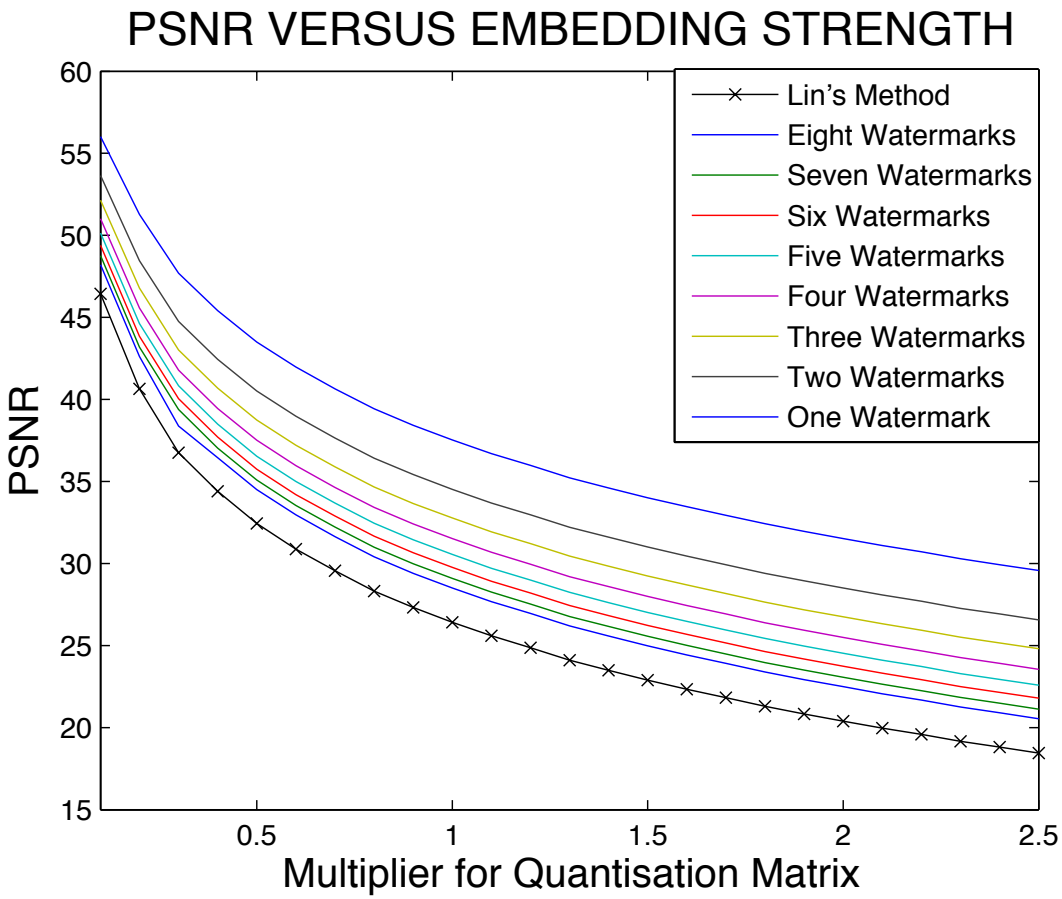

Figure 5.7. Comparison of the ROI watermark method with Lin's algorithm. Watermarking has taken place at different embedding levels over watermark embedding strengths from 0.62 to 2.50. In this instance the multiplier to the quantisation matrix is used as the embedding strength, α. Larger levels were chosen to investigate image fidelity for a worse case type of comparison. The PSNR is shown to drop off quite rapidly for α up to 1.0. Beyond this level image deterioration is much more gradual. This characteristic is independent of the number of watermarks used for a comparison. The ROI watermarking method developed is shown to outperform Lin and Chang's technique over the range of embedding strengths tested and performs better when fewer watermarks are used. For the rectangular ROI selected, the maximum number of watermarks is 8. The best performing system is that which embeds a singular watermark which is represented by the top blue line. A detailed analysis over the target embedding levels is shown in Figure 5.8

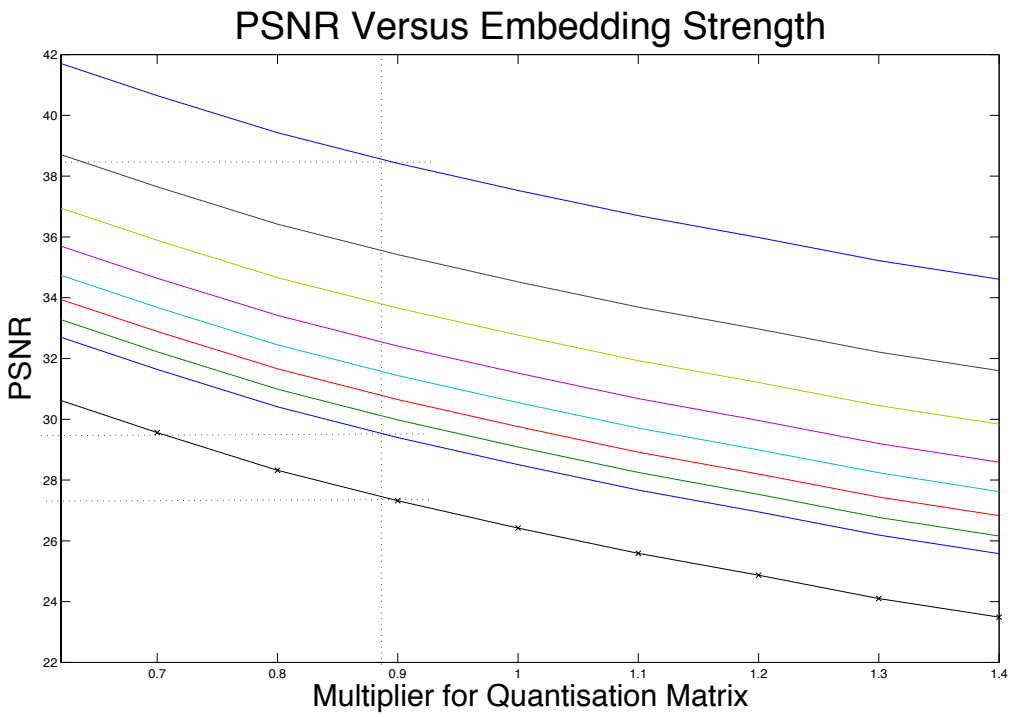

Figure 5.8. Analysis over target embedding levels. ROI watermarking shows an improved PSNR over Lin and Chang's method for the specified α range of 0.62 to 1.4. Careful inspection is drawn to the target embedding level of 0.88, which corresponds to a compression level of 1.0 Bpp. Lin's algorithm gives a PSNR of 27.4 dB, while the ROI watermarking algorithm performs much better. When 8 watermarks are used the resulting PSNR is improved by 2.1 dB at 29.5 dB. The performance is greatly enhanced when fewer watermarks are used, with a PSNR of 38.5 being reached for a singular ROI watermark. Adding more watermarks has the effect of reducing the image PSNR.

Table 5.1. Watermarked micro block, C. Taken from the ROB of the infant's fracture, the 48 and -49 signature coefficients shown in the micro block are not present prior to watermark embedding and do not correlate well with surrounding coefficients. An embedding strength, $\alpha = 0.88$ has been used. This table also depicts the efficiency of the DCT in extracting the image energy information into the top few DCT coefficients. No quantisation has been used, however integer rounding of the DCT coefficients has taken place. Because most coefficients are close to zero, the appearance of signature coefficients is quite obvious.

344	6	-1	0	0	0	0	0
0	-6	0	-1	0	0	0	48
7	6	0	0	0	0	0	-49
-7	0	0	0	0	0	0	0
-1	0	1	0	0	0	0	0
0	0	0	0	0	0	0	0
0	0	0	0	0	0	0	0
0	0	0	0	0	0	0	0

5.2.5 Comments and Discussion

The spatial distortions present in the watermarked images are shown to increase with the embedding strength and appear as checkerboard patterns. The most likely cause is signature information being present in locations of each micro block that would normally be used to represent highly localised spatial frequency information. Upon conversion back to the corresponding 8×8 pixel spatial domain where the distortions can be seen, DCT coefficients (including those used in the watermark) are multiplied with their corresponding basis functions. The signature coefficients used for the watermark do not correlate well with the surrounding coefficients not used to contain the watermark. These may be comparatively small, most probably zero and localised in the mid to upper DCT frequencies of the JPEG zigzag scan order, shown in Table 5.1. Consider the watermarked micro block C, shown in Table 5.1. In this particular block a watermark embedding strength, $\alpha = 0.88$ is used and the four bits, $v_e = 1100$ are required to be embedded into this block using semi-fragile watermarking that is robust to JPEG compression.

It is useful to follow some matrix theory to see how the watermarked micro block

Table 5.2. Original pixel values. Set of pixel values extracted from the fracture image.

44	44	44	43	43	42	42	42
44	44	44	44	44	43	43	43
43	43	44	44	44	44	44	44
42	42	42	42	43	43	43	43
41	41	41	41	41	41	41	41
43	42	42	42	41	41	40	40
46	46	45	44	43	42	41	40
49	49	47	46	44	43	42	41

Table 5.3. DCT transformed pixel values. Taking the two dimensional DCT to the set of pixels in Table 5.2.

343.7500	6.4112	-0.5576	0.1000	0	-0.0471	-0.0396	0.0973
-0.3736	-5.9332	-0.2222	-0.5327	0.3691	-0.2061	0.1734	0.7534
7.0576	6.4721	0.0732	-0.2859	-0.2310	-0.1097	-0.4268	-0.0566
-7.0405	0.1792	0.1470	0.0167	0.2514	0.0621	0.2859	0.0439
-0.5000	0.1125	0.6929	0.0637	-0.2500	-0.3204	-0.2870	0.0752
0.4027	-0.1474	-0.0982	0.2085	-0.2830	-0.1883	0.1097	0.2827
0.0532	-0.2222	0.0732	-0.1832	0.0957	0.3715	0.4268	-0.2107
-0.0706	-0.1001	-0.2107	-0.3974	-0.3089	0.0708	-0.0345	0.1048

values are obtained for this example. Consider the set of 8×8 pixel values, $\tilde{X}_P$, where $\tilde{X}_P \in Z$ for $Z = 1:255$. The pixel values corresponding to the unwatermarked version of an arbitrary ROB micro block C are shown in Table 5.2 and have been taken from the Infant's Fracture shown in Chapter 1.

The DCT is applied to 8×8 adjacent pixel blocks, which are quantised and rounded to integers prior to watermark embedding. This results in a micro block F_P, depicted in Table 5.3, where $F_P = \text{DCT}(\tilde{X}_P)$.

In this example, a watermark embedding strength, $\alpha = 0.88$ is used and the JPEG quantisation matrix Q is scaled accordingly. The micro block values, F_P are quantised and rounded to $\tilde{f}_p$ according to Equation 5.1:

$$\tilde{f}_p = \text{ROUND}[\frac{F_P}{\alpha Q}]. \tag{5.1}$$

Table 5.4. Quantised micro block coefficients. This is shown to very closely resemble the watermarked micro block shown in Table 5.1 with the exception of a watermark. The occurrence of many zeros after DCT quantisation and rounding provides for efficient entropy encoding of coefficients $p_1 : p_{64}$ following the JPEG zigzag scan.

344	6	-1	0	0	0	0	0
0	-6	0	-1	0	0	0	**0**
7	6	0	0	0	0	**0**	**0**
-7	0	0	0	0	**0**	**0**	**0**
-1	0	1	0	**0**	**0**	**0**	**0**
0	0	0	**0**	**0**	**0**	**0**	**0**
0	0	**0**	**0**	**0**	**0**	**0**	**0**
0	**0**	**0**	**0**	**0**	**0**	**0**	**0**

A new set of quantised micro block coefficients $\tilde{f}_p$ are presented in Table 5.4. Feature information in this block can mostly be retained if the coefficients are unquantised with multiplication by αQ and quantised again for smaller values of α.

Embedding of the signature bits $b = 1,1,0,0$ is localised to the last 28 coefficients of the JPEG zigzag scan, shown in bold in Table 5.4. One value of b is embedded into a sequential set of 7 values of $\tilde{f}_p$. As all of the watermark coefficients in this micro block are zero, embedding is relatively simple. The least significant bits of the seven integers $\tilde{f}_p$ are exclusive-or'd together to obtain the present bit value b_e. In this trivial case each $b_e = 0$, however the four bits that are required to be embedded are $1,1,0,0$. Hence bit flipping is required for the embedding of the first two bits, where $b \neq b_e$, but not for the second two bits. As one bit is embedded in every 7 coefficients, only the first 14 coefficients following the JPEG zigzag scan order of the last 28 coefficients are used to host the two signature bits $1,1$

Flipping the LSB of one of the quantised coefficients $\tilde{f}_p$ allows the embedding process to be made possible.

The bit to flip is the one that results in smallest error when the watermarked coefficient is unquantised by multiplying by its respective quantisation multiplier $\alpha.Q$, where Q is defined in Section 4. Hence it is desired to minimise the error $\Delta(F_P - \alpha Q\tilde{f}_p)$.

Table 5.5. Coefficients Involved in Flipping. Seven DCT coefficients are used to embed one bit. For the first two payload bits, $b = 1,1$, four columns are shown. The first two pertain to the first bit and the second two to the second bit. Columns 1 and 3 contain the original unquantised DCT coefficients, while columns 2 and 4 contain the unquantised DCT values if the LSB is flipped.

F_P (First Bit)	C_W Flipped (First Bit)	F_P (Second Bit)	C_W Flipped (Second Bit)
0.7534	48	-0.2107	-83
-0.4268	-60	-0.1832	-76
0.0621	76	-0.2830	-71
-0.2500	-59	-0.3204	-95
0.2085	56	0.2859	70
0.0732	68	-0.0566	-49
-0.1001	-80	0.0439	54

The LSB of f_p is flipped by either adding or subtracting 1 depending on the sign of the unquantised value F_P. This approach is very similar to a method adopted by Cox *et al.* (2001). The unquantised original and unquantised watermarked host coefficients are shown in Table 5.5. To minimise the error $\Delta F_P - \alpha Q \tilde{f}_p$, it is necessary to flip the LSB of the quantised coefficient which corresponds to the minimum error for the bits $b_1, b_2 = 1,1$. The minimum errors in this instance from Table 5.5 are easily shown when $\tilde{f}_p$ is flipped corresponding to the positions of F_P values 0.7534 and -0.0566 for the respective first and second bit that are required to be embedded. After these bits are flipped and multiplied by their respective quantisation multipliers, watermarked coefficients, C_W are shown with values 48 and -49. This explains the appearance of Table 5.1, where $C_W = Q\tilde{f}_p$.

The placement of one or more signature coefficients in the highest 28 DCT regions has the effect of introducing the checkerboard type of distortion corresponding to basis functions that the coefficient position corresponds to. These patterns are shown in Figure 5.9. This is part of the JPEG decompression process which is caused by conversion from DCT coefficient representation to spatial (pixel-based) form. The most likely reasons for the ROI watermark approach outperforming Lin and Chang's method at comparable embedding levels is due to significantly less area being devoted to the watermark. If there is less area used to place a watermark there will be fewer artifacts

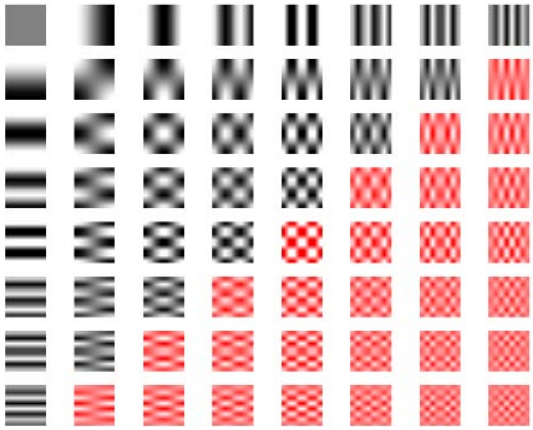

Figure 5.9. Spatial Basis Functions. This set of patterns is used to reconstruct images from DCT coefficients present in a JPEG file in each micro block to sets of 8×8 pixels. The injection of signature coefficients into the upper DCT regions allows for any of the basis functions shaded red to be used as part of the reconstructed micro block. This is the underlying cause of the distortions introduced by watermarking and the appearance of checkerboard-like distortions.

present for the same value of α. This gives an improved PSNR, as there are less differences between the watermarked and original host image. Even if a different shape was used for the ROI and the number of watermarks increased to fill the entire image, the ROI watermark system would still outperform Lin and Chang's Method as there still remains less area containing a watermark.

5.3 Compression Effectiveness

5.3.1 Aim

Earlier testing found that the ROI watermarking system and the method proposed by Lin and Chang could survive acceptable levels of DCT quantisation. This was a specific JPEG distortion, but did not include the entire set of distortions encountered during the complete JPEG compression process. This test will ensure that both the signature contained in the ROI and the surrounding outside watermark can survive acceptable levels of complete JPEG compression including DCT quantisation. Entropy coding of the DCT coefficients is a lossless compression and decompression stage which is also tested. As a side issue, the extent of lossy JPEG-2000 compression which can be applied without loss of watermark is also tested.

5.3.2 Hypothesis

The watermark robustness testing found that the Embedding Strength, α was a good indication of the expected survival rate to block-based DCT quantisation distortions. Hence it can be assumed that as α is increased, survival of JPEG compression may also be greater. Complete JPEG compression involves introducing additional distortions that are not accounted for during the quantisation testing process. These distortions include integer rounding and decimation, which occur in the JPEG decompression process. Additional rounding and decimation should lead to an increase in the error rate between the signature and watermark if the same threshold, $\pi_0 = 85\%$ is used to discriminate a match. A loss in compression performance could be expected. Additional error should lead to decreased robustness to compression at comparable quantisation levels.

Additional errors are found during the JPEG decompression process, which is the reverse of the encoding process. Please refer to Appendix C for useful flow diagrams that depict these processes. Such errors include rounding and decimation when image micro blocks are converted to 8×8 pixel sets and must be converted back to 8-bit integer values. It is not anticipated that the lossless JPEG compression stage of Huffman encoding (Huffman 1952) will result in any loss of watermark as no changes take place to the encoded coefficients.

As an additional blind test, survival to JPEG-2000 compression is dependent on the ability of the JPEG-2000 compressor to encode the signal represented by the watermark. There are two problems which make this difficult to guess. Firstly, JPEG-2000 is known to have superior bit-rate performance to conventional JPEG, so the overall picture could be encoded more efficiently and should require fewer bits. Secondly, the authentication system is based on the DCT that has been designed to survive conventional DCT-based JPEG compression.

5.3.3 Methods

JPEG-based image compression algorithms include both the JPEG and JPEG-2000 standards. Compression testing involves converting the source image into a file and uncompressing again to extract the watermark. JPEG compression includes 3 common

processes including transformation, quantisation and entropy coding. The decoding process is simply the reverse of the encoding method, to recover the reconstructed image. These processes are illustrated in Figure 5.10.

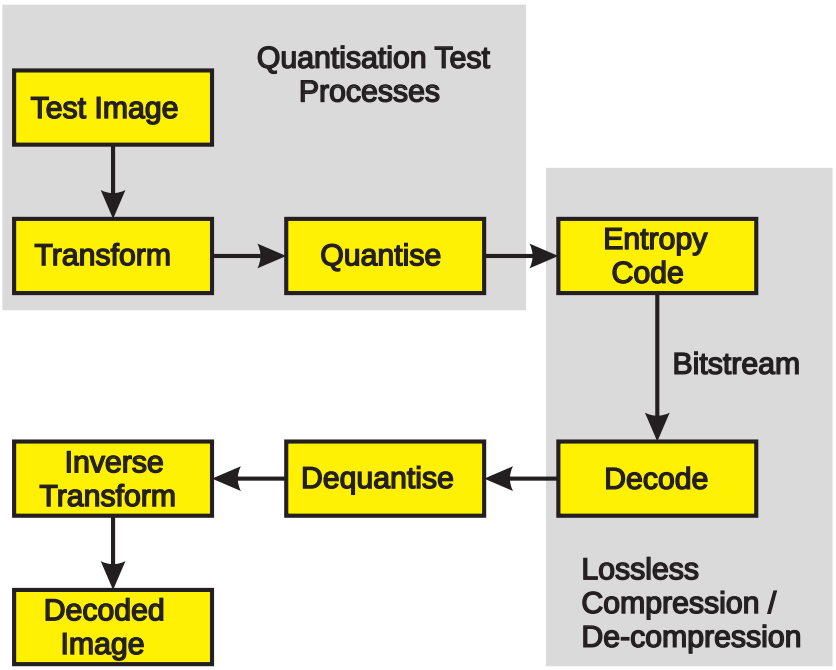

Figure 5.10. Stages of the JPEG compression and decompression process. The purpose of transforming the original image is to decorrelate the energy of the image into coefficients. This makes it possible to eliminate coefficients that are relatively unimportant. Scalar quantisation reduces the amount of data used to represent the image information by limiting the number of possible values that the transformed coefficients may have. At this point the image can no longer be identically reconstructed. Entropy coding is a reversible compression process that maps the quantised coefficients into a set of symbols, based on the probability of occurrence. Huffman coding is used for conventional JPEG. The top region shaded in grey depicts the first three stages of the JPEG compression process used for the quantisation testing. This was necessary as the quantisation stage is the most likely point of error as it introduces most significant change to the image, as all coefficients are scaled and quantised. The region shaded on the right highlights the lossless compression stage, which should not introduce distortions to the watermark or signature. Final conversion to reconstruct the compressed image introduces additional rounding and decimation error when DCT coefficients are converted to pixel values.

The images that have been used to test performance and make comparisons between systems include a sample set of 500 uncompressed greyscale medical images with resolutions varying from 512×512 to 2048×2048 pixels. These were saved as bitmap (BMP) images with a encoded bit depth of 8 Bpp.

Embedding strengths of 0.62, 0.88 and 1.4 are used that correspond to expected survival of the watermark given the target bit rates. These are tested for watermark survival to complete JPEG compression over a range of 0.1 to 2.0 Bpp. Survival of the watermark is reflected in the percentage of images detected as authentic. The system to test the compression effectiveness is illustrated in Figure 5.11. JPEG-2000 compres-

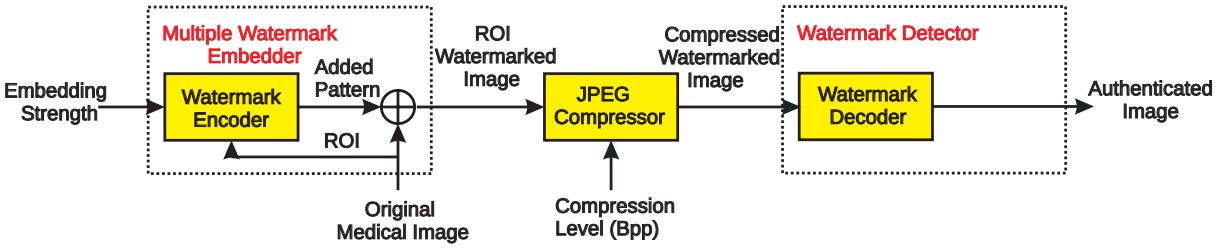

Figure 5.11. System to test watermark survival to compression. A fixed embedding strength, α is used to embed a ROI watermark in a sample set of images using the same process used for the quantisation testing in Section 5.1.3. Watermarked images are compressed from 0.1 to 2.0 Bpp. A threshold of at least 85% matching bits is required for the resulting image to be authentic. This process is repeated with a JPEG-2000 image compressor.

sion testing also took place as there was potential for both compression systems to be used at the low target bit rate of 1.0 Bpp, yet maintain survival of the watermark. Images were watermarked with $\alpha = 0.88$ corresponding to a level expected to survive conventional JPEG compression of 1.0 Bpp. Success is determined by survival of the watermark to JPEG-2000 compression at this compression level.

Image Compressors Used

Two types of JPEG image compressors are used. For the purposes of conventional DCT-based JPEG compression, a compressor is provided by the Matlab Image Processing Toolbox. This is a good system to use, as it performs floating point arithmetic, except when DCT coefficients are rounded and when pixel values are clipped and rounded during the JPEG decompression process. Hence errors that are introduced

to the system have been accounted for. Precision is limited to 0.05 Bpp for the baseline JPEG compressor. The type of JPEG-2000 compression used is an implementation of Part 1 of the JPEG-2000 standard. It is designed to be fully conformant with "profile-1," "class-2," as specified in Part 4 of the standard. The software was developed by Taubman and Marcellin (2001) in an implementation called Kakadu. Irreversible lossy JPEG-2000 compression is used and the bit rate specified to the compressor directly as a floating point number.

5.3.4 JPEG Compression Effectiveness Results

The ROI watermarking scheme was tested against Lin and Chang's semi-fragile watermarking algorithm for survival to complete JPEG compression, shown in Figure 5.12.

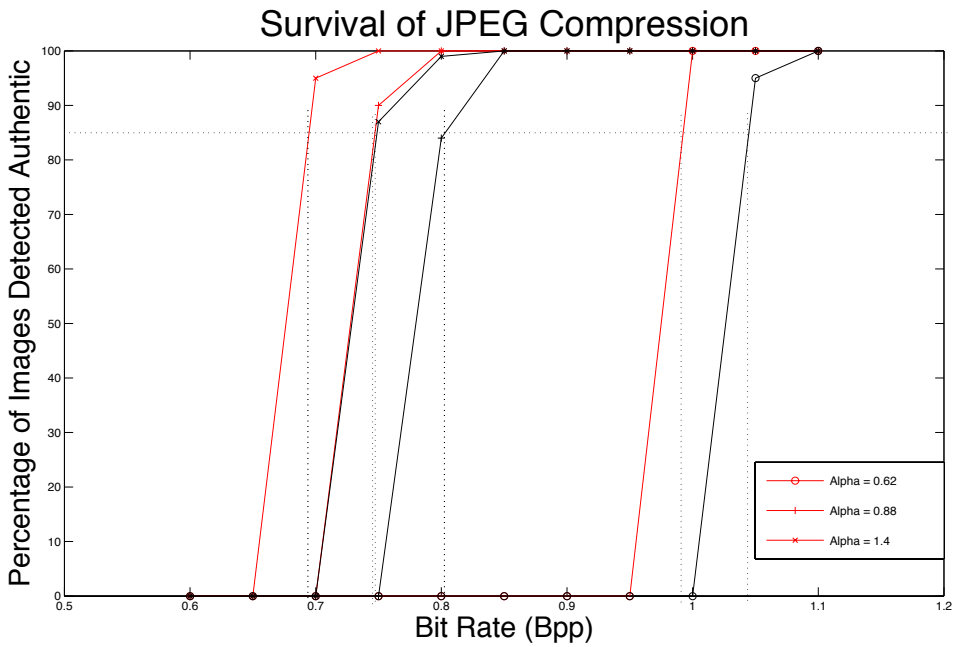

Figure 5.12. Compression results for the ROI watermark method and Lin's algorithm. To analyse robustness to JPEG compression, the three embedding strengths of 0.62, 0.88 and 1.40 are used. A threshold of 85% matching bits in the signature and watermark is used to discriminate a match. 85% of the images must also be detected as authentic for system success. Unlike the quantisation test, fewer bits per pixel (Bpp) are indicative of survival to greater amounts of compression. Watermark survival of both systems is shown to increase with the embedding strength, α. The ROI watermark system is shown in red, for comparison to Lin's method in black. For $\alpha = 0.62$, the ROI watermark survives bit rates no lower than 0.99 Bpp. At an increased embedding strength of 0.88 authentication is possible for bit rates of 0.75 Bpp and above. Increasing the embedding strength to 1.40 maintains ROI watermark integrity at bit rates down to 0.69. The ROI watermarking scheme can survive greater levels of JPEG compression and achieve smaller bit rates than for Lin's method at each for each embedding strength used. For $\alpha = 0.62$, Lin's approach survives bit rates no lower than 1.04 Bpp. At an larger embedding strength of 0.88 authentication is possible for bit rates of 0.80 Bpp and above. Increasing the embedding strength to 1.40 maintains survival of Lin's watermark at bit rates down to 0.75 Bpp. To summarise, for $\alpha = 0.62$, 0.88 and 1.40 the ROI watermark outperforms Lin's method by allowing the bit rate to be exceeded by respective levels of 0.05, 0.05 and 0.06 Bpp.

5.3.5 JPEG-2000 Compression Effectiveness Results

Results to JPEG-2000 compression are shown in Figure 5.13.

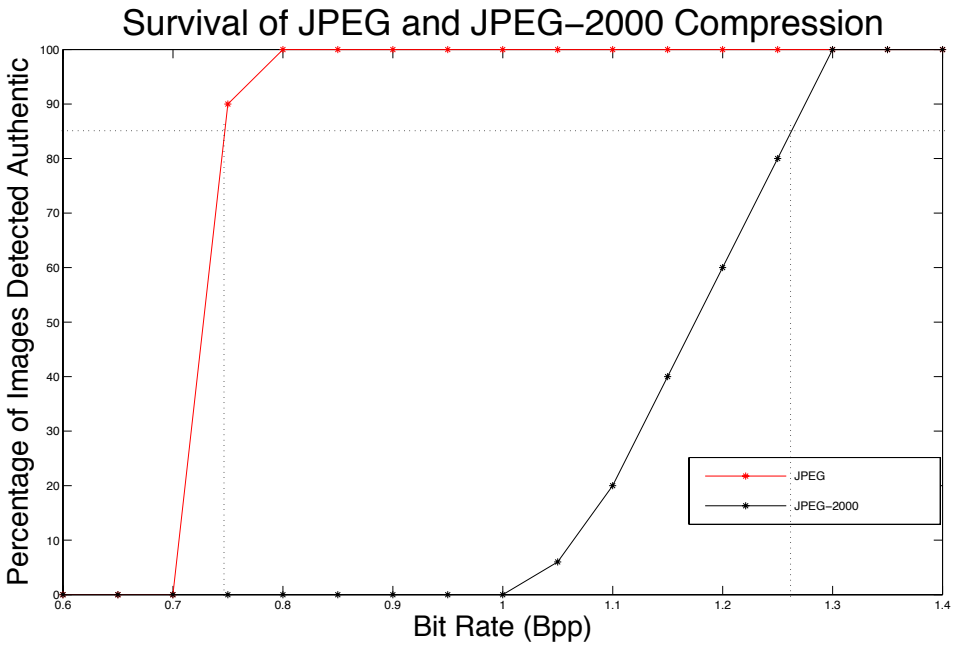

Figure 5.13. Compression Results for JPEG and JPEG-2000. Compression was applied to the same set of ROI watermarked works used for the conventional JPEG compression test. It is apparent that survival to JPEG-2000 compression fails when the compression level is between 1.2 and 1.3 Bpp. Hence the watermarking method fails to authenticate JPEG-2000 images compressed to target bit rates of 1.0 Bpp. To the contrary, survival to baseline JPEG compression is a success as the watermark can be compressed 0.3 Bpp past the expected survival rate of 1.0 Bpp. Survival to JPEG-2000 compression was found to be independent of α.

5.3.6 Comments and Discussion

The ROI watermarking system and the method proposed by Lin and Chang (2001) are able to authenticate conventional JPEG imagery to specified bit rates that are dependent on an appropriate choice of α. Compression performance of the ROI watermark method is shown to consistently outperform Lin's method. The most likely reasons have been addressed in the quantisation tests, which include increased robustness resulting from using a smaller signature for the ROI technique and the use of multiple watermarks. The increased performance is most likely to be for the same reasons, as

the compression tests only introduce extra rounding errors than for the quantisation testing because of the additional conversion from transform to pixel format. These errors appear to be insignificant, as the compression levels obtained correspond well with the quantisation levels found in the robustness testing. Significant rounding error would otherwise reduce the compression performance.

Research has shown that medical imagery can be compressed near-losslessly and without loss of diagnostic information if it is compressed to a bit rate of 1.0 Bpp (Slone *et al.* 2003), (Kocsis *et al.* 2003a). The most appropriate choice of α would be 0.62, as the ROI watermark system fails very rapidly after this threshold shortly after the target bit rate of 1.0 Bpp. This would eliminate the undesirable outcome of the watermark surviving unacceptable and excessive compression levels when larger values of α are chosen.

To the contrary, JPEG-2000 Compression effectiveness was not a success, as bit rates above 1.3 Bpp were required for survival of the ROI authentication watermark. As this compression standard is comparatively much more complex than baseline JPEG, it would not be considered cost-effective to compress the DCT-based authenticated images using this method. The only logical reason for poor JPEG-2000 watermark survival is because authentication information is embedded in the micro block DCT transform domain, which is specifically designed for survival of DCT quantisation. As JPEG-2000 is based on the DWT, survival of the watermark can only result if lossless or near-lossless compression levels are used, which require larger bit rates. This will ensure that pixel values remain unchanged and the watermark is retained.

5.4 Chapter Summary and Open Questions

The results of testing the performance of the ROI watermarking system are promising. They show that the technique outperforms earlier methods with improved robustness, image fidelity and compression performance. The JPEG quantisation tests have shown that the watermark will remain embedded in the image after increased levels of JPEG quantisation are used if the ROI watermark system is adopted rather than the proposed approach by Lin and Chang.

This would appear to be a significant result, as greater than anticipated signal distortions can be applied without loss to image quality as essential feature information is

retained. Improved quantisation performance would appear to be a result of adopting a ROI watermark approach, rather than embedding into all regions of the image.

A smaller signature implies that there are fewer bits that can be corrupted, which is reflected in increased robustness to quantisation. Watermarking is also much more efficient as fewer bits are required to authenticate the important region of a medical image. For example, if the ROI is chosen to occupy 20% of the original image, then only 20% bits are required for authentication of this region, rather than the entire image. However if many watermarks are used, an increased signature payload will be required for authentication. Investigating the false error probability for authenticating an unacceptable image with a false watermark has shown that that this probability is extremely small and does not present a significant problem.

Image fidelity has shown to be significantly improved over Lin's method with improved PSNR at all embedding strengths and when 1 to 8 watermarks were used, with fewer watermarks resulting in improved image quality. This raises an interesting question. If it were possible to increase the watermark capacity so that more signature bits could be embedded over less image area, then would this result in improved image quality?

ROI watermarking is shown to survive optimal levels of baseline JPEG compression and can maintain an authentication watermark at slightly greater compression levels than for the technique proposed by Lin and Chang (2001). This is the ultimate test in demonstrating complete survival in a wireless application as all legitimate distortions applicable to complete compression processes have occurred while maintaining watermark integrity. Although survival to lossy JPEG-2000 compression was not a success, an interesting question is, would it be possible to embed the watermark in a different way so that survival would be possible with a compression level of 1.0 Bpp? One way to approach this problem that may result in increased JPEG-2000 compression robustness would be to embed the authentication information in lower spatial frequency DCT coefficients of the JPEG zigzag scan. This may be an effective remedy, as signature information contained in these regions would be retained by more perceptible basis functions, shown in Figure 5.9. These could be removed less easily by the low-pass filtering characteristic of JPEG-2000 compression, which could be expected to conserve

the watermark at lower bit rates. Embedding would be required much closer to significant low frequency DCT coefficients, which may also compromise image quality.

5.4.1 Possible Improvements

Some of the experiments could have been tested in ways that may have given more realistic or slightly different results. Both the quantisation and compression tests have specified the ROI to be rectangular and based at the center of the test image occupying 20% of the image area. This had the benefit of allowing 8 watermarks to be embedded around the ROI, but did not provide for circumstances when this region was located near the image edges. This could have reduced the number of watermarks in test situations where the ROI was placed in an image corner, which would have resulted in 3 watermarks. One of the pressing questions is whether or not having a fewer average number of watermarks would be expected to change the results significantly?

Both the robustness and compression tests have demonstrated improvements in performance over earlier methods, however this has most likely been a result of a smaller authentication signature leading to fewer bit errors between the ROI features and the watermark after distortions had been applied. Multiple watermarks may have led to marginal improvements in quantisation and compression performance, however all of the watermarks are expected to degrade at a similar quantisation or compression levels. Hence having fewer watermarks by changing the position of the ROI in the image may not significantly change the existing results when the ROI is set to the image center. One way of rectifying this experimental limit would be to set the position of the ROI as a random variable containing of all of the possible values that one location within the ROI could take. This position could be used as a reference point. Ideally the size of the ROI should have been specified to vary within some acceptable range or limit. However such range is highly unpredictable and the ROI has been specified to occupy 20% of the image area, which represents a typical size for this region in a medical image.

One last area that could have been improved would be the method to compare the signature and watermark. These sequences were compared on a bitwise pair basis. A preferred option may have been to determine the cross correlation between the two

sequences S_1 and S_2. This would have the capability to compensate for errors involving a loss of part of the signature or watermark. Fortunately this type of loss is highly improbable, as errors resulting from acceptable image distortions typically only cause bits to flip their value.

Chapter 6

Conclusions

WIRELESS communication technology is one of the most rapidly expanding areas. The cost of transmission bandwidth is falling and data can be encoded optimally for many types of wireless communication channels. One of the most pressing challenges facing this technology are techniques to verify data integrity, particularly if the content contains critically important information. Embedded watermarking has been presented as a method to verify medical image data for this application. In this chapter a conclusion to the work presented in this thesis is drawn. Essential conclusions are presented in Section 6.1 and a summary of original contributions in Section 6.2.

6.1 Core Conclusion

Wireless telemedicine has recently proven to be an efficient and cost-effective method for diagnosis and improved specialist medical treatment to remote locations. This technology demands effective standards and quality assurance measures to be available for implementation to the user. This is especially important for the end application of teleradiology that involves the transmission of wireless medical images. Such standards are considered as a sign that the technology has reached full maturity and can be designed, implemented and deployed with less concerns for the integrity of transmitted data. Many medical images can be segmented into diagnostically significant regions and less important regions. Research focus has been to ensure image quality detailing embedded watermarking to verify the integrity of critically important diagnostic features, given the challenges and constraints of a wireless communications system.

Careful attention has been given in the design to minimise costs by facilitating the re-use of existing communications infrastructures and widespread consumer and specialist image compression standards. Cellular technology has been shown to be one of the most practical and feasible options when used in conjunction with baseline JPEG image compression.

Wireless transmission of images used in teleradiology is shown to be most rapid and effective when maximum acceptable compression levels are used. The authentication watermarking system presented is shown to maintain compatibility with JPEG. This work has optimised the speed of transmission by ensuring that the medical image authentication system is suited to the best possible bit rate, given the maximum permitted image compression level. Attention has been given to minimise degradation in diagnostically significant regions by embedding authentication information for two-level verification into the ROB.

Performance testing of the authentication watermarking system has been promising. The method presented outperforms earlier techniques with improved robustness, compression performance and image fidelity. Resilience to JPEG compression shows that the watermark will remain embedded in the image after increased levels of JPEG quantisation are used if the ROI watermark system is adopted rather than earlier methods.

Improved robustness would appear to be a result of adopting a ROI watermark approach, rather than embedding into all image regions. A smaller signature would suggest that fewer bits can be corrupted and this is reflected in an increased robustness. Image fidelity has shown to be significantly improved over earlier methods, with improved PSNR at all watermark embedding strengths used (Osborne *et al.* 2005b).

6.2 Summary of Original Contributions

The original contributions which have been presented in this thesis are highlighted in Chapter 1. To summarise they include:

1. **A Novel Technique:** A useful development in watermark technology that allows critically important feature information to be verified without introducing embedding distortions into diagnostically significant locations. Authentication information is taken from these regions and placed in less important image locations. Losses introduced into the ROI will correspond with a watermark mismatch in the ROB.

2. **Improved Performance Over Earlier Methods:** This method is shown to have superior robustness to DCT quantisation as well as complete JPEG image compression than for earlier methods. Image fidelity has also been significantly improved with less distortion introduced when watermarking embedding is used at a comparable capacity per image area compared to earlier methods.

3. **Optimised JPEG Survival Levels:** A user may specify a compression level up to where authentication must be made. This can be varied depending on the desired end application.

4. **The use of multiple robust watermarks**: The advantage being that the image can be clipped, yet is still able to be authenticated. If one watermark fails another may be used.

6.3 Chapter Summary

Conclusions have been presented as a summary of the thesis including the research problem and objectives as well as the method taken to address the challenges. Key

areas of the thesis have been highlighted as well as a concise summary of original contributions. The next chapter presents some future work for this research area as well as some promising end applications for this technique.

Chapter 7

Recommendations

FUTURE research directions are presented in this chapter as well as some potential applications, which could employ the authentication watermarking technique presented in this thesis. An approach to increase the watermark capacity is shown in Section 7.1. Measures that could be taken to improve the approximation of the point of watermark failure are discussed in Section 7.2. Protocols to identify and recall the ROI location are shown in Section 7.3. The challenge of multiply defined or non-rectangular regions of interest is presented in Section 7.4. Future work possibilities tailoring the watermark authentication system to acceptable levels of noise introduced over a wireless link are investigated in Section 7.5. This also addresses the concern of delay and jitter that can occur in a packet switched network. A plethora of possible end applications is discussed including content authentication in Section 7.6, owner identification and proof and broadcast monitoring in Sections 7.7 and 7.8.

7.1 Increased Capacity Watermark

Watermark capacity refers to the number of bits that a watermark encodes within a given image area. This definition does not state that these bits have to be unique, hence a repeated multiple watermarking method is valid for this definition. An interesting question is whether improving the capacity of the watermark will provide greater verification of the content of diagnostic features. More specifically this question addresses the importance of two variables, including the amount of feature information extracted from the ROI and the payload of information embedded into the ROB. An increased capacity may be required for the fulfilment of future standards that may define thresholds to the capacity of authentication watermark systems used in medical practice.

As specified in Section 4, the authentication watermark system extracts four bits from the most significant coefficients in the ROI, which are embedded multiply into the ROB as parts of separate watermarks. The generation of signature values is based on a relative size comparison between coefficients in the ROI.

To verify the integrity of the ROI DCT coefficients in the most complete way possible would involve extracting all of the bits that represent the picture information for the payload to a surrounding watermark. Assuming that 10 bits are used to represent each DCT coefficient (including a sign bit) and 8 coefficients are used to extract a signature, this would require 80 bits to be extracted from every micro block. It would be particularly challenging to attempt to embed this much information for the following key reasons:

- The capacity of the current watermarking method is limited to one bit per group of 7 coefficients, out of a total of 28. This limits the watermark capacity to 4 bits per micro block.
- Embedding significantly more information into the image may have the adverse effect of decreased watermark robustness as a consequence of increased numbers of watermark bits flipping their value.

If it were desired to increase the watermark capacity so that greater amounts of signature information could be placed into each micro block of the ROB, it may be possible to modify the algorithm in two ways. Firstly the number of coefficients used to contain an embedded bit, b_e could be reduced from 7 to one coefficient per bit. This would

increase the watermark capacity from 4 bits per micro block to 28 bits per block. If a greater watermark capacity was still required, it may be possible to embed more than one bit into a coefficient. This could be made possible by flipping more than one bit in the binary representation of a coefficient. The benefit of significantly greater watermark capacity would probably be outweighed by reduced survival and robustness to compression-related distortions.

Embedding a greater number of bits per ROB micro block for a systematic implementation requires modification to the sub-system that embeds four bits into a micro block. This could be implemented as shown in Figure 7.1.

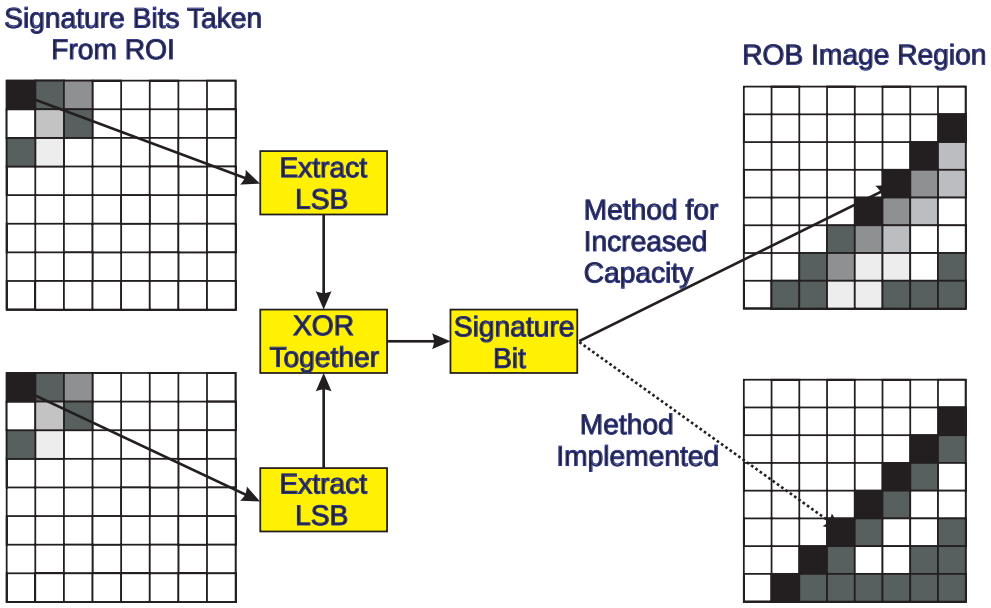

Figure 7.1. Alternative method to increase watermark embedding capacity. This option has the benefit of reducing the area required to embed a watermark by improving the capacity of the authentication system. A watermark bit, b is embedded into a group of 7 DCT coefficients by ensuring that the exclusive-or of the LSB's of each of these is equal to the signature bit, otherwise a bit is flipped. The watermark capacity can be increased by embedding b into fewer coefficients, such as four coefficients which is depicted in this diagram. This allows for 7 signature bits to be embedded into a micro block instead of 4, as there are 28 coefficients available for embedding. This increases the overall watermark capacity, but would be expected to be traded off with other system parameters, including decreased robustness to compression.

Table 7.1. Expected and actual compression survival levels. One of the challenges of the current implementation of this work is the uncertainty of the compression level where the watermark system will fail. This is a factor that is dependent on the image, embedding strength α and the threshold used to detect an authentic watermark.

Embedding Strength α	Expected Survival Level (Bpp)	Actual Survival Level (Bpp)	Difference (Bpp)
0.62	1.20	1.04	0.14
0.88	1.00	0.80	0.80
1.40	0.80	0.75	0.05

7.2 Improved Approximation to Target Bit Rates

Another intriguing area of this work that may require further scrutiny is the approximation used to select quantisation table multipliers for this system. In Appendix A a relationship was established between the amount of quantisation used and the average level of expected compression obtained. This provides some approximation to appropriate levels of quantisation and embedding strength parameters that were used to optimise system performance over the target bit rate of 1.0 Bpp. The alternative and more accurate approach may be to analyse individual images to determine the compression level resulting from variable quantisation levels. This is because the compression-quantisation relationship is specific to the image used. A broad selection of image types and resolutions were chosen so that an average quantisation-compression curve was determined for an approximation to the embedding parameter α. Determining this parameter on an individual image basis would be expected to increase the overall system complexity by increasing the number of computations required, but may be preferred for a more accurate choice of α. This factor was dependent on the watermark failure point at a given compression level, where greater α led to increased watermark survival. The previous chapter did not provide measures to ensure that the watermark would fail shortly after this level was surpassed. This problem may have been underestimated as it is equally important that the watermark fail when unacceptable or excessive compression levels are used (Osborne *et al.* 2005a). Expected and actual survival levels for ROI watermark compression performance are illustrated in Table 7.1. There is shown to be a difference from the actual and expected points of watermark

failure depending on the choice of α. It may be more appropriate to optimise the algorithm for individual images. This could be expected to give a more accurate choice of α, which would decrease the error shown in Table 7.1. Hence the point of watermark failure could be predicted more easily. Assuming that the ROI has been appropriately defined, the algorithm could be modified in the following way:

1. Perform JPEG compression on the target image to determine the multiplier to the quantisation table Q, that results in a target bit rate of 1.0 Bpp. Leave the image uncompressed. Use this value to estimate the embedding strength α.

2. Embed the authentication information into the image using the value of α as the embedding strength. Test the image to JPEG compression by compressing it to the desired bit rate and test for the positive detection of a watermark.

3. If it survives the test, then lower the choice of α and repeat the first two steps. An optimised choice of α should result in the positive detection of a watermark, but should result in a negative detection when the desired bit rate is exceeded beyond an acceptable threshold. This would have to be appropriately chosen based on the acceptable levels of JPEG compression, for example 0.8 to 1.2 Bpp is taken as an acceptable range used in this thesis. Hence 1.0 Bpp should result in the positive detection of a watermark, but any level beyond 0.8 Bpp should result in loss of the watermark.

The only trade-off to make would be a slight increase in system complexity and time to encode the watermark resulting from a repetition of watermark embedding processes that would otherwise only be implemented once.

7.3 Automated ROI Identification and Location Recall

Any type of authentication system is most effective if it is designed to be minimally invasive and transparent to the user. Watermarking has previously been used on mammograms without interfering with automatic feature detection methods (K. Engan and Josefsen 2003). One of the most useful tools to complement this type of system could be the automated mechanism for ROI identification. A known image could then be

be authenticated and transmitted without prior analysis by a specialist. Specialised software could be used to discriminate the ROI from the ROB and may require a prior knowledge of the image type for the analysis involved. For example, methods have been presented to detect cysts in a sonographic images (Janet *et al.* 2005), skin lesions using gradient vector flow snakes (Erkol *et al.* 2005) and circumscribed masses in mammograms (Herredsvela *et al.* 2005).

Automated image segmentation processes have the advantage of avoiding the need of manual inspection. This would be cost-effective for wireless teleradiology as it would allow for a ROI to be determined automatically and could minimise the number of tasks required by specialists. Figure 7.2 provides a flow of how these automated systems would operate. Recalling the location of the ROI in the original image is also a

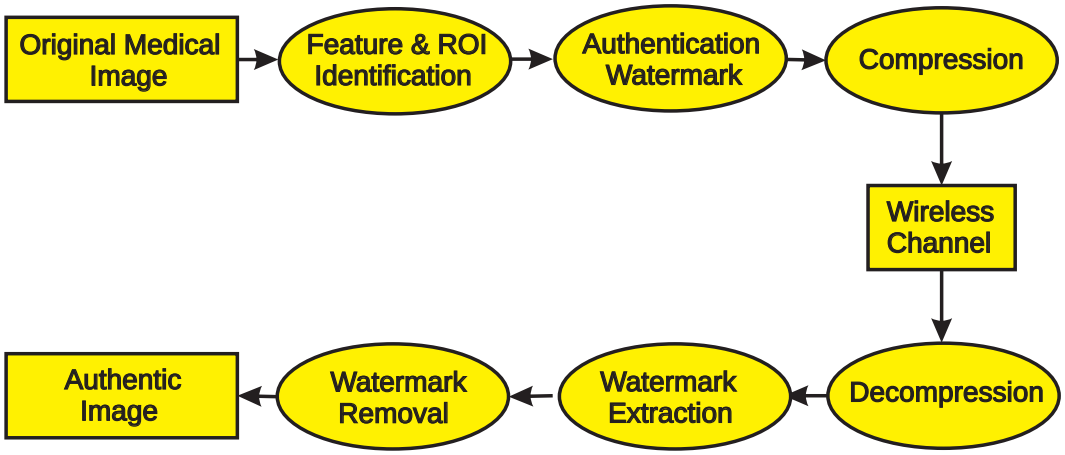

Figure 7.2. Automatic feature and ROI identification. System flow diagram used to depict the ideal flow of authentication processes desired for the overall system to be as transparent as possible to the end user. Ideally this would involve only the acquisition and viewing of the image without the need of identification of the ROI by a specialist.

challenge which was not raised in this thesis. A ROI watermark demands a known diagnostic region at transmitting and receiving ends of the communication channel. This is particularly important at the receiving end where there must be knowledge of the ROI location in the image. This information must also be transmitted in the channel and could be instigated in two ways, including:

- Appending the ROI location information the end of the JPEG file or within the encoded file structure. For example, stored this information in the JPEG file header.

- Embedding the location information in known positions as part of the authentication watermark.

It is preferable to design the authentication scheme to be as transparent as possible to image transmission and acquisition modalities. For these reasons, it may be more desirable to transmit region information as part of the watermark in a known position not containing the ROI. This would be transparent to the user as it would not require prior knowledge of the ROI to be entered manually. It would also avoid modification to JPEG compression standards by appending extra information to part of the encoded file structure.

A rectangular ROI could be specified by four numbers that define the top, bottom, left and right edges. Assuming typical image resolutions, these could be contained in a maximum of 4 digit integers each. Hence 16 integers would be required, corresponding to $16 \times 3 = 48$ bits. This could effectively be stored as a semi-fragile watermark in 12 micro blocks assuming that an embedding payload of 4 bits per micro block is used. Alternatively all the micro blocks contained in the image could be numbered by in such a way that the ROI could be specified by an index. Large medical image resolutions imply that there will probably be thousands of micro-blocks and this will still demand that valid edge points of the ROI are specified.

Alternatively, an algorithm could be used to discern between watermarked and unwatermarked regions. Such an algorithm would be quite simple, especially if it is comparing DCT coefficients that may contain a watermark. Regions that do not contain authentication information would be characterised by containing DCT coefficients with a high probability of being zero after integer rounding, while watermark coefficients would be apparent as highly localised independent values. As discussed in Section 4, these will result from flipping of the LSB of a DCT coefficient and multiplication with the necessary quantisation value to maintain b_e after JPEG compression.

7.4 Multiple or Different Shaped ROI

In some diagnostic images, there may be essential feature regions defined in multiple locations. This presents an especially challenging problem as it may no longer be feasible to embed watermarks into the outside regions that are comparable with the size of

the ROI. This would result from limited image resolution. Authentication of another ROI may require that the existing method be modified so that the watermark occupies less area. A useful way of making this possible could be to adopt an approach proposed by (Wakatani 2002), who introduced the idea of placing multiple watermarks around a ROI by wrapping them around in a spiral-like manner shown in Figure 7.3. If there is still insufficient space available for placement of a singular watermark, it

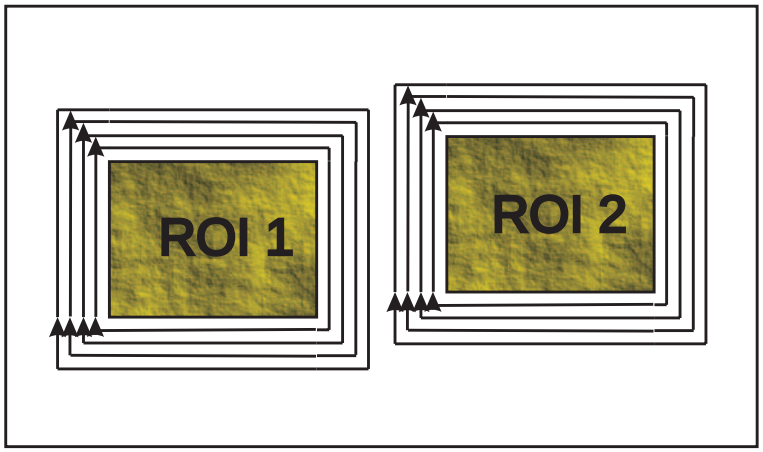

Figure 7.3. Wrapping the watermark around the ROI. An exceptional case where two ROI's must be defined. For this type of image, both regions need to be authenticated and this can only result if fewer watermarks are used or a 'wrapping' style is adopted.

may be necessary to increase the capacity of the watermark as described in Section 7.1. A reduction in the required watermark area would be made possible, but may have to be traded off with other system parameters such as watermark robustness.

Another more complex problem may involve the selection of a non-rectangular ROI. This presents an interesting challenge as it may be impractical to embed in the same shape of the ROI. This challenge is depicted in Figure 7.4 with an elliptical ROI. One way to authenticate this region and minimise the complexity involved could be to translate the ROI into a rectangular region of closest fit. All of the micro blocks contained in the rectangular region would then need to be authenticated. This approach may be more cost-effective than using complex micro block numbering and reference systems that define the ROI, which would also have to be transmitted with the watermarked JPEG file.

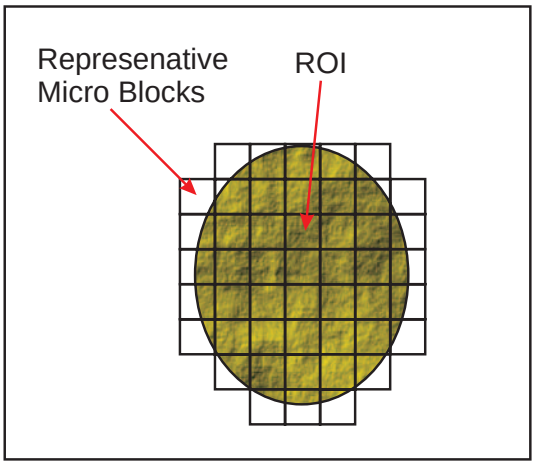

Figure 7.4. An elliptical ROI. A non-rectangular ROI can be represented by a localised set of micro-blocks whose number and position are more complex to determine than for a rectangular ROI. This would have the disadvantage of requiring the additional transmission of the ROI location, which could be more difficult to define than for a rectangular region.

7.5 Robustness to Channel Noise

Critical examination of a typical wireless mobile channel suggests that the introduction of noise to the transmitted image may compromise its integrity (Osborne *et al.* 2004a). Future work needs to investigate the effect of channel noise on the proposed watermarking scheme as this has previously been shown to be a problem that could result in image degradation. Image authentication methods have been presented in literature to survive losses in wireless environments. One such work was by Sun *et al.* (2005), who proposed an authentication scheme to survive both lossy compression and packet losses. As outlined in Chapter 1, medical images are highly important and these types of losses should be treated with much caution as they may lead to an erroneous diagnosis (Osborne *et al.* 2004c).

There are a number of very important questions that need to be addressed to quantify the degree of acceptable loss over a mobile channel. It would be assumed that these losses would result from errors that are not corrected through the channel coding process. The probability of this type of loss occurring is quite small given the superior FEC methods that are available. Moreover, the probability of this type of loss occurring without perceptible loss is very small. It may be desired to quantify acceptable levels of introduced noise to the transmitted image and ensure that the authentication

scheme does not survive noise distortions beyond this threshold. The analysis of noise in a JPEG compressed medical image may be especially hard to determine given that:

- Natural levels of noise may already be present in the medical image.
- Lossy JPEG compression schemes will introduce additional noise to the image.
- If the loss introduced over the mobile channel is very minor, it may be challenging to differentiate between noise introduced through JPEG compression and that introduced over the channel.

Hence the noise introduced to the overall image, N_i is equal to the root-square-sum of the natural level of noise present in the original image, N_n, the noise introduced as a result of compression, N_c and the noise introduced over the wireless link, N_w,

$$N_i = \sqrt{N_n^2 + N_c^2 + N_w^2},$$

assuming the noise sources are uncorrelated.

Existing methods that have been reviewed in this thesis that have investigated thresholds to the compression bit rate used in medical images for more rapid wireless transmission (Slone *et al.* 2003).

If it were required to bound the acceptable level of noise introduced to the medical image over a mobile link, then a number of steps would be required:

1. The noise level found to correlate with the target bit rate would need to be evaluated.
2. Medical images could be compressed to the target bit rate.
3. Further noise used to simulate a mobile channel could be introduced to the images. Diagnostic loss could be interpreted subjectively by a group of specialists until an acceptable threshold is found. There are many software tools that could be used to model the noise over a mobile link including the Communications Blockset found in Matlab.

After finding a bound to the acceptable level of injected noise, modification to the existing authentication system may be required. This is outside of the scope of this thesis.

7.5.1 Further Wireless Considerations

The initial research focus of this thesis involved investigating the transmission of digital imagery to remote locations in the rural areas of Australia. Hence the most probable transmission modality would be expected to be based on a packet based mechanism rather than a circuit switched network. Two areas of concern for this type of transmission modality include the challenges of delay and jitter for the packets that are transmitted over the wireless link. This may be a concern that needs to be addressed for medical images if the order in which the packets are received differ from that which was originally transmitted. One useful area of future work could investigate the effect of the authentication watermark scheme in verifying medical image integrity given this possible scenario.

7.6 Content Authentication

Verifying data integrity with watermarking is part of the broader area of content authentication. This is continually becoming more of a challenging area as it is very easy to modify multimedia content. For example, digital images can be tampered with modern software in ways that are difficult to detect. The image authentication method presented in this thesis allows an authorised user to generate a secret feature sequence from a known source image, which can be compared to an embedded watermark. An adversary who may try to change the image cannot create a new signature and will either modify the ROI or the surrounding watermark which will not allow the image to be authenticated. Embedding signature information in the image is advantageous for any images that required authentication, as the signature could otherwise be lost. If this information was stored in the header of a JPEG file and the image was converted to another file format, the authentication information could easily be lost and image integrity could no longer be verified (Cox *et al.* 2001).

A design focus for robustness to JPEG compression distortions ensures that the watermark remains in the image over an acceptable range of compression levels which can be specified by the user. This ensures that the system is resilient to legitimate distortions but fails if illegitimate image distortions are applied. One potential application would be for authenticating JPEG image files in digital cameras. A user may choose to store and authenticate a more highly compressed version of a photograph stored on

his/her flash memory card. The level of lossy JPEG compression found in most cameras does not vary over a large range which allows for the authentication system to be tailored to the device.

7.7 Owner Identification and Proof

Textual copyright information is frequently used to identify the owner of a work. This has limitations as the text can easily be removed if it is copied. For example a person copying pages out of a magazine may forget to scan in the copyright notice in the footer. Textual copyright notices for images may also be visually obtrusive and may cover an area of the visual work. By placing this information in less critical regions of the image, they are more likely to be lost if the image is copied. Embedded watermarks are inseparable from the image they are authenticating and have an advantage over conventional methods of content verification that may append authentication data to the cover work. This makes it increasingly difficult for an adversary to remove or corrupt this information without degrading the watermarked image. ROI watermarking can be used to prove copyright ownership as well as identifying ownership without introducing distortions into crucial image regions. To achieve the level of security required for proof of ownership it would be mandatory to limit the availability of the watermark detector. Because the watermarking system requires a knowledge of the ROI location and the seed required to generate a signature, it is very difficult for an adversary to remove the watermark.

It may be difficult to prove the original owner if a watermarked image is filtered. Poor watermark survival to JPEG-2000 suggests that the scheme will be particularly frail against low-pass filtering distortions that quickly destroy the watermark. This is because the lossy wavelet-based compression processes retain greater low-frequency information and discard higher spatial frequency content. This may not result in perceptible image degradation, but may render the image unable to be authenticated without containing evidence of previously being watermarked. This is a challenge for the end application of owner identification and proof. One possible way that the algorithm could be modified so that any loss of watermark resulted in perceptible degradation of image quality could involve embedding the watermark in lower frequency DCT coefficients. This may prove to be a costly trade-off as this could not occur without degrading perceptually significant DCT coefficients.

7.8 Broadcast Monitoring

Broadcast monitoring is a method to ensure that advertisers receive all of the air time that they purchase. This was previously monitored with human observers to take subjective recordings of what was broadcasted. It is considered cost-effective to replace such systems with automated protocols. According to Cox *et al.* (2001), there are two types of broadcast monitoring that include active and passive monitoring systems. Passive monitoring systems function by reorganising the content that is broadcasted. A computer can be used to monitor broadcasts that can be compared to databases of known programs for identification without the requirement of transmitted side information. This has the disadvantage of complexity in comparing the received signal to a database. The signal is typically broken down to individual frames of video, which are used as signatures. As the wireless signal can be degraded easily and each frame contains millions of bits of information that can be used for a comparison, this process may be challenging to design, develop and deploy effectively.

Active monitoring systems rely on side information that is transmitted with the broadcast content. Encoded information has conventionally been placed in the Vertical Blanking Interval (VBI) for analogue television. This is transmitted between frames. One drawback is the disadvantage of its inability to survive format transformation from analog to digital. Embedded watermarking is a cost-effective alternative to ensure that side information can be coded for an active monitoring system for digital broadcasts. As analog transmissions are replaced with their digital counterparts, this approach is promising for the future. Effective channel encoding techniques will also ensure fewer transmission losses. Lower bit error rates will provide the opportunity to use embedded watermarking for active broadcast monitoring that may otherwise be difficult to implement without high margins for error.

DCT-based watermarking may be particularly favorable, as digital transmissions are based on the MPEG-2 standard for digital video compression, which is also based on the DCT. The breakdown of MPEG video to the DCT-based micro block level is depicted in Figure 7.5. One of the most challenging design criteria in deploying this type of monitoring system would be to ensure that the image quality has not been compromised to keep the end user satisfied. Image quality could be optimised either by keeping the embedding parameter α as low as possible or removing the watermark as

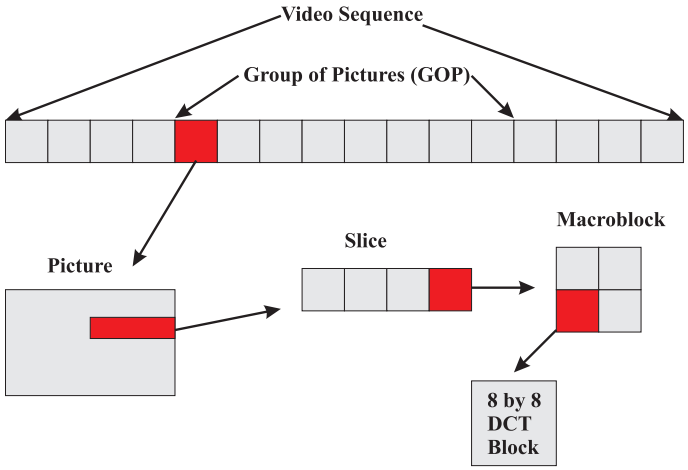

Figure 7.5. MPEG video at the micro block level. Digital video transmission of MPEG video is fundamentally based on the DCT. If the watermarking method is robust to this type of distortion, it could have potential applications for broadcast monitoring.

part of the MPEG-2 decoding process.

Ones such approach was investigated by Wang *et al.* (2000), who identified temporal regions of interest in video for embedding a watermark. However no watermark was placed within individual video frames.

7.9 Closing Comments

Wireless communication technology is expanding in application and areas that were not previously envisaged. Techniques to encode data for communication channels have reached maturity and have allowed for fast and efficient communication of a broad range of data types. Many applications may demand measures or metrics to provide quality assurance and verification of data content that has not previously been provided effectively by transmission alone. Wireless telemedicine is one application which has not reached full maturity and demands effective quality assurance procedures to verify critical data content. This thesis has shown that embedded watermarking can be used for this type of end application. This has helped pave the path for the evolving paradigm of wireless telemedicine. Cost-effective measures have been developed to verify critically important information within the framework of existing compression standards to optimise compatibility with current imaging systems.

Appendix A

Pre-Experimental Preparation

A Few pre-experimental processes and implementations are required to ensure correct system performance and optimise system parameters. These include a test that investigates the average relationship between compression and quantisation rates, which is shown in Section A.1. Preliminary quantisation tests have also been conducted to verify consistent behavior of earlier works found in literature as well as watermark functioning at the increased embedding levels used in this thesis. These experiments are shown in Section A.2.

A.1 Pre-Experimental Test

A relationship needs to be established between the amount of quantisation used and the average level of expected compression obtained. This provides some approximation to appropriate levels of quantisation, which gives an indication of the embedding strength parameter, α. This ensures that system performance can be optimised over the target bit rate of 1.0 Bpp.

A.1.1 Hypothesis

It would be expected that increasing the level of quantisation would on average reduce the number of DCT coefficients encoded in the JPEG bitstream. This should result in increased compression levels, reflected in a decrease in the bit rate for each image. Hence an inverse relationship is expected between the applied quantisation level and the resulting compression level or bit rate.

A.1.2 Test Process Involved

The test procedure used to establish this relationship is illustrated in Figure A.1 and is based on JPEG compression. The images used to establish this relationship include a sample set of 50 uncompressed greyscale medical images with resolutions varying from 512×512 to 2048×2048 pixels. These are saved as bitmap (BMP) images with an encoded bit depth of 8 Bpp. Floating point arithmetic has been used in all calculations. After the DCT coefficients have been quantised and rounded they are passed to the Huffman encoder. This was originally written by Karl Skretting (*Stavanger University, Signal Processing Group* 1999) and has been modified for use in this experiment. Quantisation levels ranging from 0.1 to 3.0 are used, which are expected to coincide with a bit rate of 1.0 Bpp at some point in this range.

A.1.3 Results

The average relationship between applied quantisation level and resulting compression is depicted in Figure A.2. See Figure A.3 for a closer inspection over the target bit rate.

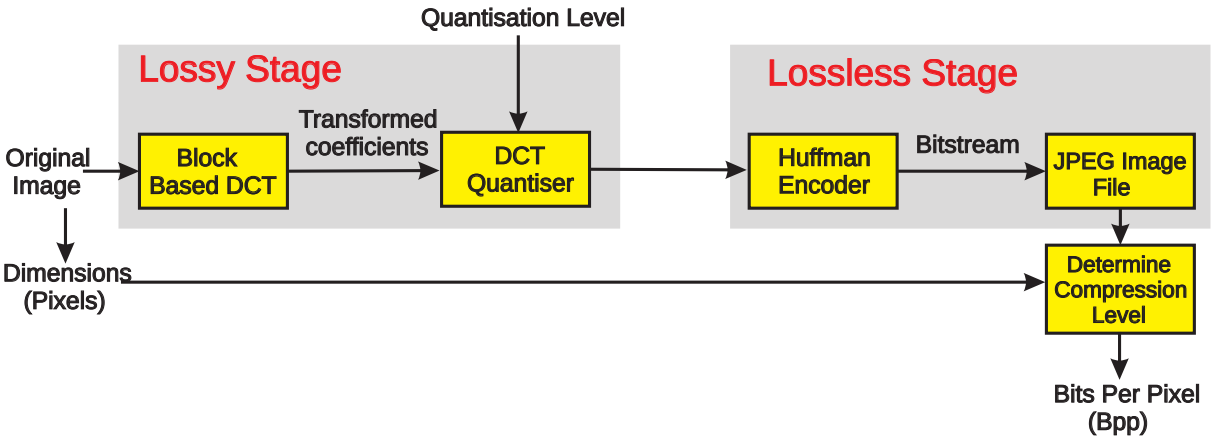

Figure A.1. Test used to establish a relationship between quantisation and compression. Two stages of the JPEG compression process are shown that include the lossy and lossless compression stage. The bit rate dependent on the level of quantisation used on each micro block. This is specified as an input parameter to the system and represents the multiplier used to the quantisation matrix, Q. The JPEG file consists of Huffman encoded DCT transform coefficients that have been rounded to integers.

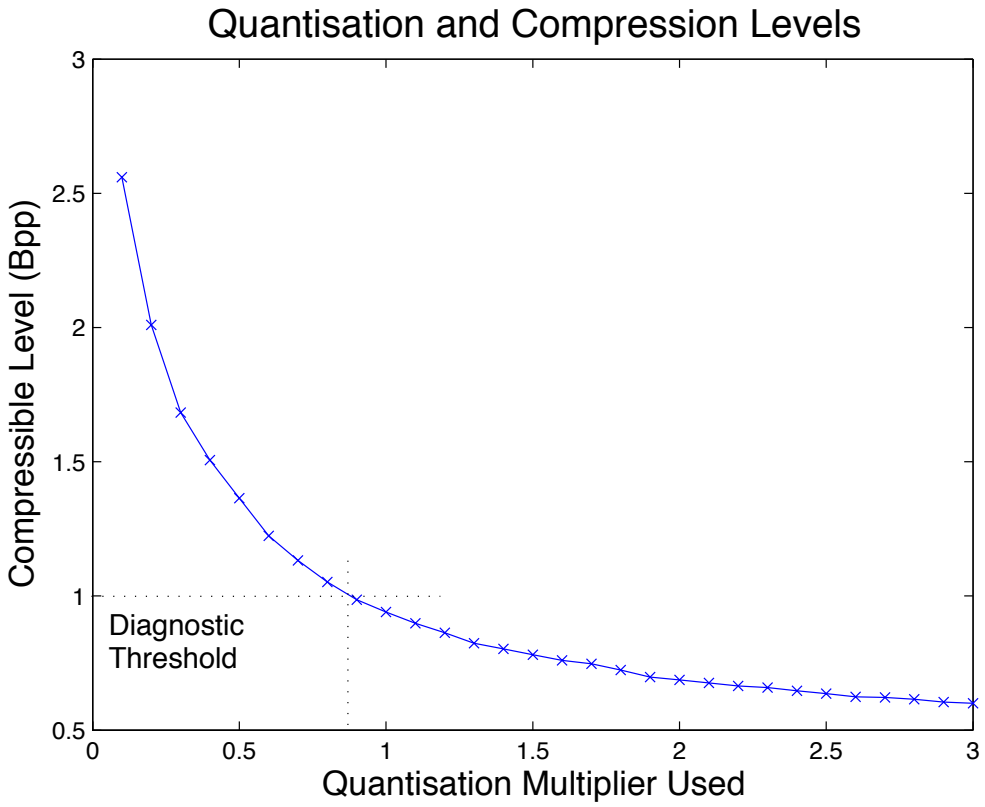

Figure A.2. Inverse relationship between quantisation level and bit rate. The quantisation multiplier varies between 0.1 and 3.0. This is inversely reflected in the compression level, which varies from slightly lossy (2.5 Bpp) to very lossy (less than 0.5 Bpp). Note that for lossless JPEG compression, the bit rate would be 8 Bpp. For the medical image to be diagnostically acceptable it must not exceed a bit rate of 1.0 Bpp. On average, this corresponds to using a quantisation multiplier of 0.88.

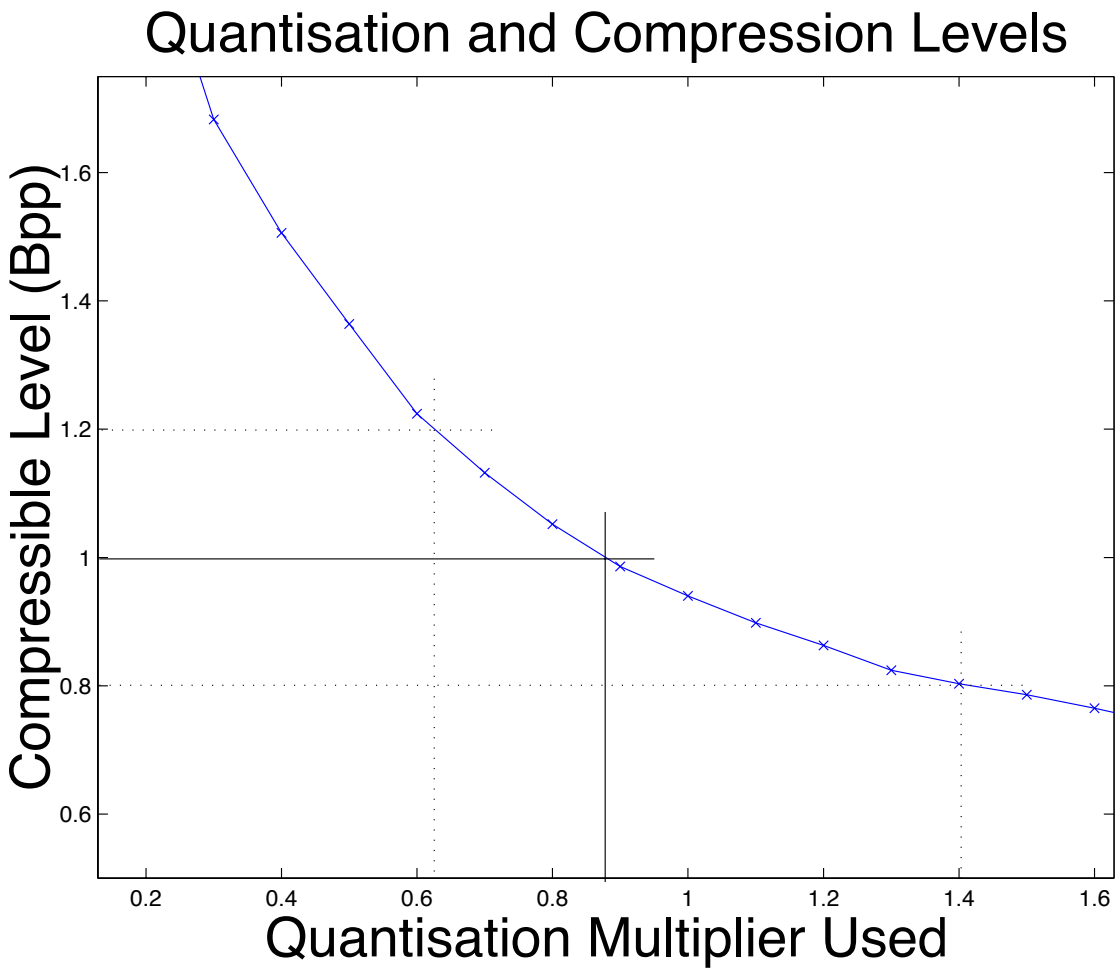

Figure A.3. Close up of area of interest. Analysing the behavior of the curve shown in Figure A.2 over the target bit rate of 1.0 Bpp. The selected compression range of interest is from 0.8 to 1.2 Bpp which corresponds to using quantisation levels of 0.62 to 1.40.

A.1.4 Conclusion

To achieve a target bit rate of 1.0 Bpp, a quantisation multiplier of 0.88 is required, however it may be more practical to use quantisation levels that correspond to an acceptable bit rate range. To ensure that the watermarking systems are functioning effectively over the target bit rate, a range has been selected that is shown shown in Figure A.3. These quantisation multipliers can be specified to the watermarking system as the maximum level of quantisation that the watermark should survive. Testing the watermark robustness at different embedding strengths makes it possible to:

- Ensure that the watermarking system survives JPEG-based distortions up to and including the embedding strength used.

- Performance of the watermark method is consistent over an acceptable range of embedding strengths.

These parameters are used for the next experiment where an earlier watermarking method proposed by Lin and Chang (2001) is tested.

A.2 Quantisation Testing Method Proposed by Lin and Chang

The objective of this section is to test and verify that an earlier robust watermarking technique proposed by Lin and Chang (2001) will survive levels of JPEG DCT quantisation with that found in earlier literature as well as increased quantisation levels that are used in this thesis. There are two parts to this experiment. Firstly there is a need to reproduce the results found in literature to show that robustness is consistent at previous levels tested. This involves testing both watermark and signature robustness. Secondly, additional quantisation levels must also be tested that include those corresponding to the desired bit rate ranges. In the previous experiment this was found to correspond with using embedding strengths ranging from 0.62 to 1.4. It is sufficient to test only the watermark robustness to DCT quantisation for this part, as additional errors in complete compression testing only result from integer rounding and decimation. Results from this experiment are intended to provide assurance that watermark embedding and extraction methods are completely functional so that they can be modified and extended for future use in this thesis.

A.2.1 Hypothesis

Inspection from results shown by Cox *et al.* (2001) demonstrate that when an embedding strength, $\alpha = 0.3$ is used, the watermarking technique proposed by Lin and Chang (2001) survives DCT quantisation levels up to and including this level. Two methodological approaches are adopted in testing this method, including:

1. Ensuring that the watermark is sufficiently robust to acceptable levels of DCT quantisation. An independent externally generated signature is used as a payload for the watermark.

2. Confirming that the same method using a signature extracted from each micro block also survives similar distortion levels. The watermark is then dependent on a unique signature extracted from the image.

It has been shown by Cox *et al.* (2001) that both methods survive JPEG DCT quantisation up to the embedding strength. Both watermarks are lost shortly after quantisation levels exceed this level. Similar type of behavior is expected when increased embedding levels are used.

A.2.2 Methods Used

Two methods are used, both of which test robustness to DCT quantisation. A threshold $\pi_0 = 85\%$ matching pair-wise bits between the signature and watermark is used to differentiate an authentic image from an inauthentic one. Floating point arithmetic is also used except that DCT coefficients are rounded after quantisation. Both of these experiments are designed to watermark complete images and extract signature information from all micro blocks. A sample set of 500 uncompressed greyscale medical images with resolutions varying from 512×512 and 2048×2048 pixels is used to test these algorithms. These are saved as bitmap (BMP) images with a encoded bit depth of 8 Bpp.

Flow diagrams have been used to illustrate how the experiments were set up. An overview of the approach used to test the robustness of Lin and Chang's algorithm with an external signature is shown in Figure A.4. Systematic processes used are depicted in Figure A.5. Please see Figure A.6 for systematic processes to test robustness when a self signature is used for an embedding strength, $\alpha = 0.3$.

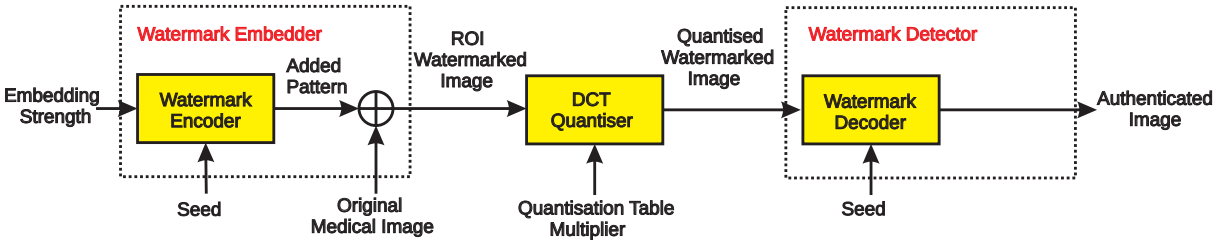

Figure A.4. Overview of the method to test Lin and Chang's algorithm. A randomly generated binary signature is used as the payload for the watermark. The embedding strength, α is specified to the watermark encoder as the maximum permissable level of quantisation that the watermark must survive. The watermark detector reproduces the original signature with an external seed. This is compared to the feature sequence extracted from the watermark. If the percentage of pair-wise matching bits is above the stated threshold of 85%, the image is declared as authentic. This process is repeated for the sample set of 500 images and ensures that the watermarking method is sufficiently robust when an externally generated signature is used.

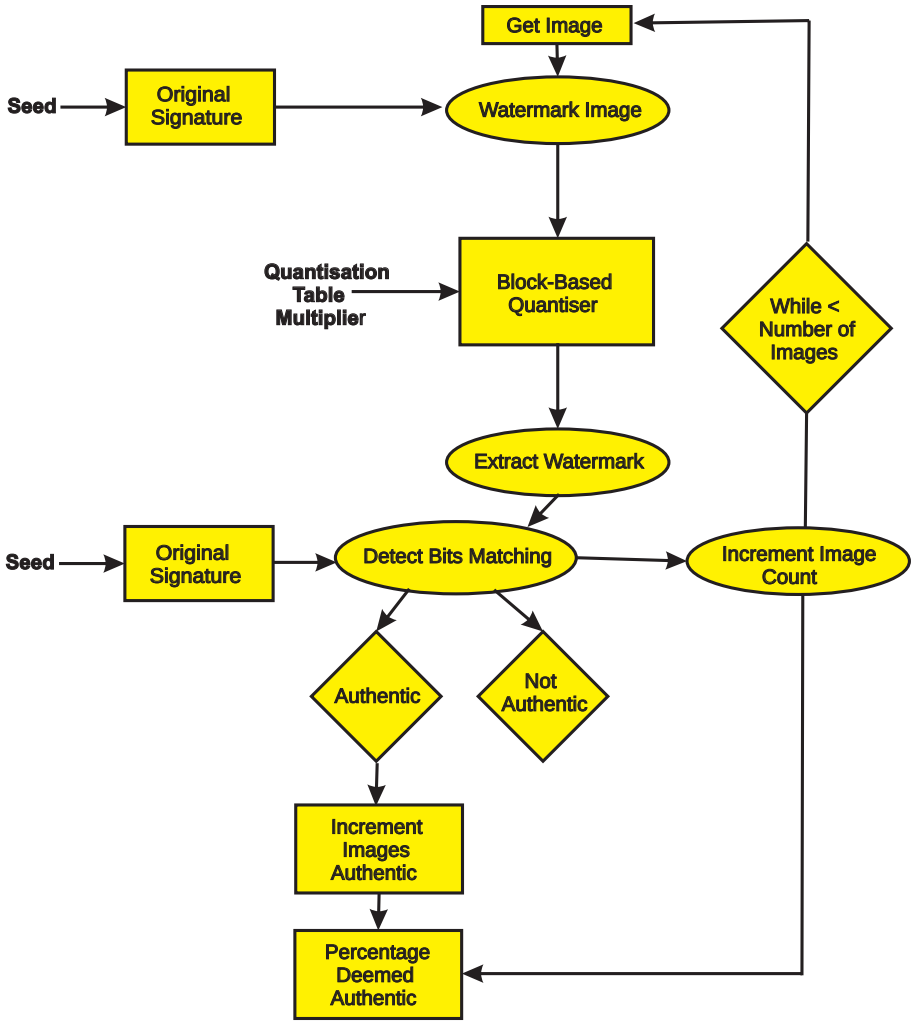

Figure A.5. Systematic processes to test robustness of Lin and Chang's watermarking algorithm. These images undergo the simulated distortion of JPEG block-based DCT quantisation. The watermark is extracted and compared to the known signature. If 85% of the watermark bits match the signature pairwise, the image is declared as authentic.

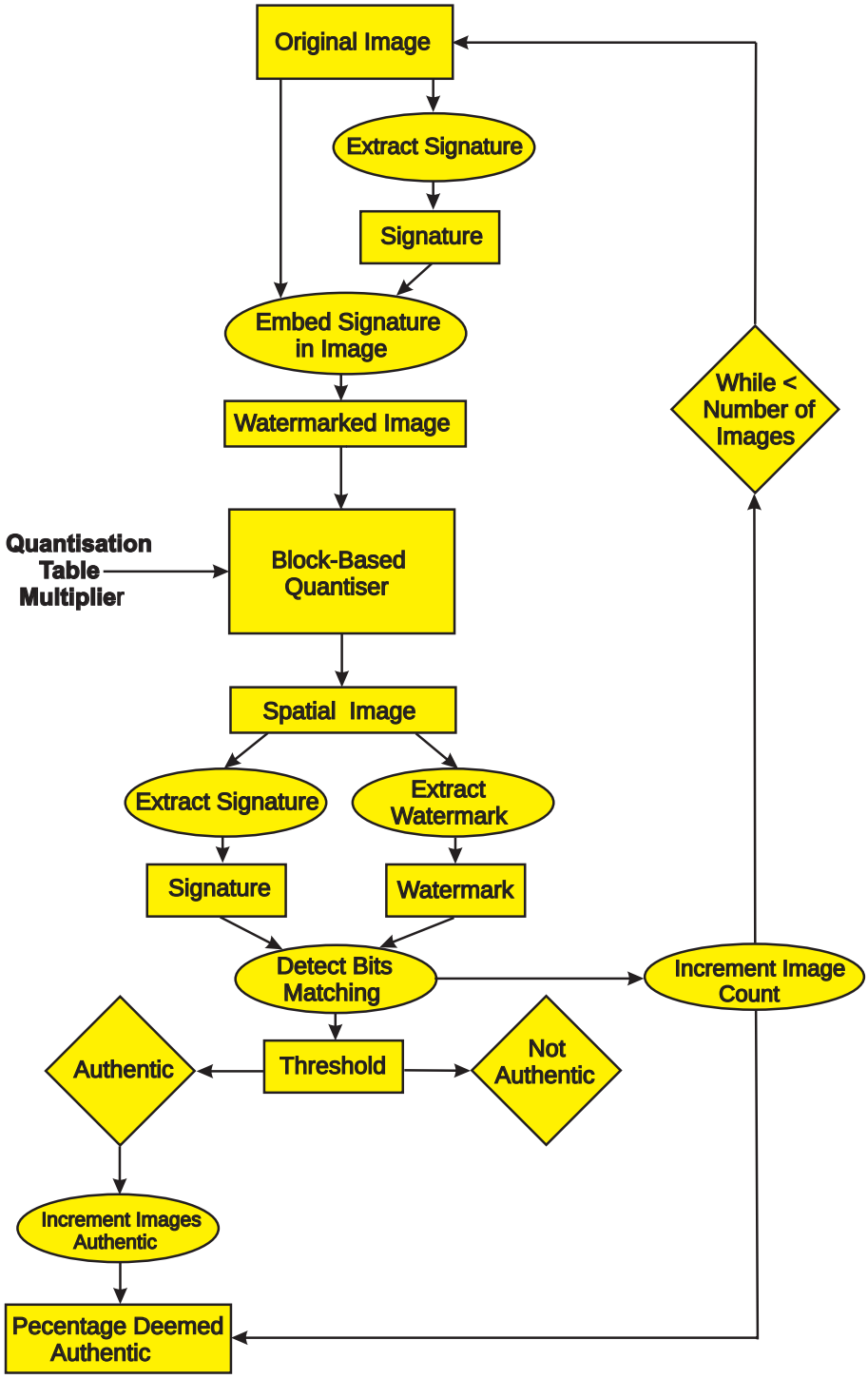

Figure A.6. System to test the robustness of the semi-fragile watermarking scheme using a semi-fragile signature. This system extracts a signature from the entire image rather than using an externally generated random bit sequence. The signature is extracted and embedded prior to the application of DCT quantisation. The signature and watermark can then be extracted and compared against a threshold to discriminate a match for an authenticated image.

A.2.3 Results

The effect of varying the applied DCT quantisation in Lin and Chang's scheme is shown in Figure A.7. For this part, an embedding strength of 0.3 is used. The results

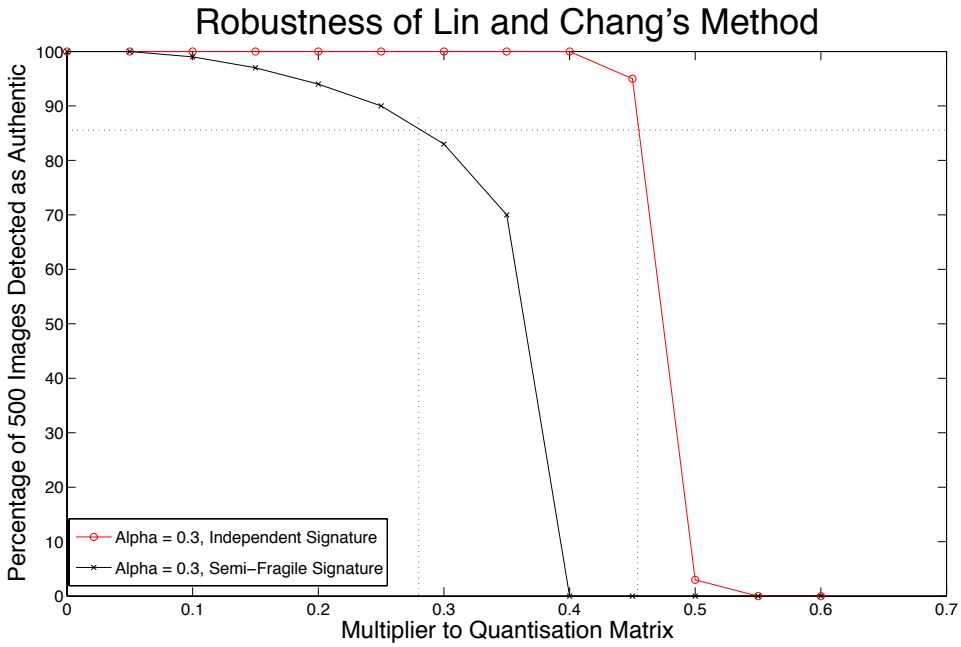

Figure A.7. Testing the robustness of Lin and Chang's algorithm. An embedding strength of 0.3 is used, which was also used by Cox *et al.* (2001). The watermarking scheme using a randomly generated signature is shown in red. This survives greater levels of DCT quantisation than for the same system incorporating a signature based on properties of the image, in black. A threshold of 85% images detected as authentic is used to indicate system success. The signature-based system fails at a quantisation level of 0.28. The system using an externally generated signature fails at 0.45, when the same embedding strength is used. This system using an independent signature also deteriorates much sooner and gradually than for the scheme using a signature based on properties of the image. These results are almost identical to those presented by Cox.

of the watermark robustness test to increased quantisation levels of 0.62, 0.88 and 1.4 are shown in Figure A.8. These levels have been selected to correspond to respective compression levels of 1.2, 1.0 and 0.8 Bpp.

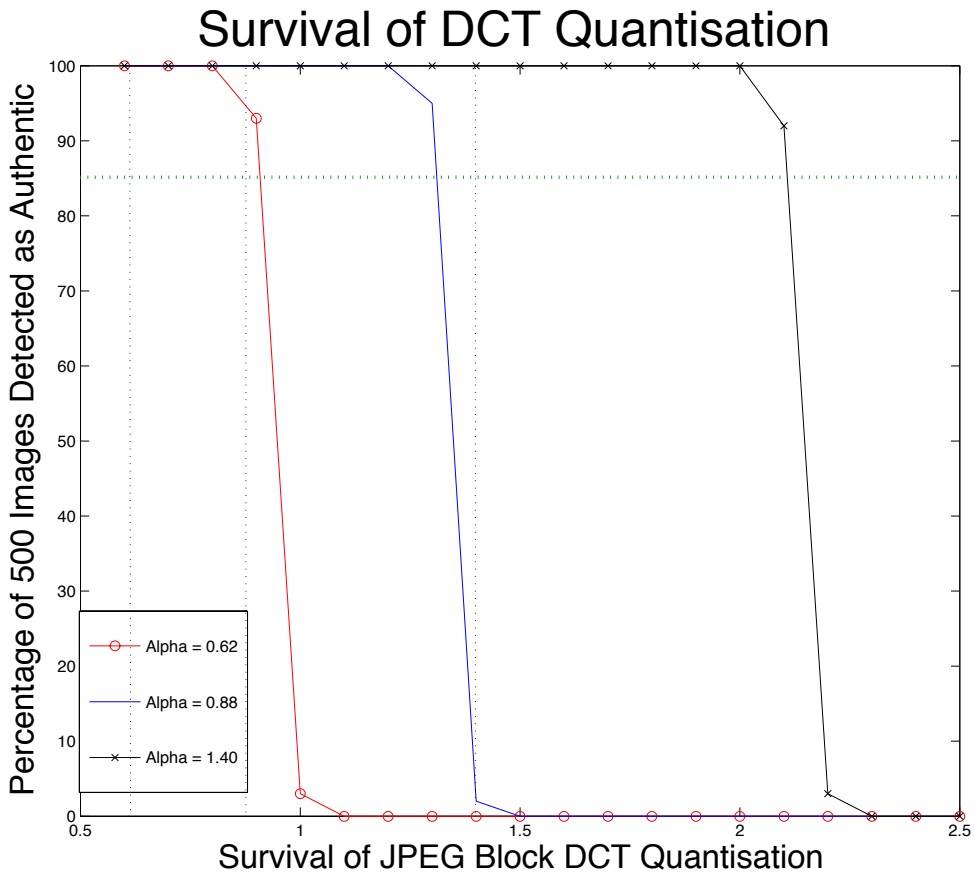

Figure A.8. Embedding strength of 0.62, 0.88 and 1.4. Testing the robustness of 500 images with the semi-fragile watermarking scheme designed to withstand JPEG compression up to this level. Embedding strengths of 0.62, 0.88 and 1.4 are shown in red, blue and black respectively. These embedding strengths have been chosen to correlate with compression levels of 0.8 to 1.2 Bpp. The quantisation factor of 0.88 corresponds to the target compression value of 1.0 Bpp. Identical thresholds have been used to determine system failure points as for Figure A.7.

Results from Figure A.8 show that robust performance is consistent when the quantisation levels exceed the embedding strength, α. For the target quantisation level of 0.88 the watermark fails for a level of quantisation of 1.4. This implies that the level of quantisation can be exceeded by 0.52 before the system can be expected to fail. This corresponds to increasing the amount of compression by 0.7 from the target 1.0 Bpp on inspecting the compression and quantisation curve shown in Figure A.2. The greater the embedding strength, the more quantisation can be applied prior to watermark failure. For an embedding strength of 0.62 the watermark fails when quantisation level exceeds 0.26. For an embedding strength of 1.4, the watermark fails after increasing the quantisation by 0.7 as failure is present at 2.1.

A.2.4 Discussion

The overall loss of watermark at increased quantisation levels has consistent behavior at each embedding strength. Careful attention should be drawn to the watermark surviving increased quantisation levels at greater embedding levels, α. This is important as it is undesirable for the watermark to survive excessive quantisation. This may lead to unacceptable loss of image detail while maintaining the watermark integrity. Attempting to optimise the embedding strength parameter to ensure that the watermark does fail at the target quantisation level may be a particularly challenging exercise. Additional errors may be introduced to the system when entire JPEG compression is used. This would result from additional rounding and decimation and should corrupt the watermark at lower quantisation levels. To summarise this experiment demonstrates that the earlier robust watermarking technique proposed by Lin and Chang (2001) will survive levels of JPEG DCT quantisation comparable with that found in earlier literature. It is also robust when increased quantisation levels are used.

Appendix B

Software Design and Matlab Code

EFFECTIVE implementation of the ROI watermark method demands careful and well coded software. Architectural and interface design has proved to be very effective with software flow diagrams. These illustrate core relationships between important parameters used in this thesis. Systems have been designed to be highly modular and have been re-used wherever practically possible. Top-down design methodologies have ensured that software modules are very easy to test and re-use. These are also loosely coupled to minimise complexity. Subsystems have been identified by being shaded in green and can be cross-referenced with corresponding Matlab code used to implement these modules.

Matlab 7.0 was used to implement All of the software modules described in this thesis. Matlab is a high-level technical, mathematical-based computing language, developed by the MathWorks. It contains built in support for a large number of mathematical functions as well as numerous systematic implementations of commonly used signal processing algorithms. Many Matlab toolboxes have been used in this thesis, which include:

- The Image Processing Toolbox
- The Statistics Toolbox
- The Communications Toolbox.

B.1 Code Description

Software design of the ROI watermark system includes three key stages that include signature extraction, watermark embedding and extraction. The following sections have included highly modular software flow diagrams as well as the Matlab code to implement these systems. This is only a portion of the software developed for this research. Matlab scripts have also been coded, such as experimental tests to generate plots. Please contact the author for specific details with regard to the software coding methodologies.

The Matlab files described below have been copied to the attached CD.

Signature Extraction -
randomize blocks.m This function randomly selects micro block pairs from the ROI as part of the signature extraction process.
extract signature.m This function extracts a signature from a pre-defined ROI by comparing DCT coefficients that are invarient to JPEG compression. This is described in Section 4 and depicted in the flow diagrams of Figure B.1.

Watermark Embedding -
eroi.m Highest level function to embed a ROI watermark in an image. This is presented by the flow diagrams shown in Figures B.2 and B.3

embed watermark in region.m This function embeds a singular authentication signature into one image region. This is similar to the method proposed by Lin and Chang (2001) and is depicted in Figure B.4.

embed four bits in a block.m This function takes four signature bits and embeds them into one micro block in the ROB, shown in Figure B.5.

embed one bit in a block.m This function takes one watermark bit b_e, which is embedded into a selection of 7 DCT coefficients. This is the lowest level embedding function and is illustrated in Figure B.6.

assign new coefficients.m A matlab function designed to replace unwatermarked DCT coefficients with watermarked DCT values.

get dctq matrix.m This function scales the standard JPEG luminance quantisation matrix, which is used for greyscale images.

Watermark Extraction -

droi.m Highest level function to decode the ROI watermark by extracting the signature and watermark from the received image, which is illustrated in the flow diagrams of Figures B.7 and B.8.

extract watermark from region.m This function extracts a singular watermark from an image region in the ROB. The software flow structure shown in Figure B.4 is re-used for this function.

extract four bits from a block.m This function extracts four embedded bits from a singular micro block. Similarly this re-uses the flow structure depicted in Figures B.5 and B.6, with the exception that embedded bits are only extracted.

Other Functions -

compress.m A Matlab function used to compress a singular micro block by quantising its DCT values. This is called repeatedly using a block processing operation supplied by the Image Processing Toolbox to quantise all micro block in an image region.

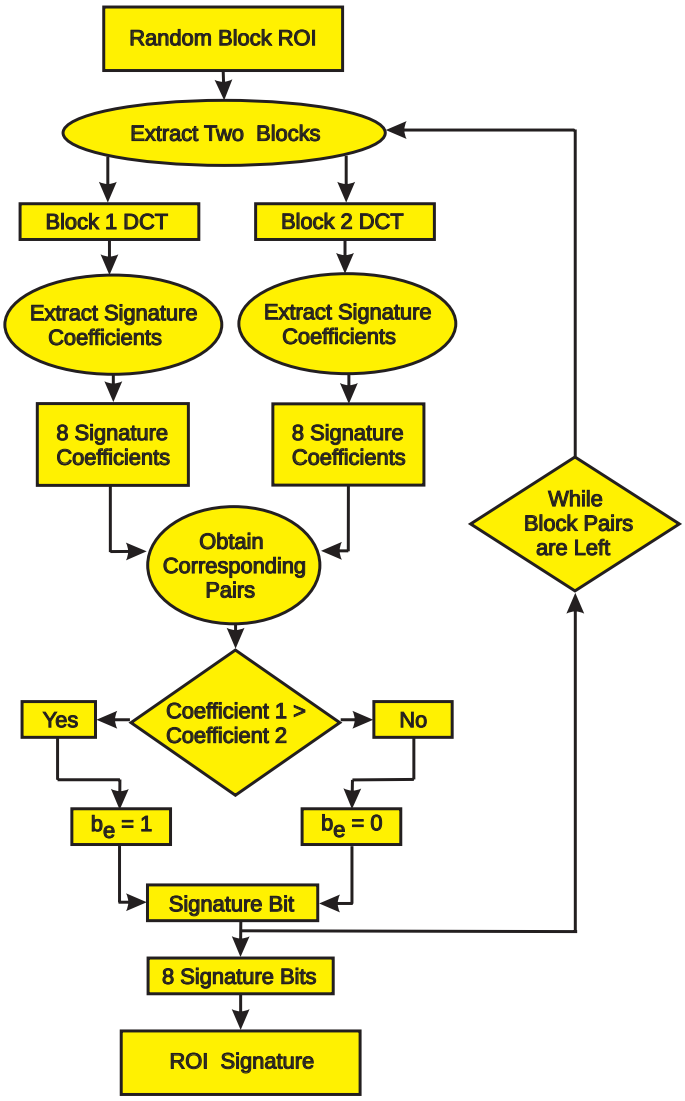

Figure B.1. Function which extracts a signature from a ROI. Two randomly selected micro blocks are extracted from the ROI and the signature coefficients are determined. These are calculated from the first 8 coefficients following the JPEG zig-zag scan depicted in Appendix C. Corresponding coefficients are compared with each other to generate feature codes as described in the system method. This process is repeated until there are no longer any block pairs left. The Matlab code used to randomly select micro blocks from the ROI has been included after the code describing the signature extraction process.

```
%%%%%%%%%%%%%%%%%%%%%%%%%%%%%%%%%%%%%%%%%%%%%%%%%%%%%%%%%%%%%%%%%%%%%%%%%%%%
%%%%%%%%%%%%  Function to Extract a Signature from a ROI   %%%%%%%%%%%%
%%%%%%%%%%%%%%%%%%%%%%%%%%%%%%%%%%%%%%%%%%%%%%%%%%%%%%%%%%%%%%%%%%%%%%%%%%%%

function signature = extract_signature(randomized_roi,tilesize)

% Arguments
% roi: the region of interest from which to extract a signature
% width: width of the ROI
% height: height of the ROI
% seed: a different signature is extracted for each value of seed
% sig_bits: the resulting signature

% Dominic Osborne
% The University of Adelaide
% July 2003

roi = randomized_roi;
size_roi =  size(roi); %Define the size of the region of interest
width_roi = size_roi(1,2); tiles_wide = width_roi/tilesize;
height_roi = size_roi(1,1); tiles_high = height_roi/tilesize;
% Get the number of tiles in the region of interest
num_tiles = tiles_wide*tiles_high;

%Now tiling and performing DCT to each tile
x_ref = 1;            % Define a starting point for application of the DCT
y_ref = 1;            % Define a starting point for application of the DCT
signature_ref = 1;

   while y_ref <= height_roi  % for the ROI
        x_ref = 1;  % initialise to the left side of the image
        while x_ref < width_roi %Center loop for application of DCT

              tile1 = roi(y_ref:y_ref + tilesize -1,
              x_ref:x_ref + tilesize -1);
```

```
x_ref = x_ref + tilesize;
%Move right to the immediate next tile
tile2 = roi(y_ref:y_ref + tilesize -1,x_ref:
x_ref + tilesize -1);
t1 = tile1;
t2 = tile2;
tile1_dct = [t1(1,1),t1(1,2),t1(2,1),t1(3,1),t1(2,2),
             t1(1,3),t1(1,4),t1(2,3)];
tile2_dct = [t2(1,1),t2(1,2),t2(2,1),t2(3,1),t2(2,2),
             t2(1,3),t2(1,4),t2(2,3)];

% Now compare corresponding bits

if tile1_dct(1) < tile2_dct(1)
   bit1 = 0;
else bit1 = 1;
end
if tile1_dct(2) < tile2_dct(2)
   bit2 = 0;
else bit2 = 1;
end
   if tile1_dct(3) < tile2_dct(3)
   bit3 = 0;
else bit3 = 1;
end
if tile1_dct(4) < tile2_dct(4)
   bit4 = 0;
else bit4 = 1;
end
 if tile1_dct(5) < tile2_dct(5)
   bit5 = 0;
else bit5 = 1;
end
if tile1_dct(6) < tile2_dct(6)
```

```
            bit6 = 0;
        else bit6 = 1;
        end
            if tile1_dct(7) < tile2_dct(7)
            bit7 = 0;
        else bit7 = 1;
        end
        if tile1_dct(8) < tile2_dct(8)
            bit8 = 0;
        else bit8 = 1;
        end

        signature(signature_ref:signature_ref + 7) =
        [bit1, bit2, bit3, bit4, bit5, bit6, bit7, bit8];
        signature_ref = signature_ref + 8;


        x_ref = x_ref + tilesize;
        %Move right to the immediate next tile
    end
     y_ref = y_ref + tilesize; %Move down to a lower tile
end
```

```
%%%%%%%%%%%%%%%%%%%%%%%%%%%%%%%%%%%%%%%%%%%%%%%%%%%%%%%%%%%%%%%%%%%%%%%%%%%%
%%%%%%%%%%  Function to Randomise Micro Blocks in the ROI   %%%%%%%%%%%%
%%%%%%%%%%%%%%%%%%%%%%%%%%%%%%%%%%%%%%%%%%%%%%%%%%%%%%%%%%%%%%%%%%%%%%%%%%%%

function randomized_roi=randomize_blocks(roi,tilesize)

% Arguments
% roi: the region of interest from which to extract a signature
% width: width of the ROI
% height: height of the ROI
% seed: a different signature is extracted for each value of seed
% sig_bits: the resulting signature

% Dominic Osborne
% The University of Adelaide
% July 2003

size_roi =  size(roi); width_roi = size_roi(1,2); tiles_wide =
width_roi/tilesize; height_roi = size_roi(1,1); tiles_high =
height_roi/tilesize;
% Get the number of tiles in the region of interest
%num_tiles = (height/tilesize)*(width/tilesize);

% Create random entries for the rearranged tiles
rand('state',0); rand_width_entries =
((randperm(tiles_wide)).*tilesize) - tilesize + 1;
rand_height_entries = (randperm(tiles_high)).*tilesize - tilesize +
1;

% Now loop through the ROI and rearrange the tiles

%Now tiling and performing DCT to each tile
x_ref = 1;       % Define a starting point for application of the DCT
y_ref = 1;       % Define a starting point for application of the DCT
```

```
x_count = 1;     % Simply used as indices for rand_width_entry vector
y_count = 1;     % Simply used as indices for the rand_height_entry vector
rearranged_roi = zeros(size(roi));

   while y_ref <= height_roi  % for the ROI
        x_ref = 1;  % initialise to the left side of the image
        x_count = 1;
        while x_ref < width_roi %Center loop for application of DCT

              current_tile = roi(y_ref:y_ref + tilesize -1,x_ref:x_ref +
              tilesize -1);

              % Now we have a particular tile from the ROI...
              % place it randomly
              % according to the 2-D permutation
              width_point = rand_width_entries(x_count);
              height_point = rand_height_entries(y_count);

              rearranged_roi(height_point:height_point + tilesize -1,
              width_point:width_point + tilesize -1) = current_tile;


              x_ref = x_ref + tilesize;
              %Move right to the immediate next tile
              x_count = x_count + 1;
        end
         y_ref = y_ref + tilesize; %Move down to a lower tile
         y_count = y_count + 1;
   end

   randomized_roi = rearranged_roi;
```

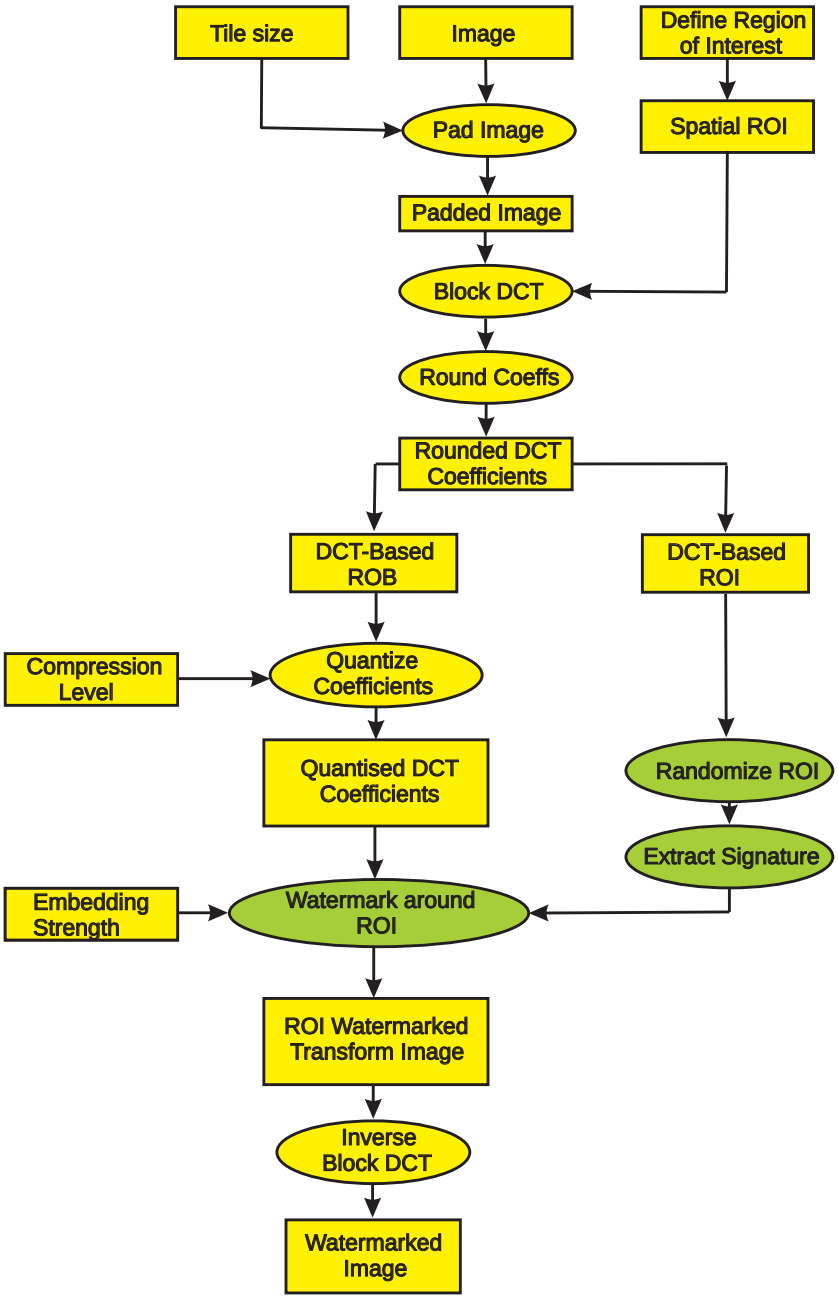

Figure B.2. System used to watermark an image with a specified ROI. A ROI is specified and copied from an image that undergoes a block-based DCT and quantisation to significantly reduce the number of non-zero coefficients for the purposes of high compression. Extraction of the signature takes place using the function in Figure B.1. Watermarking around the ROI is performed as shown in the flow diagram of Figure B.3.

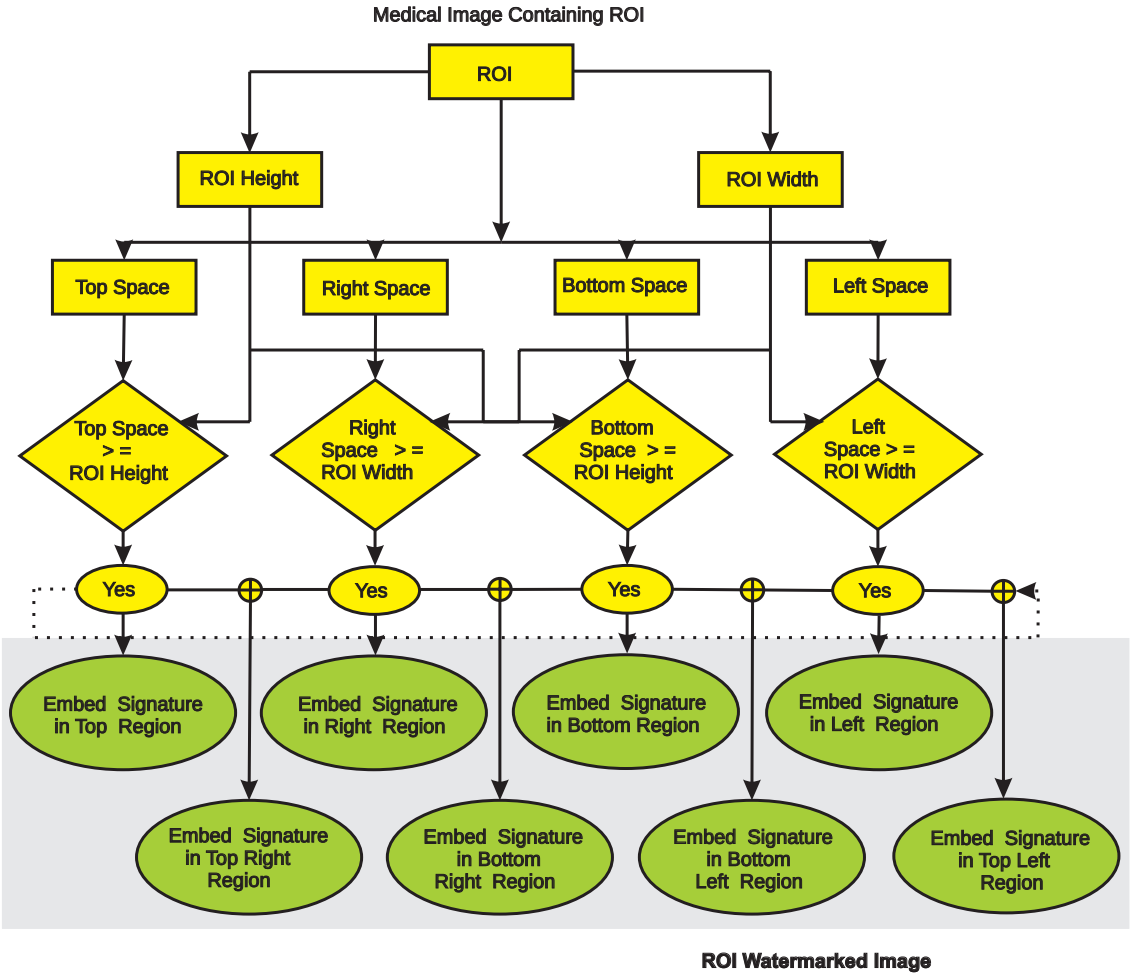

Figure B.3. Multiple embedding around the ROI. Software design flow for embedding multiply around a given ROI eight times after first checking for appropriate space given the region size and the image resolution. The bottom shaded area represents the multiply watermarked ROI compressed image. The embedding process for a singular watermark is shaded in green, with sub-function shown Figure B.4.

```
%%%%%%%%%%%%%%%%%%%%%%%%%%%%%%%%%%%%%%%%%%%%%%%%%%%%%%%%%%%%%%%%%%%%%%%%%%%%
%%%%%  Top Level Script for Multiple ROI Watermark Embedding eroi.m %%%%
%%%%%%%%%%%%%%%%%%%%%%%%%%%%%%%%%%%%%%%%%%%%%%%%%%%%%%%%%%%%%%%%%%%%%%%%%%%%

% Dominic Osborne
% The University of Adelaide
% August 2003

% Define Embedding Strength, read image from file.
% Convert to double precision
alpha = 0.88; orig = imread('medical_image.bmp'); orig =
double(orig);

% Define the constraints of the entire image as required
size_orig = size(orig); full_width = size_orig(1,2); full_height =
size_orig(1,1); image_bottom = full_height; image_top = 1;
image_left = 1; image_right = full_width; tilesize = 8;


% Extend the size of the image to cover full tiles
if rem(full_width,tilesize) > 0
    width_to_fill = (tilesize-rem(full_width,tilesize));
else width_to_fill = 0; end

if rem(full_height,tilesize) > 0
    height_to_fill = (tilesize-rem(full_height,tilesize));
else height_to_fill = 0; end
% Just fill in the extenstions with zeros
orig(1:full_height,full_width + 1:full_width + width_to_fill) = 0;
orig(full_height + 1:full_height + height_to_fill,1:full_width +
width_to_fill) = 0;
% Convert to whole image to transform representation
fun = @dct2; orig_trans = blkproc(orig,[8 8],fun);
% round the transform coefficients for packing to get the original
```

```
% image with rounded transformed coefficients.
c = round(orig_trans);

% Define a ROI in transform representation that is unquantised
% For simplicity the ROI is specified manually and as a complete
% number of micro blocks.
roi_top = 265; roi_bottom = 480; roi_left = 129; roi_right = 256;
roi = c(roi_top:roi_bottom,roi_left:roi_right); size_roi =
size(roi); width_roi = size_roi(1,2); height_roi = size_roi(1,1);
num_tiles = width_roi*height_roi/(tilesize*tilesize);

% Uncorrelate micro blocks
randomized_roi = randomize_blocks(roi,tilesize);
% Extract a signature from the ROI
signature = extract_signature(randomized_roi,tilesize);
original_signature_bits = reshape(signature, 4, num_tiles);
original_signature_bits = original_signature_bits';

% Embedding can be done.
% Based on the ROI define the available spaces
bottom_space = image_bottom - roi_bottom + 1; top_space = roi_top-1;
left_space = roi_left-1; right_space = full_width - roi_right;

% Define top region for embedding
if   top_space < height_roi
     disp('Not Enough Room to Embed above ROI')
else
     top_area = c(roi_top - height_roi:roi_top - 1,roi_left:roi_right);
     region = top_area;
     watermarked_transform_region = embed_watermark_in_region(region,
     width_roi,height_roi,alpha,original_signature_bits,tilesize);
     c(roi_top - height_roi:roi_top - 1,roi_left:roi_right) =
     watermarked_transform_region;
end
```

```
% Define top right region for embedding

if   top_space < height_roi | right_space < width_roi
     disp('Not Enough Room to Embed top right region')
else
     top_right_area = c(roi_top - height_roi:roi_top - 1,
     roi_right+1:roi_right+width_roi);
     region = top_right_area;
     watermarked_transform_region = embed_watermark_in_region(region,
     width_roi,height_roi,alpha,original_signature_bits,tilesize);
     c(roi_top - height_roi:roi_top - 1,roi_right+1:roi_right+width_roi) =
     watermarked_transform_region;
end

% Define right region for embedding
if   right_space < width_roi
     disp('Not Enough Room to Embed to the right of the ROI')
else
     right_area = c(roi_top:roi_bottom,roi_right+1:roi_right+width_roi);
     region = right_area;
     watermarked_transform_region = embed_watermark_in_region(region,
     width_roi,height_roi,alpha,original_signature_bits,tilesize);
     c(roi_top:roi_bottom,roi_right+1:roi_right+width_roi) =
     watermarked_transform_region;
end

% Define bottom right region for embedding
if   right_space < width_roi | bottom_space < height_roi
     disp('Not Enough Room to Embed bottom right region')
else
     bottom_right_area = c(roi_bottom + 1:roi_bottom + height_roi,
     roi_right+1:roi_right+width_roi);
     region = bottom_right_area;
     watermarked_transform_region =
     embed_watermark_in_region(region,width_roi,height_roi,alpha,
```

```
     original_signature_bits,tilesize);
     c(roi_bottom + 1:roi_bottom + height_roi,roi_right+1:
     roi_right+width_roi) = watermarked_transform_region;
end

% Define a bottom region for embedding
if   bottom_space < height_roi
     disp('Not Enough Room to Embed below bottom region')
else bottom_area = c(roi_bottom + 1:roi_bottom + height_roi,
     roi_left:roi_right);
     region = bottom_area;
     watermarked_transform_region = embed_watermark_in_region(region,
     width_roi,height_roi,alpha,original_signature_bits,tilesize);
     c(roi_bottom + 1:roi_bottom + height_roi,roi_left:roi_right) =
     watermarked_transform_region;
end

% Define a bottom left region for embedding
if   bottom_space < height_roi | left_space < width_roi
     disp('Not Enough Room to Embed bottom left region')
else bottom_left_area = c(roi_bottom + 1:roi_bottom +
     height_roi,roi_left-width_roi:roi_left - 1);
     region = bottom_left_area;
     watermarked_transform_region = embed_watermark_in_region(region,
     width_roi,height_roi,alpha,original_signature_bits,tilesize);
     c(roi_bottom + 1:roi_bottom + height_roi,roi_left-width_roi:
     roi_left - 1) = watermarked_transform_region;
end

% Define left region for embedding
if   left_space < width_roi
     disp('Not Enough Room to Embed to the left of the ROI')
else left_area = c(roi_top:roi_bottom,roi_left-width_roi:roi_left -
1);
     region = left_area;
```

```
     watermarked_transform_region = embed_watermark_in_region(region,
     width_roi,height_roi,alpha,original_signature_bits,tilesize);
     c(roi_top:roi_bottom,roi_left-width_roi:roi_left - 1) =
     watermarked_transform_region;
end

% Define top left region for embedding
if   left_space < width_roi | top_space < height_roi
     disp('Not Enough Room to Embed to the top left of the ROI')
else
     top_left_area = c(roi_top - height_roi:roi_top - 1,
     roi_left-width_roi:roi_left - 1);
     region = top_left_area;
     watermarked_transform_region = embed_watermark_in_region(region,
     width_roi,height_roi,alpha,original_signature_bits,tilesize);
     c(roi_top - height_roi:roi_top - 1,roi_left-width_roi:roi_left - 1) =
     watermarked_transform_region;
end

%Convert to spatial representation needed for imwrite
fun = @idct2; watermarked_image = blkproc(c,[8 8],fun);
norm_watermarked_image = watermarked_image./255;
%imshow(norm_watermarked_image)

%Write watermarked images to a bitmap image
imwrite(norm_watermarked_image,'watermarked_image.bmp','bmp');
```

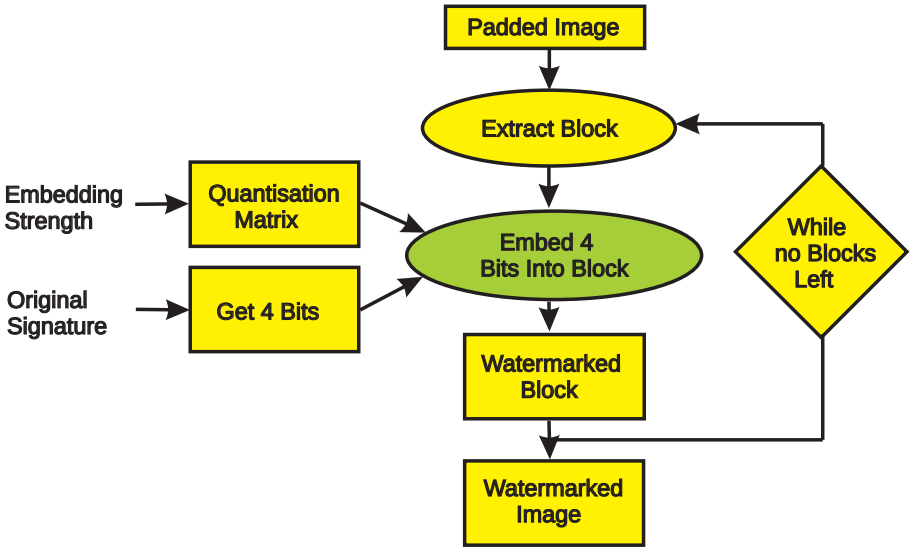

Figure B.4. Flow diagram of the function to embed a singular watermark in one image region. The input parameters for this sub-function include four bits from the signature and a specified embedding strength, α. This last factor is used as a multiplier to the standard JPEG quantisation matrix. Watermarking takes place in each micro block in a stepwise fashion from top left to bottom right. Four bits are embedded into each micro block that is depicted in the sub-function shown in Figure B.5. This function is also re-used in the watermark extraction process. An exception is that bits are only extracted instead of embedded in the sub-function that embeds four bits in a block.

```
%%%%%%%%%%%%%%%%%%%%%%%%%%%%%%%%%%%%%%%%%%%%%%%%%%%%%%%%%%%%%%%%%%%%%%%%%%%%
%%%% Embedding Function to Embed a Watermark in a singular Region  %%%%%%
%%%%%%%%%%%%%%%%%%%%%%%%%%%%%%%%%%%%%%%%%%%%%%%%%%%%%%%%%%%%%%%%%%%%%%%%%%%%

% Dominic Osborne
% The University of Adelaide
% April 2003

function watermarked_transform_region =
embed_watermark_in_region(region,
width_roi,height_roi,alpha,original_signature_bits,tilesize)

quant_matrix = get_dctq_matrix(alpha);
%Calls a function to get and scale the quantisation matrix.
%embed 4 bits in each block

%Now tiling and performing DCT to each tile
x_ref = 1;            % Define a starting point for application of the DCT
y_ref = 1;            % Define a starting point for application of the DCT
signature_row_reference = 1;

   while y_ref <= height_roi
        x_ref = 1;
        while x_ref < width_roi %Center loop for application of DCT

              current_tile = region(y_ref:y_ref + tilesize -1,x_ref:
              x_ref + tilesize -1);

              % Get the watermark bits used to embed 4 bits.

              four_bits_to_embed = original_signature_bits
              (signature_row_reference,1:4);
              signature_row_reference = signature_row_reference + 1;
```

```
            watermarked_transform_tile = embed_four_bits_in_a_block
            (quant_matrix,current_tile,four_bits_to_embed);

            watermarked_transform_region(y_ref:y_ref + tilesize -1,
            x_ref:x_ref + tilesize -1) = watermarked_transform_tile;
            watermarked_spatial_region(y_ref:y_ref + tilesize -1,
            x_ref:x_ref + tilesize -1) =
            IDCT2(watermarked_transform_tile);


            x_ref = x_ref + tilesize; %Move right to the next tile

    end
     y_ref = y_ref + tilesize; %Move down to a lower tile
end
```

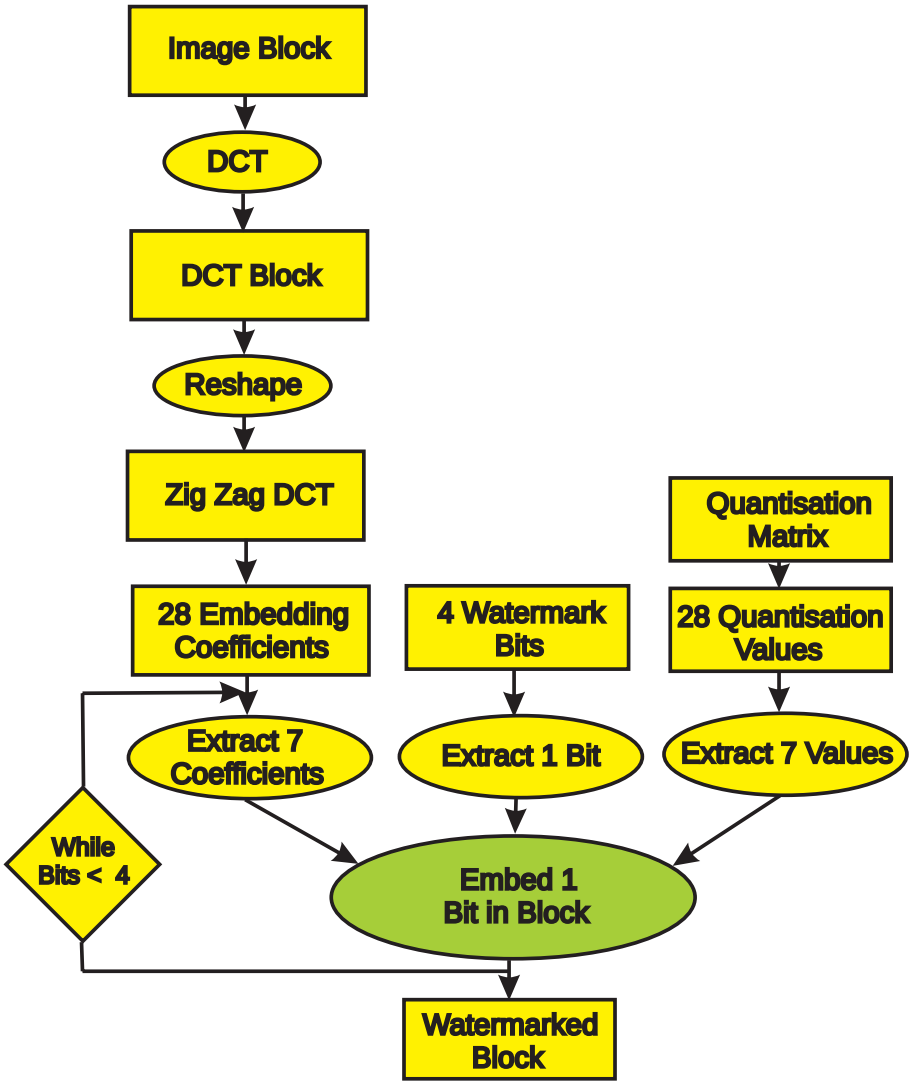

Figure B.5. Flow diagram of the function to embed 4 bits in a micro block. For each micro block, 28 of the last DCT coefficients of the JPEG zigzag scan are used to host four signature bits. This also requires corresponding quantisation values obtained from the quantisation matrix that determines the extent of watermark embedding. The lowest level function that embeds one bit in a selection of 7 of these coefficients is shown in Figure B.6. This module is also re-used for the watermark system that extracts four bits from a block. An exception is that only extraction takes place and the central flow structure containing watermark bits is not used.

```
%%%%%%%%%%%%%%%%%%%%%%%%%%%%%%%%%%%%%%%%%%%%%%%%%%%%%%%%%%%%%%%%%%%%%%%%%%%%
%%%%% Third Level Embedding Function for Four Bits Per Micro Block %%%%%
%%%%%%%%%%%%%%%%%%%%%%%%%%%%%%%%%%%%%%%%%%%%%%%%%%%%%%%%%%%%%%%%%%%%%%%%%%%%

function  watermarked_transform_tile=embed_four_bits_in_a_block
(quant_matrix,current_tile,four_bits_to_embed)

% Embed 4 bits into each block
% Quantisation_values: Vector containing the set of 28 quantisation values
% Embed four bits into this block and then quantise and clip or until all
% bits are correctly embedded

% Dominic Osborne
% The University of Adelaide
% April 2003

% Getting the relevant coefficients
current_transform_tile = current_tile;

p = current_transform_tile; %for Convenience to specify the DCT vector

% Converting the whole DC-transform tile to a zigzag vector
zigzag_dct_vector =
[p(1,1),p(1,2),p(2,1),p(3,1),p(2,2),p(1,3),p(1,4),
                    p(2,3),p(3,2),p(4,1),p(5,1),p(4,2),p(3,3),p(2,4),
                    p(1,5),p(1,6),p(2,5),p(3,4),p(4,3),p(5,2),p(6,1),
                    p(7,1),p(6,2),p(5,3),p(4,4),p(3,5),p(2,6),p(1,7),
                    p(1,8),p(2,7),p(3,6),p(4,5),p(5,4),p(6,3),p(7,2),
                    p(8,1),p(8,2),p(7,3),p(6,4),p(5,5),p(4,6),p(3,7),
                    p(2,8),p(3,8),p(4,7),p(5,6),p(6,5),p(7,4),p(8,3),
                    p(8,4),p(7,5),p(6,6),p(5,7),p(4,8),p(5,8),p(6,7),
                    p(7,6),p(8,5),p(8,6),p(7,7),p(6,8),p(7,8),p(8,7),
                    (8,8)];
embedding_coefficients = [zigzag_dct_vector(37:64)];
```

```
x = quant_matrix; zigzag_quant_vector =
[x(1,1),x(1,2),x(2,1),x(3,1),x(2,2),x(1,3),x(1,4),
                      x(2,3),x(3,2),x(4,1),x(5,1),x(4,2),x(3,3),x(2,4),
                      x(1,5),x(1,6),x(2,5),x(3,4),x(4,3),x(5,2),x(6,1),
                      x(7,1),x(6,2),x(5,3),x(4,4),x(3,5),x(2,6),x(1,7),
                      x(1,8),x(2,7),x(3,6),x(4,5),x(5,4),x(6,3),x(7,2),
                      x(8,1),x(8,2),x(7,3),x(6,4),x(5,5),x(4,6),x(3,7),
                      x(2,8),x(3,8),x(4,7),x(5,6),x(6,5),x(7,4),x(8,3),
                      x(8,4),x(7,5),x(6,6),x(5,7),x(4,8),x(5,8),x(6,7),
                      x(7,6),x(8,5),x(8,6),x(7,7),x(6,8),x(7,8),x(8,7),
                      x(8,8)];
quantisation_values = zigzag_quant_vector(37:64);
coefficient_pointer = 0;

    for i = 1:4
        set_of_7_original_coeffs =  embedding_coefficients
        (coefficient_pointer+1:coefficient_pointer + 7);
        quantisation_7_values = quantisation_values
        (coefficient_pointer+1:coefficient_pointer + 7);
        bit_to_embed = four_bits_to_embed(i);

        new_set_of_7_coeffs = embed_one_bit_in_a_block
        (set_of_7_original_coeffs,quantisation_7_values,bit_to_embed);

        new_coefficients(coefficient_pointer+1:coefficient_pointer + 7) =
        new_set_of_7_coeffs;
        coefficient_pointer = coefficient_pointer + 7;
    end

   %Assign the modified coefficients to the current transform tile
   watermarked_transform_tile = assign_new_coefficients
   (new_coefficients,current_transform_tile);
```

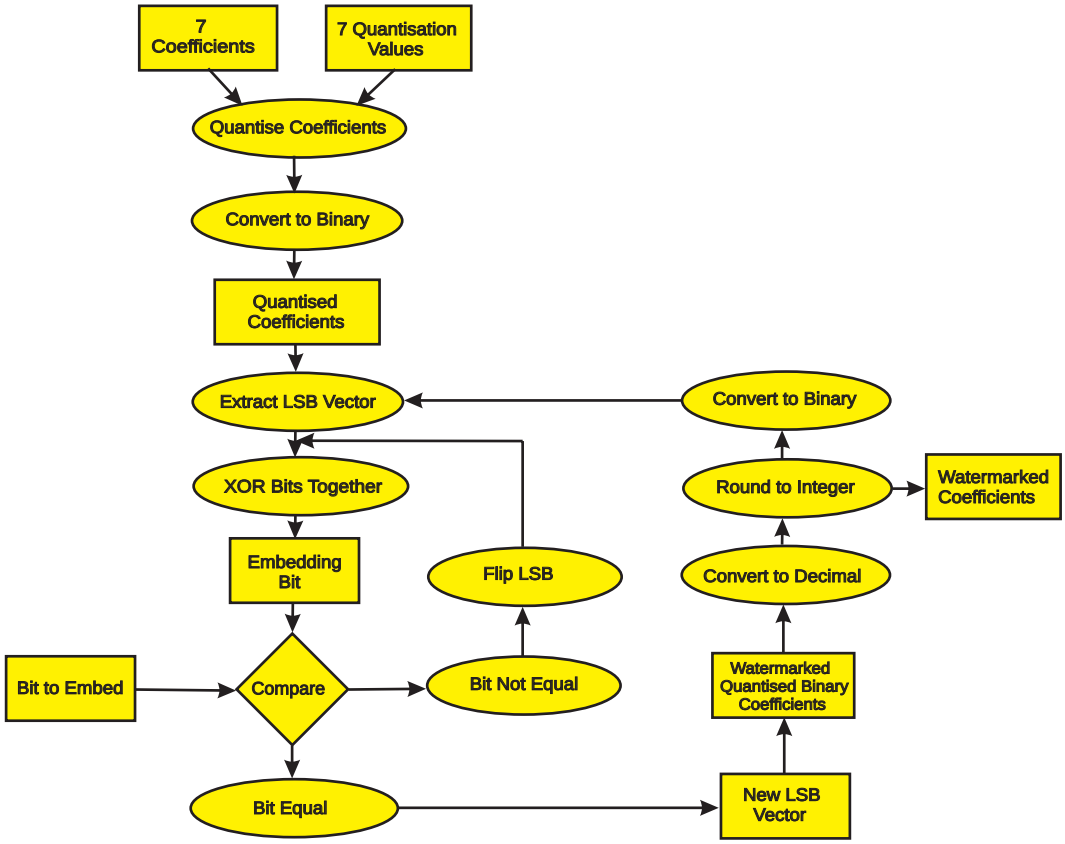

Figure B.6. Flow diagram of the function that embeds 1 bit in a selection of 7 DCT coefficients. Three input parameters are specified including seven DCT coefficients from the ROB micro block as well as the corresponding quantisation values that are used to determine the extent of embedding for each coefficient. After being quantised, rounded to the nearest integer and converted to binary, the Least Significant Bit (LSB) vector is extracted from the 7 DCT coefficients. These individual bits are exclusive-or'd together and are compared to the the present signature bit value, b_e that is to be embedded. If these bits do not match, the bit resulting in the least amount of distortion from the LSB vector is flipped. This results in a new LSB vector, which contains the bit b_e as an embedded watermark. This replaces the original LSB vector and the coefficients are converted back to decimal. This process is repeated several times to ensure that the bit is embedded correctly and is not lost as a result of clipping and rounding from binary to decimal conversion. System structures that are re-used in the watermark extraction process include those on the left side of the figure. In order to extract one bit from a selection of 7 coefficients, the first six processes are used to extract an embedded bit.

```
%%%%%%%%%%%%%%%%%%%%%%%%%%%%%%%%%%%%%%%%%%%%%%%%%%%%%%%%%%%%%%%%%%%%%%%%%%%%
%%%%% Fourth Level Embedding Function: One Bit per Micro Block %%%%%%%%
%%%%%%%%%%%%%%%%%%%%%%%%%%%%%%%%%%%%%%%%%%%%%%%%%%%%%%%%%%%%%%%%%%%%%%%%%%%%

% Dominic Osborne
% The University of Adelaide
% April 2003

function new_set_of_7_coeffs=embed_one_bit_in_a_block
(set_of_7_original_coeffs,quantisation_7_values,bit_to_embed)

%Out of the 7 coefficients selected from the set of 28 coefficients:
%Divide each of the coefficients by its corresponding quantisation
%factor and round to the nearest integer, that it:
%Quantisation_7_values: a set of 7 quantisation
%values chosen from the set of 28

new_set_of_7_coeffs = set_of_7_original_coeffs; %initialise coefficients

    for iterations = 1:10 %Repeat the embedding process

                % Perform the quantising step of JPEG compression
                resultant_quantised_coeffs = round(new_set_of_7_coeffs./
                (quantisation_7_values));
                %Take the LSB of each of the resulting integers and XOR
                %them together to obtain the current
                %bit value represented by these coefficients
                resultant_quantised_coeffs_bin =
                dec2bin(abs(resultant_quantised_coeffs)) - '0';
                %To convert to a string
                size_bin_coeff_vector =
                size(resultant_quantised_coeffs_bin);
                num_ls_bits = size_bin_coeff_vector(1,1);
                %which represents the number of rows, 7 of course
                ls_column = size_bin_coeff_vector(1,2);
```

```
%the actual column in which reside the ls bits
ls_bits = resultant_quantised_coeffs_bin
(1:num_ls_bits,ls_column);
%Getting the lsb vector from 7 coeffs

% XOR the bits together

b_e = bitxor(ls_bits(1,1),ls_bits(2,1));
b_e = bitxor(b_e,ls_bits(3,1));
b_e = bitxor(b_e,ls_bits(4,1));
b_e = bitxor(b_e,ls_bits(5,1));
b_e = bitxor(b_e,ls_bits(6,1));
b_e = bitxor(b_e,ls_bits(7,1)); %current bit value

if b_e ~= bit_to_embed

       %Then we must flip the lsb of one of the integers.
       %Then we must flip the lsb of one of the integers.
       % The one to flip is the one that will cause the
       %least fidelity impact.
       for i = 1:7 %For each quantised coefficients
       %Find out what the new value of each of the
       %coefficients if we flip the lsb
            if set_of_7_original_coeffs(i) <
               quantisation_7_values(i)*
               resultant_quantised_coeffs(i);
               flipped_ci = resultant_quantised_coeffs(i)
               - 1;  %Then subtract a bit
            else
               flipped_ci = resultant_quantised_coeffs(i)
               + 1;  %Otherwise add a bit to it
            end

            %Find the quantisation factor multiples that
            %get closest to the current coefficient values
```

```
                    flip_error(i) = abs(quantisation_7_values(i)
                    *flipped_ci - set_of_7_original_coeffs(i));
                end

            %Get the position in the flip error vector
            %containing the smallest error
            [min_value,position] = min(flip_error);
            %flip the lsb of the selected coefficient

                    if set_of_7_original_coeffs(position) <
                        quantisation_7_values(position)*
                        resultant_quantised_coeffs(position);
                        flipped_ci = resultant_quantised_coeffs
                        (position) - 1;
                    else
                        flipped_ci = resultant_quantised_coeffs
                        (position) + 1;
                    end
                    resultant_quantised_coeffs(position) =
                    flipped_ci;
        end

    new_set_of_7_coeffs = round(resultant_quantised_coeffs.*
    quantisation_7_values);
end
```

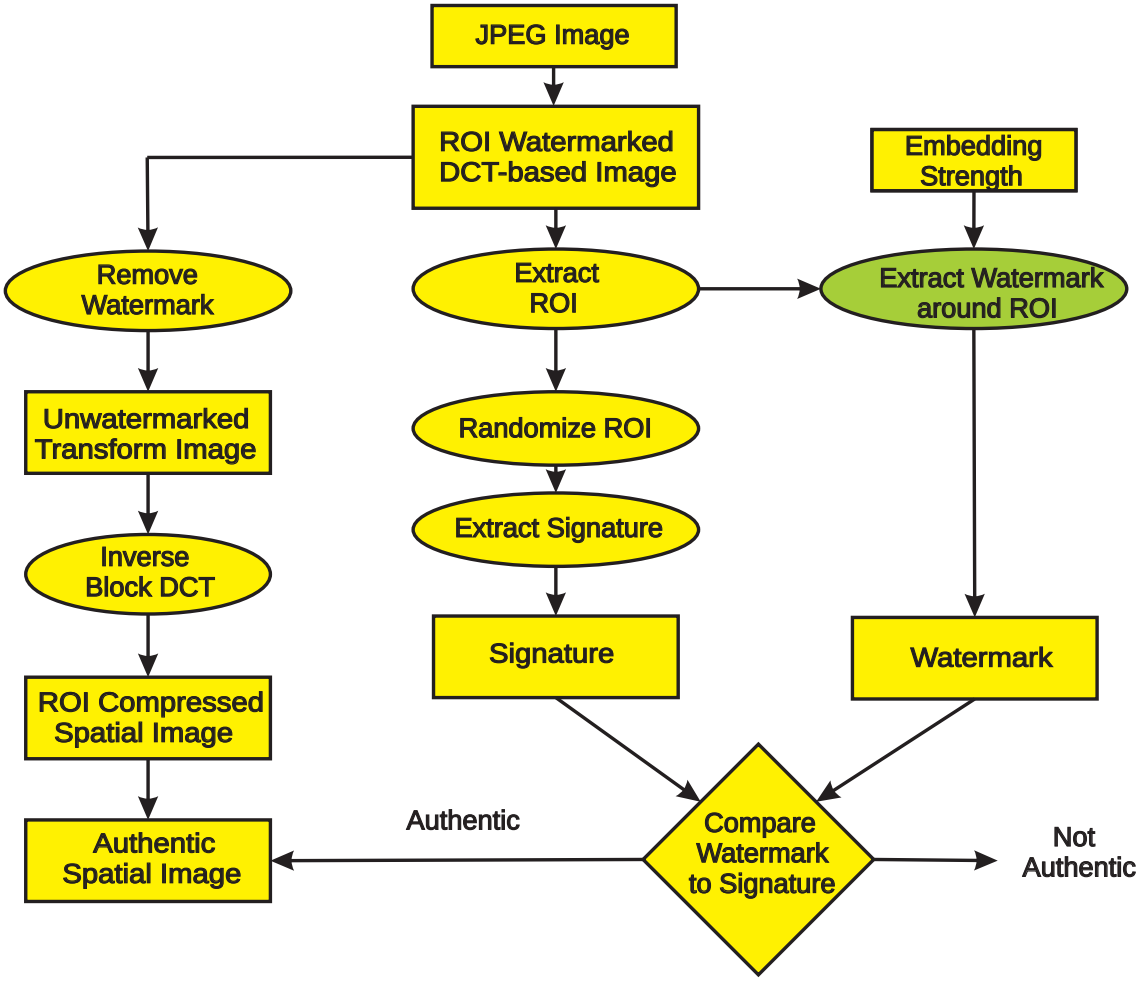

Figure B.7. Top level function for watermark extraction. A JPEG file is examined for ROI content authentication. Three stages take place, which include signature and watermark extraction as well as the optional process of watermark removal. This algorithm requires that the ROI location is pre-specified. Extraction of the signature is implemented by re-using the software modules shown in Figure B.1, which is depicted by the the software processes 'Extract ROI' to 'Extract Signature.' Extraction of the watermark from the ROB takes place using the sub-function shown in Figure B.8. Bits in the signature and watermark are then compared pair-wise against a threshold of $\pi_0 = 85\%$ to discriminate an acceptable match from a watermark loss.

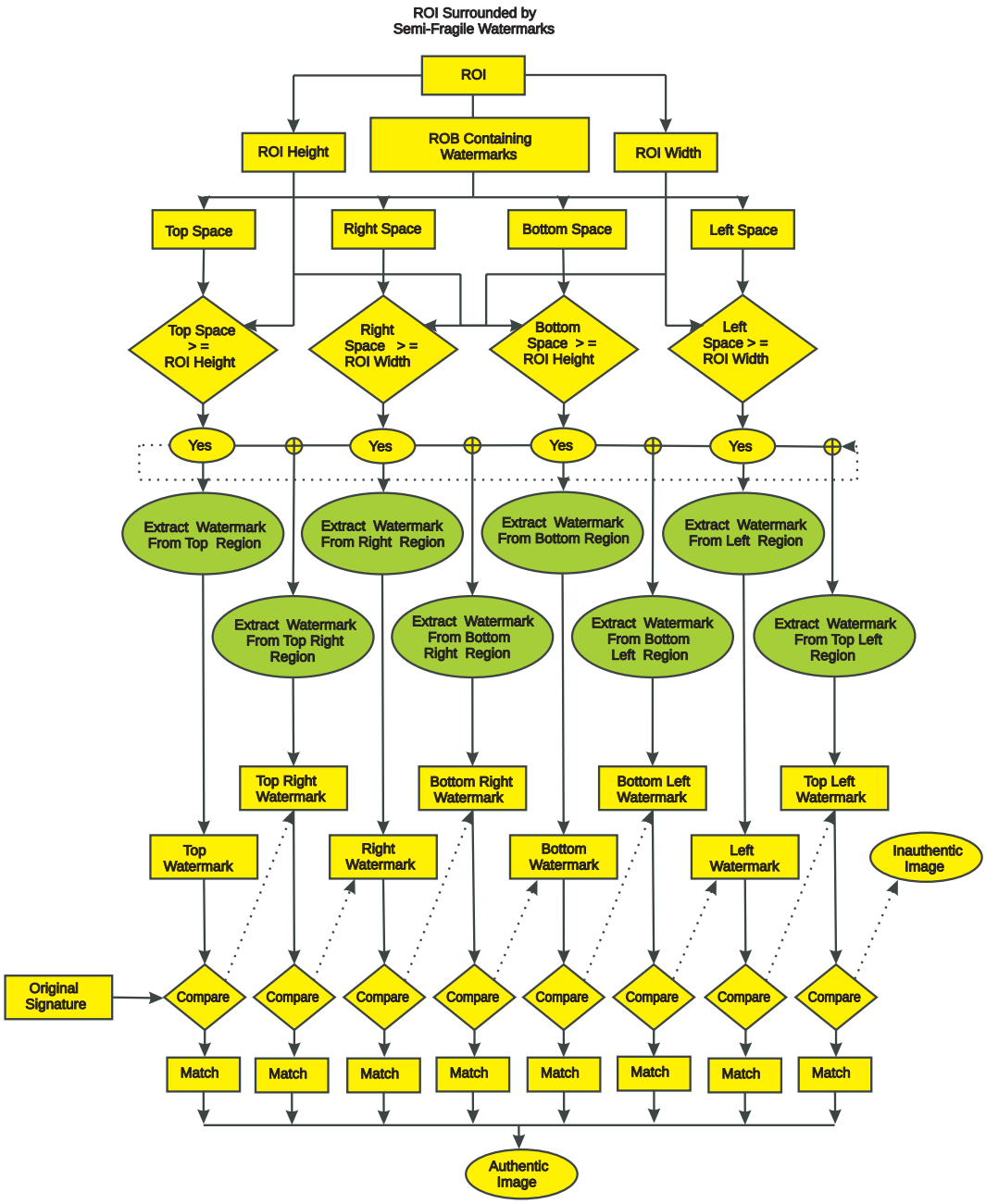

Figure B.8. Sub-function for watermark extraction around the ROI. Two input arguments are required including the position of the ROI and the watermarked image in its DCT transform representation. On knowing the position of the ROI, this system can easily determine the available space in the ROB where authentication information is placed. Watermarks can be extracted sequentially in the event that a watermark does not match the original signature given an acceptable threshold, π_0. If an acceptable match is not found, the image is declared as inauthentic. Extracting a singular watermark is performed by re-using the software modules depicted in Figures B.4, B.5 and B.6.

```
%%%%%%%%%%%%%%%%%%%%%%%%%%%%%%%%%%%%%%%%%%%%%%%%%%%%%%%%%%%%%%%%%%%%%%%%%%%%
%%%%%  Top Level Function for Extracting Multiple Watermarks   %%%%%%%%
%%%%%%%%%%%%%%%%%%%%%%%%%%%%%%%%%%%%%%%%%%%%%%%%%%%%%%%%%%%%%%%%%%%%%%%%%%%%

function  [signature,extracted_signature_bits]=
          D_ROI(watermarked_transform_image)

% Top level function D_SFSIG
% Tests the Authenticity of an image file by
% 1) Extracting a signature using the protocols from the embedder
% 2) Extracting a watermark and comparing it to the signature
% 3) 85% bits must match for an authentication

% Get the image.  In this case the JPEG file has been converted
% to a bitmap for ease of calculation.

% Dominic Osborne
% The University of Adelaide
% August 2003

watermarked_image = imread('watermarked_image.bmp');
%load('test.mat')
alpha = 1.44; %which is used as the embedding strength

%Convert to transform representation for extraction of watermark
fun = @dct2; watermarked_transform = blkproc(watermarked_image,[8
8],fun); watermarked_transform = round(watermarked_transform); c =
watermarked_transform;

size_vector = size(c); % To get the size in pixels
full_height = size_vector(1,1); full_width = size_vector(1,2);
image_bottom = full_height; image_top = 1; image_left = 1;
image_right = full_width; tilesize = 8;

% Re-define a ROI
```

```
roi_top = 265; roi_bottom = 480; roi_left = 129; roi_right = 256;
roi = c(roi_top:roi_bottom,roi_left:roi_right); size_roi =
size(roi); width_roi = size_roi(1,2); height_roi = size_roi(1,1);
num_tiles = width_roi*height_roi/(tilesize*tilesize);

% Uncorrelate the image blocks side to side
randomized_roi = randomize_blocks(roi,tilesize);

% Extract a signature from the ROI
ex_signature = extract_signature(randomized_roi,tilesize);



% Perform Extraction:
bottom_space = image_bottom - roi_bottom + 1; top_space = roi_top-1;
left_space = roi_left-1; right_space = full_width - roi_right;

% Set flag pointer to zero
extraction_successful = 0; while extraction_successful == 0

    %top region
    if   top_space < height_roi
         disp('No watermark in top region')
    else
        region = c(roi_top - height_roi:roi_top - 1,roi_left:roi_right);
        watermark = extract_watermark_from_region(region,width_roi,
        height_roi,alpha,tilesize);
    end

    bit_errors = biterr(ex_signature,watermark);
    percentage_bit_error = 100*bit_errors/prod(size(ex_signature))
    if percentage_bit_error < 15
        extraction_successful = 1;
    end

        %top right region
```

```
if   top_space < height_roi
     disp('No watermark in top right region')
else
    region = c(roi_top - height_roi:roi_top - 1,
    roi_right+1:roi_right+width_roi);
    watermark = extract_watermark_from_region(region,width_roi,
    height_roi,alpha,tilesize);
end

bit_errors = biterr(ex_signature,watermark);
percentage_bit_error = 100*bit_errors/prod(size(ex_signature));
if percentage_bit_error < 15
    extraction_successful = 1;
end

    %right region
if   right_space < width_roi
     disp('No Watermark in Right Region')
else
    region = c(roi_top:roi_bottom,roi_right+1:roi_right+width_roi);
    watermark = extract_watermark_from_region(region,width_roi,
    height_roi,alpha,tilesize);
end

bit_errors = biterr(ex_signature,watermark);
percentage_bit_error = 100*bit_errors/prod(size(ex_signature));
if percentage_bit_error < 15
    extraction_successful = 1;
end

    %bottom right region
if   right_space < width_roi | bottom_space < height_roi
     disp('No watermark in bottom right region')
else
    region = c(roi_bottom + 1:roi_bottom + height_roi,
```

```
    roi_right+1:roi_right+width_roi);
    watermark = extract_watermark_from_region(region,width_roi,
    height_roi,alpha,tilesize);
end

bit_errors = biterr(ex_signature,watermark);
percentage_bit_error = 100*bit_errors/prod(size(ex_signature));
if percentage_bit_error < 15
    extraction_successful = 1;
end

    %bottom region
if   bottom_space < height_roi
     disp('No watermark in bottom region')
else
    region = c(roi_bottom + 1:roi_bottom + height_roi,
    roi_left:roi_right);
    watermark = extract_watermark_from_region(region,width_roi,
    height_roi,alpha,tilesize);
end

bit_errors = biterr(ex_signature,watermark);
percentage_bit_error = 100*bit_errors/prod(size(ex_signature));
if percentage_bit_error < 15
    extraction_successful = 1;
end
    %bottom left region
if   bottom_space < height_roi | left_space < width_roi
     disp('No watermark in bottom left region')
else
    region = c(roi_bottom + 1:roi_bottom + height_roi,
    roi_left-width_roi:roi_left - 1);
    watermark = extract_watermark_from_region(region,width_roi,
    height_roi,alpha,tilesize);
end
```

```
bit_errors = biterr(ex_signature,watermark);
percentage_bit_error = 100*bit_errors/prod(size(ex_signature));
if percentage_bit_error < 15
    extraction_successful = 1;
end

    %left region
if   left_space < width_roi
     disp('No watermark in left region')
else
    region = c(roi_top:roi_bottom,roi_left-width_roi:roi_left - 1);
    watermark = extract_watermark_from_region(region,width_roi,
    height_roi,alpha,tilesize);
end

bit_errors = biterr(ex_signature,watermark);
percentage_bit_error = 100*bit_errors/prod(size(ex_signature));
if percentage_bit_error < 15
    extraction_successful = 1;
end

    %top left region
if   left_space < width_roi | top_space < height_roi
     disp('No watermark in top left region')
else
    region = c(roi_top - height_roi:roi_top - 1,
    roi_left-width_roi:roi_left - 1);
    watermark = extract_watermark_from_region(region,
    width_roi,height_roi,alpha,tilesize);
end

bit_errors = biterr(ex_signature,watermark);
percentage_bit_error = 100*bit_errors/prod(size(ex_signature));
if percentage_bit_error < 15
```

```
        extraction_successful = 1;
    end

    if extraction_successful == 1
       disp('Watermark Extraction Succesful')
    else
        extraction_successful = 1;
        disp('Watermark Extraction Not Succesful')
    end
end



%%%%%%%%%%%%%%%%%%%%%%%%%%%%%%%%%%%%%%%%%%%%%%%%%%%%%%%%%%%%%%%%%%%%%%%%%%%%
%%%  Second Level Function for Extracting a Watermark from a Region   %%%
%%%%%%%%%%%%%%%%%%%%%%%%%%%%%%%%%%%%%%%%%%%%%%%%%%%%%%%%%%%%%%%%%%%%%%%%%%%%

% Dominic Osborne
% The University of Adelaide
% April 2003

function watermark = extract_watermark_from_region
         (region,width_roi,height_roi,alpha,tilesize)

quant_matrix = get_dctq_matrix(alpha);
%Calls a function to get and scale the quantisation matrix.
%embed 4 bits in each block

%Now tiling and performing DCT to each tile
x_ref = 1;           % Define a starting point for application of the DCT
y_ref = 1;           % Define a starting point for application of the DCT
signature_row_reference = 1; watermark_pointer = 0;

   while y_ref <= height_roi
        x_ref = 1;
        while x_ref < width_roi %Center loop for application of DCT
```

```
            current_transform_tile = region(y_ref:y_ref + tilesize -1,
            x_ref:x_ref + tilesize -1);

            signature_row_reference = signature_row_reference + 1;

            extracted_four_bits = extract_four_bits_from_a_block
            (quant_matrix,current_transform_tile);

            watermark(watermark_pointer+1:watermark_pointer+4) =
            extracted_four_bits;
            watermark_pointer = watermark_pointer + 4;

            x_ref = x_ref + tilesize;
            %Move right to the immediate next tile

        end
         y_ref = y_ref + tilesize; %Move down to a lower tile
    end


%%%%%%%%%%%%%%%%%%%%%%%%%%%%%%%%%%%%%%%%%%%%%%%%%%%%%%%%%%%%%%%%%%%%%%%%%%%%
%%% Third Level Function for Extracting Four Bits From a Micro Block   %%
%%%%%%%%%%%%%%%%%%%%%%%%%%%%%%%%%%%%%%%%%%%%%%%%%%%%%%%%%%%%%%%%%%%%%%%%%%%%

% Dominic Osborne
% The University of Adelaide
% April 2003

function  extracted_four_bits = extract_four_bits_from_a_block
(quant_matrix,current_transform_tile)

p = current_transform_tile; %for Convenience to specify the DCT vector

% Converting the whole DC-transform tile to a zigzag vector
```

```
zigzag_dct_vector = [p(1,1),p(1,2),p(2,1),p(3,1),p(2,2),p(1,3),
    p(1,4),p(2,3),p(3,2),p(4,1),p(5,1),p(4,2),p(3,3),p(2,4),
    p(1,5),p(1,6),p(2,5),p(3,4),p(4,3),p(5,2),p(6,1),p(7,1),
    p(6,2),p(5,3),p(4,4),p(3,5),p(2,6),p(1,7),p(1,8),p(2,7),
    p(3,6),p(4,5),p(5,4),p(6,3),p(7,2),p(8,1),p(8,2),p(7,3),
    p(6,4),p(5,5),p(4,6),p(3,7),p(2,8),p(3,8),p(4,7),p(5,6),
    p(6,5),p(7,4),p(8,3),p(8,4),p(7,5),p(6,6),p(5,7),p(4,8),
    p(5,8),p(6,7),p(7,6),p(8,5),p(8,6),p(7,7),p(6,8),p(7,8),
    p(8,7),p(8,8)];

embedding_coefficients = [zigzag_dct_vector(37:64)];

x = quant_matrix; zigzag_quant_vector =
[x(1,1),x(1,2),x(2,1),x(3,1),x(2,2),
    x(1,3),x(1,4),x(2,3),x(3,2),x(4,1),x(5,1),x(4,2),x(3,3),
    x(2,4),x(1,5),x(1,6),x(2,5),x(3,4),x(4,3),x(5,2),x(6,1),
    x(7,1),x(6,2),x(5,3),x(4,4),x(3,5),x(2,6),x(1,7),x(1,8),
    x(2,7),x(3,6),x(4,5),x(5,4),x(6,3),x(7,2),x(8,1),x(8,2),
    x(7,3),x(6,4),x(5,5),x(4,6),x(3,7),x(2,8),x(3,8),x(4,7),
    x(5,6),x(6,5),x(7,4),x(8,3),x(8,4),x(7,5),x(6,6),x(5,7),
    x(4,8),x(5,8),x(6,7),x(7,6),x(8,5),x(8,6),x(7,7),x(6,8),
    x(7,8),x(8,7),x(8,8)];
quantisation_values = zigzag_quant_vector(37:64);
coefficient_pointer = 0; extracted_four_bits = zeros(1,4);
bit_pointer = 1;

    for i = 1:4

        set_of_7_original_coeffs =  embedding_coefficients
        (coefficient_pointer+1:coefficient_pointer + 7);
        quantisation_7_values = quantisation_values
        (coefficient_pointer+1:coefficient_pointer + 7);

                new_set_of_7_coeffs = set_of_7_original_coeffs;
                % Perform the quantising step of JPEG compression
```

```
                resultant_quantised_coeffs = round(new_set_of_7_coeffs./
                (quantisation_7_values));
                % Convert host DCT coefficients to binary to extract lsb
                resultant_quantised_coeffs_bin =
                dec2bin(abs(resultant_quantised_coeffs)) - '0';
                size_bin_coeff_vector =
                size(resultant_quantised_coeffs_bin);
                num_ls_bits = size_bin_coeff_vector(1,1);
                ls_column = size_bin_coeff_vector(1,2);
                ls_bits = resultant_quantised_coeffs_bin
                (1:num_ls_bits,ls_column);

                % XOR the least significant bits together
                b_e = bitxor(ls_bits(1,1),ls_bits(2,1));
                b_e = bitxor(b_e,ls_bits(3,1));
                b_e = bitxor(b_e,ls_bits(4,1));
                b_e = bitxor(b_e,ls_bits(5,1));
                b_e = bitxor(b_e,ls_bits(6,1));
                b_e = bitxor(b_e,ls_bits(7,1)); %current bit extracted
                extracted_four_bits(1,bit_pointer) = b_e;

        new_coefficients(coefficient_pointer+1:coefficient_pointer + 7) =
        new_set_of_7_coeffs;
        coefficient_pointer = coefficient_pointer + 7;
        bit_pointer = bit_pointer + 1;
    end

%%%%%%%%%%%%%%%%%%%%%%%%%%%%%%%%%%%%%%%%%%%%%%%%%%%%%%%%%%%%%%%%%%%%%%%%%%%%
%%%%%%%%%%%%%%  Sub-Function to Assign New DCT Values   %%%%%%%%%%%%%%
%%%%%%%%%%%%%%%%%%%%%%%%%%%%%%%%%%%%%%%%%%%%%%%%%%%%%%%%%%%%%%%%%%%%%%%%%%%%

% Dominic Osborne
% The University of Adelaide
% April 2003
```

```
function watermarked_transform_tile =
assign_new_coefficients(new_coefficients,current_transform_tile)
watermarked_transform_tile = current_transform_tile;

watermarked_transform_tile(8,2) = new_coefficients(1);
watermarked_transform_tile(7,3) = new_coefficients(2);
watermarked_transform_tile(6,4) = new_coefficients(3);
watermarked_transform_tile(5,5) = new_coefficients(4);
watermarked_transform_tile(4,6) = new_coefficients(5);
watermarked_transform_tile(3,7) = new_coefficients(6);
watermarked_transform_tile(2,8) = new_coefficients(7);
watermarked_transform_tile(3,8) = new_coefficients(8);
watermarked_transform_tile(4,7) = new_coefficients(9);
watermarked_transform_tile(5,6) = new_coefficients(10);
watermarked_transform_tile(6,5) = new_coefficients(11);
watermarked_transform_tile(7,4) = new_coefficients(12);
watermarked_transform_tile(8,3) = new_coefficients(13);
watermarked_transform_tile(8,4) = new_coefficients(14);
watermarked_transform_tile(7,5) = new_coefficients(15);
watermarked_transform_tile(6,6) = new_coefficients(16);
watermarked_transform_tile(5,7) = new_coefficients(17);
watermarked_transform_tile(4,8) = new_coefficients(18);
watermarked_transform_tile(5,8) = new_coefficients(19);
watermarked_transform_tile(6,7) = new_coefficients(20);
watermarked_transform_tile(7,6) = new_coefficients(21);
watermarked_transform_tile(8,5) = new_coefficients(22);
watermarked_transform_tile(8,6) = new_coefficients(23);
watermarked_transform_tile(7,7) = new_coefficients(24);
watermarked_transform_tile(6,8) = new_coefficients(25);
watermarked_transform_tile(7,8) = new_coefficients(26);
watermarked_transform_tile(8,7) = new_coefficients(27);
watermarked_transform_tile(8,8) = new_coefficients(28);
```

```
%%%%%%%%%%%%%%%%%%%%%%%%%%%%%%%%%%%%%%%%%%%%%%%%%%%%%%%%%%%%%%%%%%%%%%%%%%%%
%%%  Sub-Function to Get the Approprate DCT Quantisation Matrix   %%%%%%%
%%%%%%%%%%%%%%%%%%%%%%%%%%%%%%%%%%%%%%%%%%%%%%%%%%%%%%%%%%%%%%%%%%%%%%%%%%%%

% Dominic Osborne
% The University of Adelaide
% April 2003

function  quant_matrix=get_dctq_matrix(alpha)

quantisation_table = [16,11,10,16,24,40,51,61;
12,12,14,19,26,58,60,55; 14,13,16,24,40,57,69,56;
14,17,22,29,51,87,80,62; 18,22,37,56,68,109,103,77;
24,35,55,64,81,104,113,92; 49,64,78,87,103,121,120,101;
72,92,95,98,112,100,103,99];

quant_matrix = [alpha.*quantisation_table];

%%%%%%%%%%%%%%%%%%%%%%%%%%%%%%%%%%%%%%%%%%%%%%%%%%%%%%%%%%%%%%%%%%%%%%%%%%%%
%%%%%%%%%%%%%%%%%%%%%%  DCT Quantisation Algorithm   %%%%%%%%%%%%%%%%%%%%%%
%%%%%%%%%%%%%%%%%%%%%%%%%%%%%%%%%%%%%%%%%%%%%%%%%%%%%%%%%%%%%%%%%%%%%%%%%%%%

% Dominic Osborne
% The University of Adelaide
% April 2003

function [new_block]=compress(x)

new_block = x; compression_level = 0.2; quantisation_table =
[16,11,10,16,24,40,51,61; 12,12,14,19,26,58,60,55;
14,13,16,24,40,57,69,56; 14,17,22,29,51,87,80,62;
18,22,37,56,68,109,103,77; 24,35,55,64,81,104,113,92;
49,64,78,87,103,121,120,101; 72,92,95,98,112,100,103,99];
quant_matrix = [compression_level.*quantisation_table]; new_block =
quant_matrix.*round(new_block./quant_matrix);
```

Appendix C

JPEG Compression Standard

JOINT Photographic Experts Group (JPEG) specification has become the most widespread standard for storing photographic still images. JPEG uses transform based coding and is exploits the property that most of the useful image content changes relatively slowly across images. This appendix presents a theoretical overview of baseline JPEG compression, shown in Section C.1 and the underlying DCT in Section C.1.1. Details that specify the bitstream configuration of JPEG are unrelated to the watermarking procedure and are not covered in this Appendix. As JPEG-2000 has been treated as a side issue in this thesis, there is no discussion covering the structure of this standard.

C.1 Theoretical Overview of Baseline JPEG

In this section a review JPEG lossy image compression standard is presented and some of the transforms involved. For simplicity, 8-bit monochromatic images are used. A systematic overview of this compression standard is shown in Figure C.1. At the input

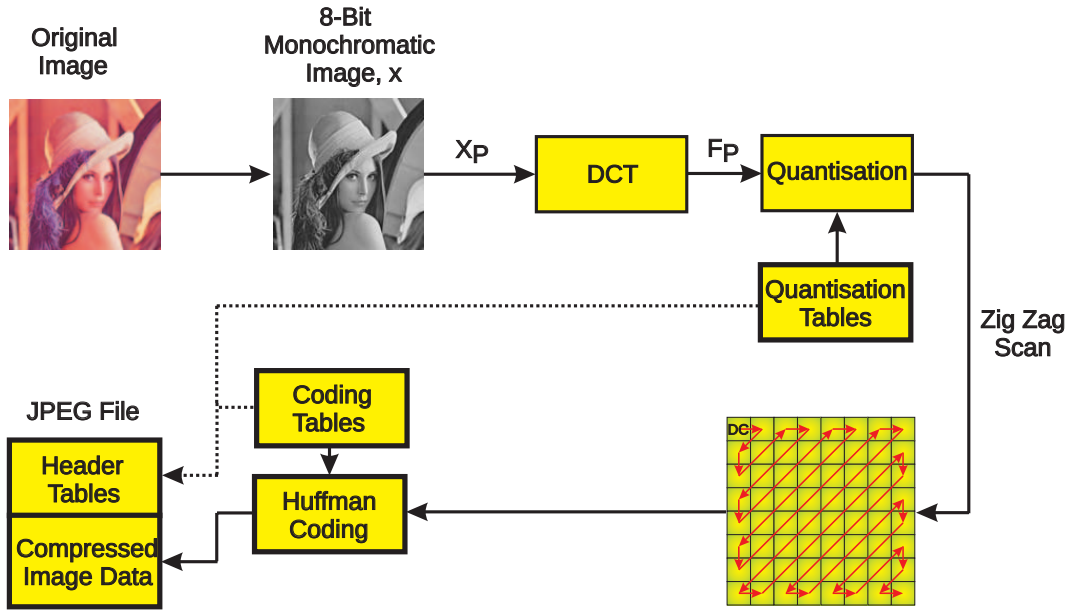

Figure C.1. Overview of the JPEG compression system. For ease of implementation, the quantisation table is typically extracted from the compressed JPEG file or estimated by analyzing the DCT coefficients of the decompressed image.

to the encoder a monochromatic image, X, is segmented into ρ adjacent 8×8 blocks, $X = \bigcup_{p=1}^{\rho} X_p$. Each block undergoes a DCT and can be rewritten as a 64×1 vector following the JPEG zigzag scan. The set of 8×8 coefficients contains values F_p, where:

$$F_p = DCT(X_p). \tag{C.1}$$

Each coefficient in the micro block is quantised uniformly by a 64-element quantisation table, Q, used on all coefficients in all micro blocks in the image. Each DCT coefficient is divided by its corresponding quantisation step size and integer rounded. The quantisation process is the key step which removes redundant DCT coefficients that are not easily noticed by the HVS. This allows for 64 pixel values to stored as a few coefficients, thus allowing for effective compression.

$$\tilde{f}_p(i) \equiv \text{ROUND}\left(\frac{F_p(i)}{Q(i)}\right). \tag{C.2}$$

For $i = 1....64$ following the zigzag scan order, where $\tilde{f}_p$ is the quantised coefficient. The quantised approximation of F_p is defined as:

$$\tilde{F}_p \equiv \tilde{f}_p(i) \cdot Q(i). \tag{C.3}$$

The reverse process is also possible where the micro blocks can be converted back to spatial domain representation, $\tilde{X}_P$. This process is called the block-based Inverse Discrete Cosine Transform (IDCT) and results in a decoded image block, comprising of 8-bit integers:

$$\tilde{X}_p = D^{-1}\tilde{F}_p. \tag{C.4}$$

These are used to represent dark to bright pixel intensities, which can have integer values from 0 to 255 for a greyscale image.

C.1.1 The Discrete Cosine Transform

The DCT defined by Ahmed *et al.* (1974), is the principal transformation used in the JPEG compression and decompression process. It has proved to be very useful for approximating linear signals with very few coefficients by converting them from the spatial domain to the frequency domain.

The DCT involves taking a set of input values and transforming them into a linear combination of weighted basis functions. These functions are representations of the different frequency characteristics of the original data set and are depicted in Figure C.2.

For an 8×8 image pixel block, it is necessary to perform a two-dimensional DCT, whereby a one-dimensional DCT is applied twice; once in the x-direction and and again in the y-direction. This results in a corresponding DCT block of the same dimensions that is shown in Figure C.3. The pixel values are replaced with a measure of spatial frequency, representing the change in intensity across the pixel block. Compression is possible as only a few coefficients are needed to approximately reconstruct the original pixel set.

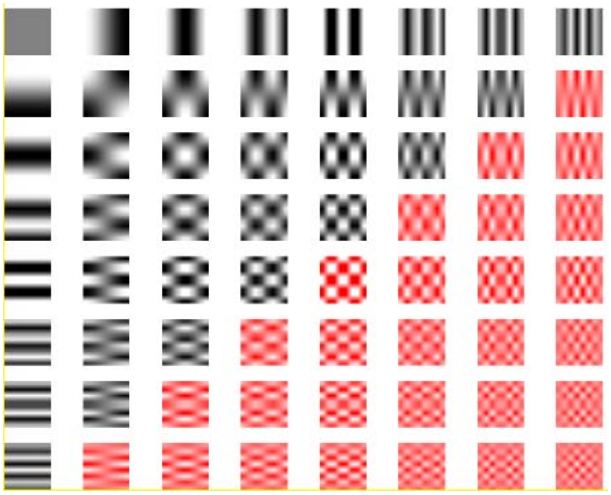

Figure C.2. Set of 8×8 basis functions used in the JPEG compression process. The top left pattern represents the DC or non-varying basis function. This represents detail most easily noticed by the HVS. Following the JPEG zigzag scan sequence to the bottom right basis function shows the highest spatial frequency pattern that would least be noticed by the HVS as it contains the most fine detail. The last 28 basis functions are shaded red to indicate the regions where signature information is placed. These functions are least probable to be used in the JPEG decompression process. This is because the DCT coefficients corresponding to their positions are most likely zero after DCT quantisation has occurred during JPEG compression.

The DCT as used in image compression standards can be defined in Equation C.5.

$$F(u,v) = \frac{1}{4} C_U C_V \sum_{x=0}^{7} \sum_{x=0}^{7} f(x,y) \cos\left(\frac{(2x+1)u\pi}{16}\right) \cos\left(\frac{(2y+1)v\pi}{16}\right)$$

$$C_U = \frac{1}{\sqrt{2}} \qquad \text{for } u = 0, C_U = 1 \text{ otherwise}$$

$$C_V = \frac{1}{\sqrt{2}} \qquad \text{for } v = 0, C_V = 1 \text{ otherwise.} \tag{C.5}$$

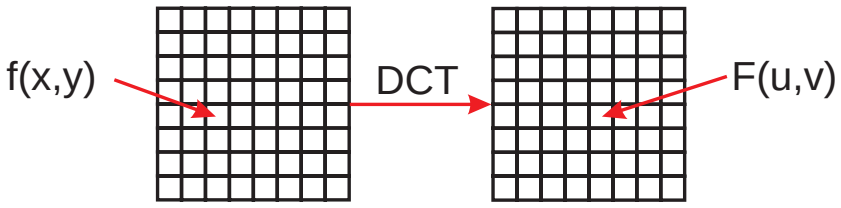

Figure C.3. Performing the DCT on a pixel block. For a set of 8×8 pixels, x and y are indices into this region. After the transformation F is applied, u and v are the resulting indices into an 8×8 array of DCT coefficients.

Appendix D

Proof of Theorems

PROOFS of two of the theorems presented by Lin and Chang are presented. These include theorems 1 and 2, which are defined in Chapter 2, which relate to the extraction of image feature information. In some software applications, truncation is used instead of integer rounding for DCT values in an image. In this instance both theorems are still valid but can be proved by **Proof 2** with identical parameter substitutions as in **Proof 1.** These proofs have been adapted from Lin and Chang (2001).

D.1 Proof 1

$\forall a, b, c \in \Re$, assume $a = A + r(a)$, $b = B + r(b)$, and $c = C + r(c)$, in which $A, B, C \in Z$ are the rounding integers of a, b, c and $-0.5 \leq r(a), r(b), r(c) < 0.5$.
Assume $a - b > c$, then substituting gives:

$$A + r(a) - B - r(b) > C + r(c)$$

therefore by rearranging,

$$A - B - C > r(c) + r(b) - r(a).$$

If c is an integer, then

$$A - B - C > -1.0.$$

But since A,B,C are integers,

$$A - B \geq C.$$

Supposing that $r(c) \neq 0$, then

$$-1.5 < r(c) + r(b) - r(a) < 1.5.$$

Because $A, B, C \in Z$

$$A - B \geq C - 1.$$

Theorem 1 can be proved by substituting a by $\frac{F_p(i)}{Q(i)}$, A by $\frac{\tilde{F}_p(i)}{Q(i)}$, by $\frac{F_q(i)}{Q(i)}$, B by $\frac{\tilde{F}_q(i)}{Q(i)}$, c by 0 and with every parameter multiplied by $Q(i)$.

D.2 Proof 2

$\forall a, b, c \in \Re$, assume $a = A + r(a)$, $b = B + r(b)$, and $c = C + r(c)$, in which $A, B, C \in Z$ are the truncated integers of a, b, c and $0 \leq r(a), r(b), r(c) < 1$. If $a - b > c$, then $A - B - C > r(c) + r(b) - r(a)$,
if c is an integer, then $-1.0 < r(c) + r(b) - r(a) < 1.0$. Hence,

$$A - B \geq C.$$

If $r(c) \neq 0$, then $-1.0 < r(c) + r(b) - r(a) < 2$. Because $A, B, C \in Z$,

$$A - B - C \geq 0 > -1.$$

Consequently,

$$A - B \geq C,$$

Satisfying the relationship $A - B \geq C - 1$. Theorem 2 can be proved with the same parameter substitutions, except c is replaced by $\frac{k}{Q(i)}$ and C with $\tilde{k}_i$.

Appendix E

List of Acronyms

ACR	American College of Radiology
Angio-C	Angiographic Cardiology
Angio-R	Angiographic Radiology
BMP	Bitmap
Bpp	Bits Per Pixel
CR	Computed Radiography
CT	Computed Tomography
DCT	Discrete Cosine Transform
DF	Digital Fluoroscopy
DICOM	Digital Imaging and Communication in Medicine
DPCM	Differential Pulse Code Modulation
DR	Direct Radiography
DWT	Discrete Wavelet Transform
EBCOT	Embedded Block Coding with Optimal Truncation
ECG	Electrocardiogram
FD	Film Digitizer
FEC	Forward Error Correction
fps	Frames Per Second
GSM	Global System for Mobile Communications
HPS	Human Patient Simulator
HVS	Human Visual System
IDCT	Inverse Discrete Cosine Transformation
ISO	International Standard Organisation
ITU	International Telecommunication Union

JPEG	Joint Picture Experts Group
Mb	Mega Bytes
MRI	Magnetic Resonance Imaging
MVSAT	Mobile Very Small Aperture Terminal
NM	Nuclear Medicine
NMSE	Normalised Mean Square Error
OCR	Object Character Recognition
PACS	Picture Archiving and Communication Systems
PDA	Personal Digital Assistant
PSNR	Peak Signal to Noise Ratio
RF	Radio Frequency
RMS	Root Mean Square
ROB	Region of Background
ROC	Receiver Operating Characteristic
ROI	Region of Interest
SMS	Short Message Service
SNR	Signal-to-Noise Ratio
SPIHT	Set Partitioning in Hierarchal Trees
TIP	telemedicine Instrumentation Pack
US	Ultrasound
VHF	Very High Frequency
VSQ	Variable Scalar Quantisation
WWW	World Wide Web
3G	Third Generation

Appendix F

List of Symbols

X	Monochromatic 8-bit image used for testing
ρ	Number of micro blocks
F_P	Coefficient vector taken from a micro block, F
$\tilde{X}_P$	8-bit pixel value
Q	Quantisation table
$\tilde{f}_p$	Quantised coefficient
α	Embedding strength
b_e	Present signature bit value
C_W	Watermarked coefficient
Z	Feature codes extracted from an image
$\Delta F_{p,q}$	Difference between coefficients p and q
k	Fixed threshold used to bound DCT coefficient differences
Z	The real set of integers
N	Number of sets of feature codes generated from an image
b_n	Number of coefficients to extract a signature
n	Signature length
M	Number of matches between signature and watermark
π	Proportion of matches between signature and watermark
π_0	Proportion of matches for an acceptable watermark
τ	Significance for accepting an inauthentic image
N_i	Noise introduced to image
N_n	Natural level of noise present in original image
N_c	Noise introduced to image as a result of compression
N_w	Noise introduced to image over a wireless link

Bibliography

ABRAMOWITZ-M., AND STEGUN-I. A. (1974). *Handbook of Mathematical Functions*, Dover Publications.

AGRAFIOTIS-D., BULL-D. R., AND CANAGARAJAH-N. (2003). Region of interest coding of volumetric medical images, *Proceedings of the IEEE International Conference on Image Processing*, Vol. 3, pp. 217–220.

AHMED-N., NATARAJAN-T., AND RAO-K. R. (1974). Discrete cosine transform, *IEEE Transactions on Computers*, **C-23**, pp. 90–93.

American College of Radiology (2005). Web. http://www.acr.org Last Checked: Febuary 3 2005.

ANAND-D., AND NIRANJAN-U. C. (1998). Watermarking medical images with patient information, *Proceedings of the IEEE Engineering in Medicine and Biology Society*, pp. 703–706.

ANASTASSOPOULOS-G. K., AND SKODRAS-A. N. (2002). JPEG2000 ROI coding in medical imaging applications, *Proceedings of the 2nd IASTED International Conference on visualisation, imaging and image processing (VIIP2002)*, pp. 783–788.

ARUNODAY-T., SUDIPTA-M., AND VIDYA-K. (2004). Segmentation-based CT image compression, *Proceedings of the SPIE - Medical Imaging 2004: PACS and Imaging Informatics*, Vol. 5371, pp. 160–169.

AVCIBAS-I., MEMON-N., AND SANKUR-B. (2003). Steganalysis using image quality metrics, *IEEE Transaction on Image Processing*, **12**(2), pp. 221–229.

AWRANGJEB-M., AND KANKANHALLI-M. S. (2005). Reversible watermarking using a perceptual model, *Journal of Electronic Imaging*, **14**(1), pp. 1–8.

CELIK-M. U., SHARMA-G., TEKALP-A. M., AND SABER-E. S. (2003). Localized lossless authentication watermark (LAW), *Proceedings of the SPIE - Security and Watermarking of Multimedia Contents V*, Vol. 5020, pp. 689–698.

CHEN-M.-J., PAN-C.-W., CHEN-J.-W., AND WENG-R.-M. (2001). Multiple region-of-interest image coding with embedded watermark, *Proceedings of the IEEE International Symposium on Circuits and Systems*, Vol. 5, Sydney, NSW, Australia, pp. 207–210.

CHEN-T. S., CHEN-J., AND CHEN-J. G. (2004). A simple and efficient watermark technique based on JPEG2000 codec, *Journal of Multimedia Systems*, **10**(1), pp. 16–26.

CLUNIE-D. (2000). Lossless compression of greyscale medical images - effectivness of traditional and state of the art approaches, *Proceedings of the SPIE - Medical Imaging 2000: PACS Design and Evaluation: Engineering and Clinical Issues*, Vol. 3980, pp. 74–84.

COATRIEUX-C., MAITRE-H., SANKUR-B., ROLLAND-Y., AND COLLOREC-R. (2000). Relevance of watermarking in medical imaging, *Proceedings of the IEEE EMBS Conference on Information Technology Applications in Biomedicine*, pp. 250–255.

COOK-L. T., INSANA-M. F., MCFADDEN-M. A., HALL-T. J., AND COX-G. G. (1995). Contrast-detail analysis of image degradation due to lossy compression, *Medical Physics*, **22**(6), pp. 715–721.

COSMAN-P. C., DAVIDSON-H. C., BERGIN-C. J., TSENG-C. W., MOSES-L. E., RISKIN-E. A., OLSHEN-R. A., AND GRAY-R. M. (1994). Thoracic CT images: Effect of lossy image compression on diagnostic accuracy, *Radiology*, **190**, pp. 517–524.

COX-I. J., MILLER-M. L., AND BLOOM-J. A. (2001). *Digital Watermarking*, Morgan Kaufmann Publishers.

CRAIG-J., AND PATTERSON-V. (2005). Introduction to the practice of telemedicine, *Journal of Telemedicine and Telecare*, **11**(1), pp. 3–9.

CURRY-G. R., AND HARROP-N. (1998). The lancashire telemedicine ambulance, *Journal of Telemedicine and Telecare*, **4**(4), pp. 231–238.

DALY-S. (1990). Application of a noise-adaptive contrast sensitivity function to image data compression, *Optical Engineering*, **29**(8), pp. 977–987.

DELBRIDGE-A., BERNARD-J. R. L., BLAIR-D., BUTLER-S., PETERS-P., AND YALLOP-C. (2001). *The Macquarie Dictionary, Revised 3rd Edition*, Macquarie Library, North Ryde, NSW, Australia.

Digital Imaging and Communication in Medicine (DICOM) (2005). web. http://medical.nema.org/ Last Checked: September 6 2005.

EASTES-L. (2001). Use of the Personal Digital Assistant for point-of-care trauma documentation, *Journal of Emergency Nursing*, **27**(5), pp. 516–518.

EFSTATHOPOULOS-E. P., COSTARIDOU-L., KOCSIS-O., AND PANAYIOTAKIS-G. (2001). A protocol-based evaluation of medical image digitizers, *British Journal of Radiology*, **74**, pp. 841–846.

ENGAN-K., LILLO-M. R., AND GULSRUD-T. O. (2005). Compression of digital mammograms with region-of-interest coding evaluated on a CAD system, *Proceedings of the SPIE: Medical Imaging 2005, Image Processing*, Vol. 5747, pp. 1018–1027.

ERKOL-B., MOSS-R. H., STANLEY-R. J., STOECKER-W. V., AND HVATUM-E. (2005). Automatic lesion boundary detection in dermoscopy images using gradient vector flow snakes, *Skin Research and Technology*, **11**(1), pp. 17–26.

ESTRIBEAU-M., AND MAGNAN-P. (2005). Pixel crosstalk and correlation with modulation transfer function of CMOS image sensor, *Proceedings of the SPIE - Sensors and Camera Systems for Scientific and Industrial Applications VI*, Vol. 5677, pp. 98–108.

FERRER-ROCA-O., CARDENAS-A., DIAZ-CARDAMA-A., AND PULIDO-P. (2004). Mobile phone text messaging in the management of diabetes, *Journal of Telemedicine and Telecare*, **10**(5), pp. 282–285.

FOOS-D. H., MUKA-E., SLONE-R. M., ERICKSON-B. J., FLYNN-M. J., CLUNIE-D. A., HILDEBRAND-L., KOHM-K. S., AND YOUNG-S. S. (2000). JPEG2000 compression of medical imagery, *Proceedings of the SPIE - Medical Imaging 2000: PACS Design and Evaluation: Engineering and Clinical Issues*, Vol. 3980, pp. 85–96.

FREEMAN-D., AND KNOWLES-G. (2004). Novel architectures for the JPEG2000 block coder, *Journal of Electronic Imaging*, **13**(4), pp. 897–906.

GAGLIANO-D., LAMONTE-M., HU-P., GAASCH-W., GUNAWARDANE-R., MACKENZIE-C., AND XIAO-Y. (2000). Design and evaluation of a real-time mobile telemedicine system for ambulance transport, *Journal of High Speed Networks*, **9**(1), pp. 47–56.

GEMMILL-J. (2005). Network basics for telemedicine, *Journal of Telemedicine and Telecare*, **11**(2), pp. 71–76.

GOKTURK-S. B., TOMASI-C., GIROD-B., AND BEAULIEU-C. (2001). Medical image compression based on region of interest with application to colon CT images, *Proceedings of the 23rd Annual International Conference of the IEEE - Engineering in Medicine and Biology Society (EMBS)*, Vol. 3, pp. 2453–2456.

GOOD-W. F., MAITZ-G. S., AND GUR-D. (1994). Joint photographic experts group JPEG compatible data compression of mammograms, *Journal of Digital Imaging*, **7**(3), pp. 123–132.

HERREDSVELA-J., GULSRUD-T. O., AND ENGAN-K. (2005). Detection of circumscribed masses in mammograms using morphological segmentation, *Proceedings of the SPIE: Medical Imaging 2005: Image Processing*, Vol. 5747, pp. 902–913.

HERSH-W., HELFAND-M., WALLACE-J., KRAEMER-D., PATTERSON-P., SHAPIRO-S., AND GREENLICK-M. (2002). A systematic review of the efficacy of telemedicine for making diagnostic and management decisions, *Journal of Telemedicine and Telecare*, **8**(4), pp. 197–209.

HESLOP-L., HOWARD-A., FERNANDO-J., ROTHFIELD-A., AND WALLACE-L. (2003). Wireless communications in acute health-care, *Journal of Telemedicine and Telecare*, **9**(4), pp. 187–193.

HJELM-N. M. (2005). Benefits and drawbacks of telemedicine, *Journal of Telemedicine and Telecare*, **11**(2), pp. 60–70.

HUFFMAN-D. A. (1952). A method for the construction of minimum-redundancy codes, *Proceedings of the Institute of Radio Engineers (IRE)*, **40**, pp. 1098–1101.

JANET-J., NATESAN-T. R., SANTHOSH-R., AND IBRAMSHA-M. (2005). Detection of cyst using image segmentation and building knowledge-based intelligent decision support system as an aid to telemedicine, *Proceedings of the SPIE - Applications of Neural Networks and Machine Learning in Image Processing IX*, Vol. 5673, pp. 134–141.

JASEMIAN-Y., AND ARENDT-NIELSEN-L. (2005). Evaluation of a realtime, remote monitoring telemedicine system using the Bluetooth protocol and a mobile phone network, *Journal of Telemedicine and Telecare*, **11**(5), pp. 256–260.

JIA-W., HE-X., AND LIN-Q. (2004). Echocardiography sequential images compression based on region of interest, *Proceedings of the 2nd International Conference on Information Technology for Application (ICITA 2004)*, pp. 232–237.

JPEG 2000 Image Coding System: ITU-T Rec. T.800 08/2002, ISO/IEC 15444-1: Core Coding System (2004).

JPEG-LS - Lossless and near-lossless compression of continuous-tone still images: ITU-T Rec. T.87, ISO / IEC 14495-1: Baseline (1999).

KAIDU-M., TOYABE-S., ODA-J., OKAMOTO-K., OZAKI-T., SHIINA-M., SASAI-K., AND AKAZAWA-K. (2004). Development and evaluation of a teleradiology and videoconferencing system, *Journal of Telemedicine and Telecare*, **10**(4), pp. 214–218.

KAJIWARA-K. (1992). JPEG compression for PACS, *Computer Methods and Programs in Biomedicine*, **37**(4), pp. 343–351.

K. ENGAN-T. O. G., AND JOSEFSEN-K. R. (2003). Watermarking of digital mammograms without interfering with automatic detection of microcalcifications, *Proceedings of the IEEE International Conference on Image Processing (ICIP)*, Vol. 1, pp. 489–492.

KOCSIS-O., COSTARIDOU-L., MANDELLOS-G., LYMBEROPOULOS-D., AND PANAYIOTAKIS-G. (2003a). Compression assessment based on medical image quality concepts using computer-generated test images, *Computer Methods and Programs in Biomedicine*, **71**(2), pp. 105–115. Elsevier science.

KOCSIS-O., COSTARIDOU-L., VARAKI-L., LIKAKI-E., KALOGEROPOULOU-C., SKIADOPOULOS-S., AND PANAYIOTAKIS-G. (2003b). Visually lossless threshold determination for microcalcification detection in wavelet compressed mammograms, *European Radiology*, **13**(10), pp. 2390–2396.

KONG-X., AND FENG-R. (2001). Watermarking medical signals for telemedicine, *IEEE Transactions on Information Technology in Biomedicine*, Vol. 5, pp. 195–201.

KUNDUR-D., AND HATZINAKOS-D. (2004). Toward robust logo watermarking using multiresolution image fusion principles, *IEEE Transactions on Multimedia*, **6**(1), pp. 185–198.

LAMMINEN-H. (1999). Mobile satellite systems, *Journal of Telemedicine and Telecare*, **5**(2), pp. 71–83.

LEE-H. K., SONG-G. S., KIM-M. A., YOO-K. S., AND LEE-W. H. (2004). A digital watermarking scheme in JPEG2000 using the properties of wavelet coefficient sign, *Conference Proceedings of Computational Science and its Applications (ICCSA)*, Vol. 1, pp. 159–166.

LIE-W.-N., HSU-T.-L., AND LIN-G.-S. (2003). Verification of image content integrity by using dual watermarking on wavelets domain, *Proceedings of the IEEE International Conference on Image Processing (ICIP)*, Vol. 2, pp. 487–490.

LIN-C.-Y., AND CHANG-S.-F. (1997). An image authenticator surviving DCT-based variable quantization table compressions, *Technical Report 490-98-24*, CU / CTR Technical Report.

LIN-C. Y., AND CHANG-S. F. (1999). Distortion modeling and invariant extraction for digital image print-and-scan process, *Proceedings of the International Symposium on Multimedia Information Processing (ISMIP 99)*.

LIN-C. Y., AND CHANG-S. F. (2001). A robust image authentication method distinguishing JPEG compression from malicious manipulation, *IEEE Transactions on Circuits and Systems for Video Technology*, **11**(2), pp. 153–168.

LI-X. (2002). Blind image quality assessment, *Proceedings of the IEEE International Conference on Image Processing (ICIP)*, **1**, pp. 449–452.

LOANE-M., AND WOOTTON-R. (2002). A review of guidelines and standards for telemedicine, *Journal of Telemedicine and Telecare*, **8**(2), pp. 63–71.

LUO-J., YU-Q., AND MILLER-M. E. (2002). A triage method of determining the extent of JPEG compression artifacts, *IEEE International Conference on Image Processing (ICIP)*, **1**, pp. 473–476.

MAITY-S. P., KUNDU-M. K., AND NANDI-P. K. (2004). Compression resilient image watermarking scheme in spatial domain, *Proceedings of the International Conference on Communication, Devices and Intelligent Systems (CODIS)*, pp. 558–561.

MARTINEZ-A., VILLARROEL-V., SEOANE-J., AND DEL POZO-F. (2004). A study of a rural telemedicine system in the Amazon region of Peru, *Journal of Telemedicine and Telecare*, **10**(4), pp. 219–225.

Medpix^{TM} Medical Image Database (2005). Web. http://rad.usuhs.mil/medpix Last Checked: April 12 2005.

MIYASHITA-T., TAKIZAWA-M., NAKAI-K., OKURA-H., KANDA-H., MURASE-S., ICHIJO-T., KARAKI-Y., OUE-T., AND YAGI-K. (2003). Realtime ultrasound screening by satellite telecommunication, *Journal of Telemedicine and Telecare*, **9**(Supplement 1), pp. 60–61.

MONTONI-M., VILLELA-K., ROCHA-A. R., AND RABELO-A. (2002). TeleCardio mobile: Development of platform-independent telemedicine applications, *Proceedings of the Mobile Computing in Medicine Conference*, pp. 119–130.

NAKATA-N., KANDATSU-S., SUZUKI-N., AND FUKUDA-K. (2005). Mobile wireless DICOM server system and PDA with high-resolution display: Feasibility of group work for radiologists, *RadioGraphics*, **25**, pp. 273–283.

OKKALIDES-D. (1998). Assessment of commercial compression algorithms, of the lossy DCT and lossless types, applied to diagnostic digital image files, *Computerized Medical Imaging and Graphics*, **22**(1), pp. 25–30.

OLGES-N. H., EICHELBERG-M., RIESMEIER-J., AND JENSCH-P. F. (2000). Integrating JPEG compression with DICOM: Experiences and technical issues, *Proceedings of the SPIE - Medical Imaging 2000: PACS Design and Evaluation: Engineering and Clinical Issues*, Vol. 3980, pp. 46–56.

OSBORNE-D., ABBOTT-D., SORELL-M., AND ROGERS-D. (2004a). Multiple embedding using robust watermarks for wireless medical images, *Proceedings of the 3rd International Conference on Mobile and Ubiquitous Multimedia (MUM-2004)*, Vol. 83 of *ACM International Conference Proceeding Series*, College Park, Maryland, U.S.A. October 27-29, pp. 245–250.

OSBORNE-D., ABBOTT-D., SORRELL-M., AND ROGERS-D. (2004b). Multiple embedding using semi-fragile watermarks for wireless medical images, *Proceedings of the IEEE: Electronics and Telecommunications (ETC-2004)*, Timisoara, Romania, October 22-23, Section 13(34), pp. 120–125.

OSBORNE-D., ROGERS-D., AND ABBOTT-D. (2005a). Embedded watermarking for wireless image content authentication, *WSEAS Transactions on Communications*, **4**(7), pp. 505–513.

OSBORNE-D., ROGERS-D., AND ABBOTT-D. (2005b). Integrity assessment of diagnostic image content, *Proceedings of the 9th WSEAS International Conference on Communications*, Vouliagmeni, Athens, Greece, July 14-16. paper 479-308.

OSBORNE-D., ROGERS-D., MAZUMDAR-J., COUTTS-R., AND ABBOTT-D. (2002). An overview of wavelets for image processing for wireless applications, *Proceedings of the SPIE: Smart Structures, Devices and Systems*, Vol. 4935, University of Melbourne, Australia December 16-18, pp. 427–435.

OSBORNE-D., ROGERS-D., SORELL-M., AND ABBOTT-D. (2004c). Embedded importance watermarking for image verification in radiology, *Proceedings of the SPIE - BioMEMS and Nanotechnology*, Vol. 5275, University of Western Australia, Perth, December 10-12, pp. 383–390.

OSBORNE-D., ROGERS-D., SORELL-M., AND ABBOTT-D. (2005c). Multiple medical image ROI authentication using watermarking, *Proceedings of the SPIE - Biomedical Applications of Micro- and Nanoengineering II*, Vol. 5651, University of New South Wales, Sydney, Australia 12-15 December 2004, pp. 221–231.

PAGANI-L., JYRKINEN-L., NIINIMAKI-J., REPONEN-J., KARTTUNEN-A., LLKKO-E., AND JARTTI-P. (2003). A portable diagnostic workstation based on a webpad: Implementation and evaluation, *Journal of Telemedicine and Telecare*, **9**(4), pp. 225–229.

PALOMBO-A., FERGUSON-J., ROWLANDS-A., PEDLEY-D., AND FRASER-S. (2003). An evaluation of a telemedicine fracture review clinic, *Journal of Telemedicine and Telecare*, **9**(Supplement 1), pp. 31–33.

PARK-D. G., AND KIM-H. C. (2003). Comparative study of telecommunication methods for emergency telemedicine, *Journal of Telemedicine and Telecare*, **9**(5), pp. 300–303.

PENEDO-M., PEARLMAN-W. A., TAHOCES-P. G., SOUTO-M., AND VIDAL-J. J. (2003). Region-based wavelet coding methods for digital mammography, *IEEE Transactions on Medical Imaging*, **22**(10), pp. 1288–1296.

PLANITZ-B. M., AND MAEDER-A. J. (2005). Medical image watermarking: A study on image degradation, *Proceedings of the APRS Workshop on Digital Image Computing: Pattern Recognition and Imaging for Medical Applications*, pp. 3–8.

PRZELASKOWSKI-A. (2004). Compression of mammograms for medical practice, *in* A. Press. (ed.), *Proceedings of the 2004 ACM Symposium on Applied Computing*, pp. 249–253.

Raytheon Pty Ltd (2003). Acessed Online November 2003: www.raytheon.com / MVSAT.

REPONEN-J., ILKKO-E., JYRKINEN-L., KARHULA-V., TERVONEN-O., LAITINEN-J., LEISTI-E. L., KOIVULA-A., AND SURAMO-I. (1998). Digital wireless radiology consultations with a portable computer, *Journal of Telemedicine and Telecare*, **4**(4), pp. 201–205.

REPONEN-J., ILKKO-E., JYRKINEN-L., TERVONEN-O., NIINIMAKI-J., KARHULA-V., AND KOIVULA-A. (2000a). Intitial experience with a wireless Personal Digital Assistant as a teleradiology terminal for reporting emergency computerized tomography scans, *Journal of Telemedicine and Telecare*, **6**(1), pp. 45–49.

REPONEN-J., MINIMAKI-J., HOLOPAINEN-A., JARTTI-P., ILKKO-E., KARTTUNEN-A., KUMPULAINEN-T., TERVONEN-O., AND PAAKKO-E. (2000b). MOMEDA - a mobile smartphone terminal for DICOM images and web-based electronic patient data, *Proceedings of the International EuroPACS 2000 Conference: Telemedicine*, pp. 274–277.

SANCHEZ-V., MANDAL-M., AND BASU-A. (2004). Robust wireless transmission of regions of interest in JPEG2000, *Proceedings of the IEEE International Conference on Image Processing (ICIP)*, Vol. 4, pp. 2491–2494.

SEIDMAN-L. P. (1997). Satellites for telemedicine and telehealth, *Journal of Telemedicine and Telecare*, **3**(Supplement 1), pp. 101–102.

SHANNON-C. E., AND WEAVER-W. (1949). *The Mathematical Theory of Communication*, University of Illinois Press.

SHERSHNEVA-M. B., AND OLSON-C. A. (2005). Education through telemedicine networks: Setting quality standards, *Journal of Telemedicine and Telecare*, **11**(3), pp. 127–134.

SILVERMAN-R. D. (2003). Current legal and ethical concerns in telemedicine and e-medicine, *Journal of Telemedicine and Telecare*, **9**(Supplement 1), pp. 67–69.

SLONE-R. M., MUKA-E., AND PILGRAM-T. K. (2003). Irreversible JPEG compression of digital chest radiographs for primary interpretation: Assessment of visually lossless threshold, *Radiology*, **228**(2), pp. 425–429.

Stavanger University, Signal Processing Group (1999). Web. http://www.ux.his.no/ karlsk Last Checked: September 7 2005.

SUN-Q., YE-S., LIN-C.-Y., AND CHANG-S.-F. (2005). A crypto signature scheme for image authentication over wireless channel, *International Journal of Image and Graphics*, **5**(1), pp. 135–148.

SU-P., WANG-H. M., AND KUO-C. J. (1999). Digital watermarking on EBCOT compressed images, *Proceedings of the SPIE: Applications of Digital Image Processing XXII: Image and Video Compression II*, Vol. 3808, pp. 313–324.

TACHAKRA-S., WANG-X. H., ISTEPANIAN-R. S., AND SONG-Y. H. (2003). Mobile e-health: The unwired evolution of telemedicine, *Telemedicine Journal and e-health*, **9**(3), pp. 247–257.

TAUBMAN-D. S., AND MARCELLIN-M. W. (2001). *JPEG2000: Image Compression Fundamentals, Standards and Practice*, Kluwer International Series in Engineering and Computer Science.

TINGBERG-A., HERRMANN-C., LANHEDE-B., ALMEN-A., SANDBORG-M., MCVEY-G., MATTSSON-S., PANZER-W., BESJAKOV-J., MANSSON-L. G., KHEDDACHE-S., CARLSSON-G. A., DANCE-D. R., TYLEN-U., AND ZANKL-M. (2004). Influence of the characteristic curve on the clinical image quality of lumbar spine and chest radiographs, *British Journal of Radiology*, **77**(915), pp. 204–215.

TONG-H., LI-M., ZHANG-H., ZHANG-C., HE-J., AND MA-W.-Y. (2005). Learning no-reference quality metric by examples, *Proceedings of the IEEE: 11th International Conference on Multi Media Modelling (MMM 2005)*, Vol. 1, pp. 247–254.

TOOLEY-M. A., FORREST-F. C., AND MANTRIPP-D. R. (1999). MultiMed - remote interactive medical simulation, *Journal of Telemedicne and Telecare*, **5**(Supplement 1), pp. 119–121.

WAKATANI-A. (2002). Digital watermarking for ROI medical images by using compressed signature image, *Proceedings of the IEEE: 35th Annual Hawaii International Conference on System Sciences (HICSS'02)*, Vol. 6, pp. 2043–2048.

WALLACE-G. K. (1991). The JPEG still picture compression standard, *Communications of the ACM*, **34**(4), pp. 30–44.

WANG-H. J., KUO-M., AND PO-CHYI-S. (1999). Digital image watermarking in regions of interest, *Proceedings of the Conference on Image Processing, Image Quality and Image Capture Systems (PICS 1999) - Image Processing Track: Image Processing - Watermarking and Security*, IS&T - The Society for Imaging Science and Technology, pp. 295–300.

WANG-R., CHENG-Q., AND HUANG-T. S. (2000). Identify regions of interest for video watermark embedment with principle component analysis, *Proceedings of the Eighth ACM International Conference on Multimedia*, pp. 459–461.

WANG-Z., BOVIK-A. C., SHEIKH-H. R., AND SIMONCELLI-E. P. (2004). Image quality assessment: From error visibility to structural similarity, *IEEE Transactions on Image Processing*, **13**(4), pp. 600–612.

WANG-Z., SHEIKH-H. R., AND BOVIK-A. C. (2002). No-reference perceptual quality assessment of JPEG compressed images, *Proceedings of the IEEE International Conference on Image Processing (ICIP)*, Vol. 1, pp. 477–480.

WEKEN-D. V., NACHTEGAEL-M., AND KERRE-E. E. (2004). Using similarity measures and homogeneity for the comparison of images, *Journal of Image and Vision Computing*, **22**(9), pp. 695–702.

WONG-H., GUAN-L., AND HONG-H. (1995). Compression of digital mammogram databases using a near-lossless scheme, *Proceedings of the IEEE International Conference on Image Processing (ICIP)*, **2**, pp. 21–24.

WOO-C.-S., DU-J., AND PHAM-B. (2005). Multiple watermark method for privacy control and tamper detection in medical images, *Proceedings of the APRS Workshop on Digital Image Computing: Pattern Recognition and Imaging for Medical Applications*, pp. 43–48.

WOOTTON-R., BLIGNAULT-I., AND CIGNOLI-J. (2003). A national survey of telehealth activity in Australian hospitals, *Journal of Telemedicine and Telecare*, **9**(Supplement 2), pp. 73–75.

YAGI-Y., AND GILBERTSON-J. R. (2005). Digital imaging in pathology: The case for standardization, *Journal of Telemedicine and Telecare*, **11**(3), pp. 109–116.

YANG-Z., CAMPISI-P., AND KUNDUR-D. (2004). Dual domain watermarking for authentication and compression of cultural heritage images, *IEEE Transactions on Image Processing*, **13**(3), pp. 430–448.

YOGESAN-K., CONSTABLE-I. J., MORGAN-W., AND SOEBADI-D. Y. (2000). International transmission of tele-ophthalmology images, *Journal of Telemedicine and Telecare*, **6**(1), pp. 41–44.

YOUNGBERRY-K. (2004). Telemedicine research and MEDLINE, *Journal of Telemedicine and Telecare*, **10**(2), pp. 121–123.

ZAMPOLO-R. F., AND SEARA-R. (2003). A measure for perceptual image quality assessment, *Proceedings of the IEEE International Conference on Image Processing (ICIP)*, Vol. 1, pp. 433–436.

ZHANG-H., AND FRITTS-J. (2004). EBCOT coprocessing architecture for JPEG2000, *Proceedings of the SPIE - Electronic Imaging: Visual Communications and Image Processing*, Vol. 5308, pp. 1333–1340.

Appendix G

Resume

Dominic Osborne received certificates of credit in the Australian Westpac Mathematics Competition in 1990 and 1992. In 1995 he achieved the Duke of Edinburgh Silver Award. In 2000 at the University of South Australia he was awarded the Entech Electronic Engineering Prize. This was awarded to the student in the Bachelor of Engineering (Electronic and Microengineering) who obtained the highest average weighted mark for all of the scheduled third year courses taken over one year. In 2001 he achieved first class honours and was placed on the Dean's merit list as a result of being in the top fifteen percent of all undergraduate students in the Division of Information Technology, Engineering and the Environment. He graduated in 2002 and was awarded an APAI Scholarship (funded by the Australian Research Council and Motorola) to undertake a PhD at the University of Adelaide in the School of Electrical and Electronic Engineering. His research was under the supervision of Professor Derek Abbott (The Centre for Biomedical Engineering) and Dr Derek Rogers (Adjunct Senior Lecturer from the School of Electrical and Electronic Engineering). Osborne has authored seven publications and has given six conference presentations. His interests include image and signal processing and expanding the developments in biomedical engineering.